Understanding HDAC8-Catalyzed Deacetylation:

From New Substrates to Diseases

by

Jeffrey E. López

A dissertation submitted in partial fulfillment
of the requirements for the degree of
Doctor of Philosophy
(Chemical Biology)
in the University of Michigan
2017

Doctoral Committee:

Professor Carol A. Fierke, Chair
Professor Anna K. Mapp
Associate Professor Patrick J. O'Brien
Professor Janet L. Smith

Jeffrey E. López

lopejeff@umich.edu

ORCID ID: 0000-0002-5329-0043

Acknowledgements

I would like to thank my advisor, Dr. Carol Fierke. Her mentorship and encouragement throughout the years has helped me improve as both an independent scientist and as a person. She always encouraged me to explore, challenge and broaden my horizons both academically and personally. I could always go to her with questions and would always leave her office with more questions than when I walked in. I am glad that I had the opportunity to work with such an amazing mentor and for her deciding to believe in my potential.

To my undergraduate mentors at the University of Delaware, particularly Dr. John Burmeister for always encouraging me to pursue my dreams even after I had that awful first semester in CHEM 111/112. Dr. Harold White, for teaching me how to think logically and critically and to always question the world around me. Dr. Burnaby Munson, always being welcoming, encouraging and igniting my passion for going into the academic field and Dr. Charles Riordan, for giving me a chance to work in his lab and learning valuable skills and habits that have stayed with me throughout my scientific career.

To the Fierke lab, you all have become an amazing group of friends. We have had tons of fun, whether it would be in the break room, eating lunch or going out. I would like to personally thank the HDAC subgroup and all its members I have interacted with throughout the years including Dr. Eric Sullivan, Dr. Byungchul Kim, Dr. Carol Ann Pitcairn, Dr. Noah Wolfson, Katherine Leng, Kelsey Diffley, Hannah Foley and George Murphy III. This has been an amazing journey through graduate school and I don't think I would have ever made it without any of you. I would also like to thank Dr. Elia Wright for being an amazing lab mentor and friend.

Finally, I would like to thank all my family, particularly my parents William and Rhyna and my grandmother Inés. Thank you for being stern, kind and an inspiration in

my life. For always supporting me and for always pushing me to strive for the best. Thank you all for showing me how to persevere and push forward in life.

TABLE OF CONTENTS

List of Figures

List of Tables

Abstract

Lysine acetylation is a dynamic post-translational modification occurring ubiquitously in cells. The histone deacetylase (HDAC) family catalyzes the removal of an acetyl group from the ε-position of lysine residues in proteins. There are 11 metal-dependent deacetylases tasked with the proper regulation of thousands of proteins. Thus, it is important to define the specificity and reactivity of each isozyme.

HDAC8 is a well characterized metal-dependent deacetylase that can be activated with Zn^{2+} or Fe^{2+} *in vitro* with a relatively unknown protein-substrate pool. To unveil new putative full- length protein substrates, we developed and optimized a chemical capture approach that can be used along with co-immunoprecipitation and proteomics to trap short-lived HDAC8-substrate interactions. Using this approach, we identified 11 potential HDAC8 substrates. These substrates were then validated using acetylated peptide mimics with an enzyme-coupled assay, determining rate constants that are at least two orders of magnitude faster than SMC3, one of the best *in vivo* validated HDAC8 protein substrates. Furthermore, we studied how Cornelia de Lange spectrum disorders are caused by HDAC8 missense mutations. Based on our results, we determined that these mutations can affect a variety of processes such as substrate binding, product release, and most interestingly, divalent metal binding; bringing to question the identity of HDAC8's catalytic divalent metal ion. Finally, we have shown that the sequence specificity of HDAC8 towards peptide substrates is dependent on the identity of the catalytic divalent metal ion in addition to the immediate sequence and potentially other post-translational modifications. Overall, this work has provided insight into the substrate specificity and regulation of HDAC8 in the cell, in addition to providing a new, alternate approach for identifying potential HDAC-specific substrates that could be adapted for other deacetylase isozymes.

Chapter 1

Metal-Dependent Deacetylases[*,†]

A General Overview

Epigenetic regulation is a key factor in cellular homeostasis. This regulation of proteins is possible due to post-translational modifications (PTMs). Many of these modifications are both dynamic and reversible. PTMs include methylation, phosphorylation, ubiquitination, acetylation, sumoylation and biotinylation, among others. Some of these modifications, such as acetylation and methylation, were originally characterized on the tails of core histone proteins and regulate access to wrapped DNA by disrupting chromatin structure[1]. Lysine acetylation has garnered increasing interest in recent years, with a trend in publication rate that rivals that of phosphorylation[2].

A major advance in the acetylation field has been the transition from analysis of acetylation (both hyper- and hypoacetylation) of specific lysine residues in core histone tails to defining and understanding the numerous proteins that undergo acetylation events. Acetylation has been shown to compete and/or cooperate with other PTMs, such as ubiquitination[3], and affect specific protein-protein interactions, protein stability, and

[*] Reproduced, in part, from Lopez, J. E., Sullivan, E. D., and Fierke, C. A., (2016) Metal-dependent Deacetylases: Cancer and Epigenetic Regulators. *ACS Chem. Bio. 11,* 706-16

[†] Original text written by Jeffrey E. Lopez and Eric D. Sullivan. The text was updated and revised by Jeffrey E. Lopez for this thesis

protein-DNA interactions[4]. Identifying HDAC-protein interactions will lead to a better understanding of the acetylome, the collection of non-histone proteins that undergo acetylation/deacetylation, and the role of acetylation in cell regulation, growth and homeostasis. (Figure 1.1)

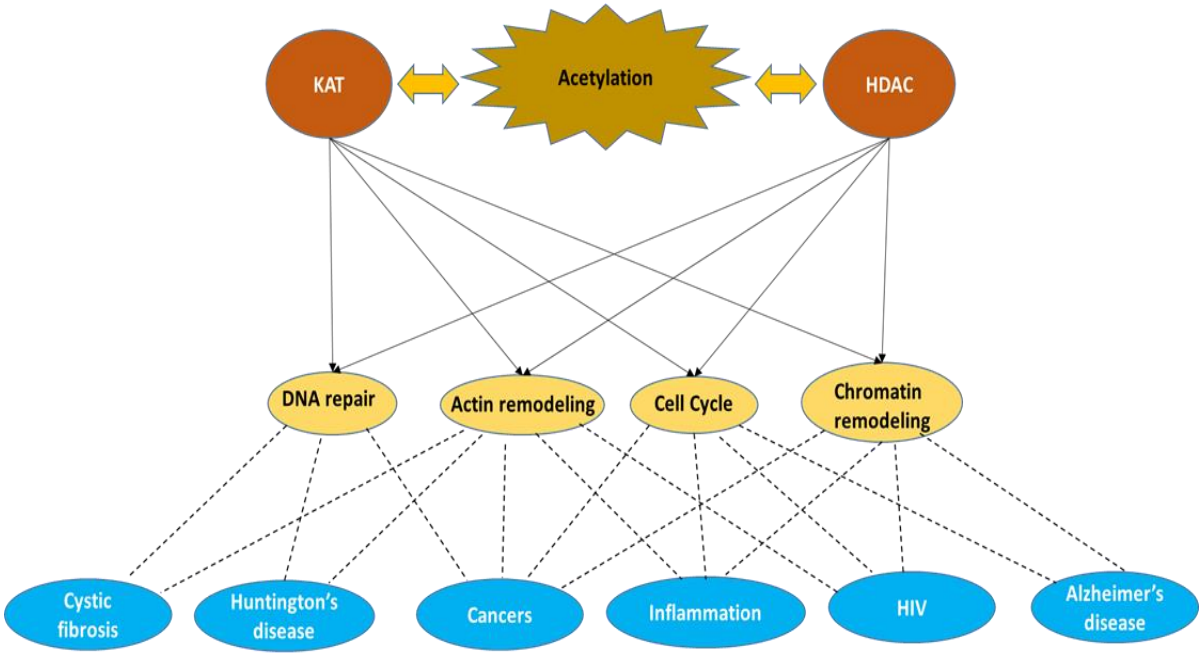

Figure 1.1: Acetylation is critical for regulation and proper cellular function

Lysine acetyltransferases (KATs) and histone deacetylases (HDACs) maintain acetylation to optimal levels. Acetylation regulates essential cellular processes such as DNA repair, chromatin and actin remodeling and proteins that serve as checkpoints during the cell cycle.

Acetylation is an enzyme catalyzed and reversible PTM in which an acetyl group is attached to the N^{ε}-position of a lysine side chain. Lysine acetyltransferases (KATs) catalyze acetylation of lysine side chains using acetyl-CoA as a cofactor, and metal-dependent deacetylases (HDACs) catalyze hydrolysis of the acetyl moiety to generate lysine and acetate. Traditionally, HDACs have been described as transcriptional repressors since they change the recruitment and interactions of many proteins, including bromodomain-containing proteins, MEF2-binding proteins and domains, to histone tails.

They are also involved in chromatin compaction[1]. However, acetylation and deacetylation of many non-histone proteins have now been discovered. In fact, currently, over 6000 acetylation sites have been discovered in the mammalian proteome, with many more being discovered through proteomics, computational and modeling analyses[5].

Considering these many non-histone HDAC targets, a more suitable name for these enzymes would be acetyl-lysine deacetylases, or acKDACs. Aberrant regulation of protein acetylation has been observed in various types of cancers including prostate[6], breast[7], and colon[8] among others, in addition to a variety of diseases, such as Cornelia de Lange-like Spectrum diseases (CdLS)[9], Huntington's disease[10], and inflammation[11].

The increasingly evident role and overexpression of HDACs in cancer has made them an interesting and attractive anticancer target. Current research shows that there are multiple mechanisms by which acetylation affects cancer development using HDAC inhibitors (HDACi) such as inducing cell growth, differentiation, senescence, and death of non-cancerous cells and tissues[12,13]. Several HDAC inhibitors have been developed to examine and combat these mechanisms; however, the current clinically approved compounds do not possess isozyme selectivity. Three pan-HDAC inhibitors - suberoylanilide hydroxamic acid (SAHA)[14], Romidepsin (cyclic peptide)[14], and belinostat (hydroxamic acid)[15] – have been approved by the FDA for treatment of T-cell lymphomas, and a fourth inhibitor, panabinostat (hydroxamic acid), has recently been approved for multiple myeloma treatment[16].

Studies have demonstrated that pan-HDACi's can also be used to increase the effectiveness of anticancer immunotherapy treatments. In one case, T-cell survival was enhanced due to prevention of activation-induced cell death by lymphocytes[12,17].

However, these effects vary significantly and can produce a variety of undesirable side effects. Additionally, HDACi's have been used to enhance vaccine strategies; namely, mice vaccinated with melanomal cells that have been pretreated with trichostatin A (TSA), a potent hydroxamic acid, show an increase in immune response towards additional tumors, effectively enhancing their tumor specific immunity mechanisms[11].

HDACs are divided into four different classes based on their phylogeny and sequence homology to yeast orthologs[13]. Class I, which shares homology with Rpd3, consists of HDACs 1, 2, 3, and 8. Class II, with homology to Hda1, can be divided into two subclasses – IIa (HDACs 4, 7, and 9) and IIb (HDACs 6 and 10). Class III, with homology to the Sir2 family, is known as the sirtuins and utilizes NAD^+ as a cofactor. Class IV, which shares homology with both class I and class II, consists solely of HDAC11. Classes I, II and IV are metal-dependent HDACs that use a divalent metal-water as a nucleophile during catalysis, which is activated by a general acid-base mechanism (Figure 1.2)[18]. In addition, the activity of HDACs can be further regulated by monovalent metal ions, such as potassium and sodium[19].

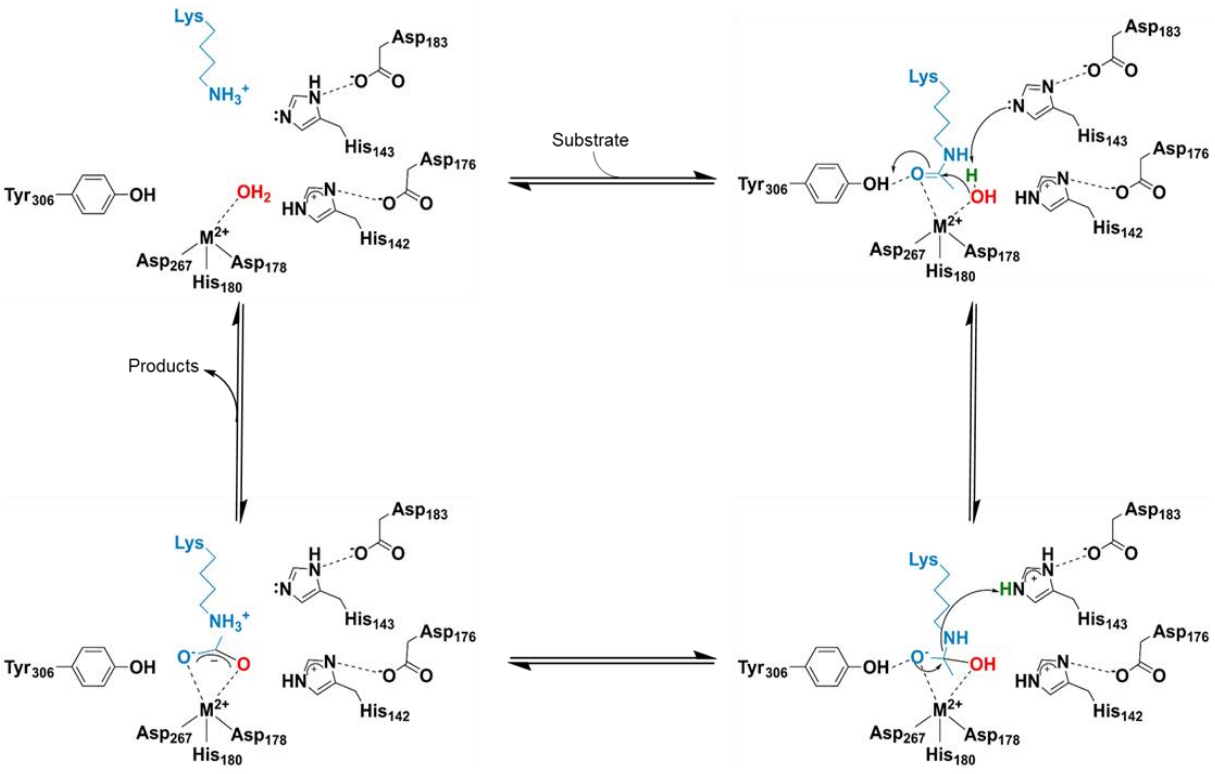

Figure 1.2: General acid/base catalytic mechanism used by metal-dependent deacetylases

A divalent metal ion is coordinated by a conserved Asp-Asp-His triad and one water molecule that functions as the nucleophile in the reaction. His143 acts as both a general acid and a general base, while Tyr306 and His143 stabilize the oxyanion intermediate.

Metal-dependent HDACs share common sequence motifs (Figure 1.3), including a deacetylase domain that is comprised of an arginase-deacetylase fold, consisting of a multistranded β-sheet surrounded by α-helices, and a divalent metal ion cofactor coordinated by an Asp-Asp-His triad[20]. Class I HDACs possess a deacetylase domain that has little sequence variation. These enzymes are localized mainly in the nucleus[13], with the exception of HDAC8, which has been observed in the cytoplasm of smooth muscle cells[21]. Class II HDACs are shuttled between the nucleus and the cytoplasm and possess additional domains, such as MEF2 binding domains. HDAC6 has the largest

array of domains with two deacetylase domains and a zinc finger binding domain[13]. Class II HDACs are expressed ubiquitously through the cell and generally have lower *in vitro* catalytic activity when compared to class I deacetylases. Finally, HDAC11, the sole class IV metal-dependent deacetylase, possesses characteristics from both class I and II deacetylases, is expressed in high abundance in specific tissues such as brain, heart and kidney[22] and has been shown to catalyze deacetylation of both methylcoumarin-bound and non-methylcoumarin bound peptides[23].

Crystal structures have been solved for HDAC1 (PDB: 4BKX), HDAC2 (PDB: 3MAX), HDAC3 (PDB: 4A69), HDAC4 (PDB: 2VQM), HDAC6 (PDB: 3PHD, 5EDU, 5EEF, 5EEI)), HDAC7 (PDB: 3C0Y; catalytic domain only), HDAC8 (2V5W), and HDAC9 (PDB: 1TQE). The isozymes that lack crystal structures are HDAC5, HDAC10 and HDAC11.

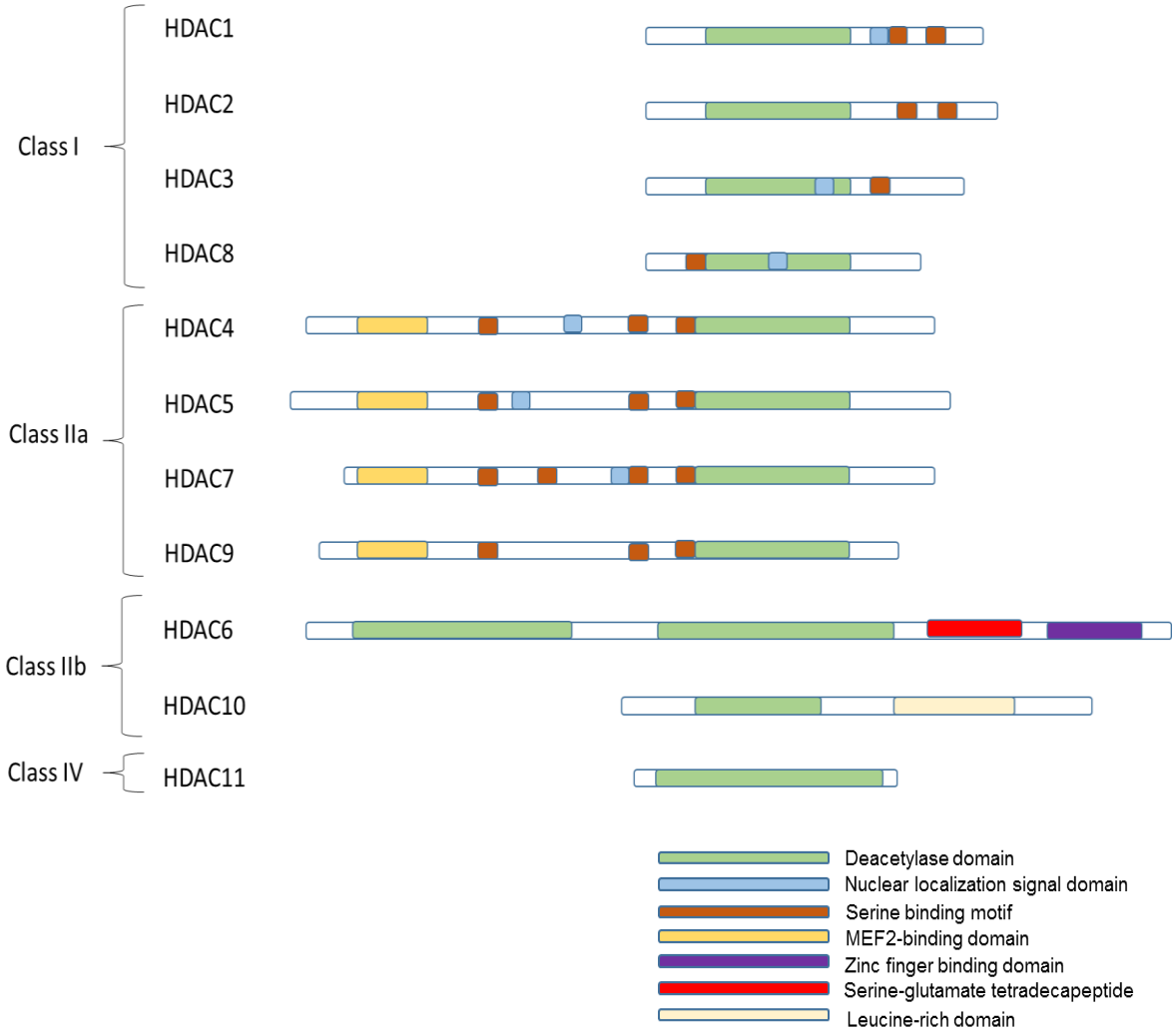

Figure 1.3: Schematic comparison of the metal-dependent deacetylases

All isozymes possess a common deacetylase domain. Class I isozymes are highly conserved and small. Class IIa isozymes have specific MEF2-binding/localization domains in addition to their conserved deacetylase domains. Class IIb isozymes contain unique domains unlike the other classes. Only the deacetylase domain has been identified in class IV.

One of the most prevalent questions in the HDAC field is the substrate selectivity of each isozyme. There are over 6000 validated mammalian acetylation sites[5] and 18 deacetylase isozymes (11 metal-dependent and 7 NAD^+-dependent enzymes). Thus, defining the substrate pool for each isozyme is essential for understanding the biological functions of acetylation. Additionally, the substrate specificity of HDACs might be regulated by oxidative stress, protein-protein interactions, and other PTMs. Elucidating HDAC substrate specificity and regulation will provide insight into the function and control of acetylation sites in proteins.

Here, we highlight some functions of each of the metal-dependent deacetylase classes regarding epigenetic regulation and homeostasis, and how acetylation/deacetylation plays a role in cell proliferation and growth in cancers, in addition to other, as of now, unknown roles.

Class I HDACs

The class I HDAC subfamily is dysregulated in cancers and is the best studied subfamily among the metal-dependent deacetylases. Overexpression of this subclass has been observed in a variety of cancers such as gastric[24], breast[7], prostate[6], and colon[8], as well as T-cell[25] and Hodgkin's lymphoma[26].

In most cases, upregulation of HDAC1 is associated with poor cancer prognosis[27]. Silencing of HDAC1 using siRNA knockouts results in cell cycle arrest, growth inhibition and induction of apoptosis in breast cancer cells[28] and induction of a plasminogen activator in neuroblastoma cells, increasing their invasive capacity[29]. Mass proteomic analyses have revealed additional HDAC1 protein-protein interactions, ranging from

short-lived interaction proteins, such as IKF2, HMG box transcription factor BBX, and activity-dependent neuroprotector homeobox protein ADNP, to proteins with methylation-related functions such as ARID5B to previously uncharacterized zinc-binding proteins and domains, such as C16orf87[30]. Additionally, HDAC1 has been shown to interact with the oncogene fusion protein PML-RAR, a protein involved in the pathogenesis of acute promyelocytic lymphoma (APL); HDAC1 diminishes the tumorigenic activity of PML-RAR by interfering with cell differentiation, impairing genetic stability, and increasing the renewal of progenitor cells. However, HDAC1 expression also enhances cell survival once they have differentiated, leading to a dual role in cancerous tissue[31].

Immunodeficient mice have been used to evaluate the role of HDAC1 in tumor formation using teratomas. In these models, HDAC1 deficiency leads to partially undifferentiated carcinomas, upregulation of HDAC2, elevated levels of SNAIL1 expression and delocalization of E-cadherin[32]. Knockouts of HDAC1 and 2 showed dramatic acceleration of leukomogenesis in preleukemic mice. HDAC1 knockouts also led to deletion of p53 and c-myc overexpression[31]. Additionally, Dovey et al demonstrated that knockouts of key components of the HDAC1/2 deacetylase complex, namely Sin3A and Mi2, decreased overall HDAC activity in T-cells and perturbed the differentiation of thymocytes into mature T lymphocytes[33]. Similarly, mice knockouts of HDAC1/2 showed that the loss of HDAC activity leads to the accumulation of thymocytes in addition to blocking early thymic development[34].

The previously described protein-protein interactions have led to the proposal that some HDACs function in large deacetylase complexes. HDAC1 and HDAC2, together with histone binding proteins RBBP4 and RBBP7, DNA/chromatin recognition motifs, and

transcription factors form core deacetylase complexes that help localize HDAC1 and HDAC2 to chromatin[35].

HDAC2 is overexpressed in lung cancer tissues and mesenchymal tumors, suggesting that it is an effector for these diseases. Silencing of HDAC2 using siRNA leads to an increase in p53 DNA binding activity, Bax activation and Bcl2 suppression[36]. These changes in Bax activation and Bcl2 suppression are consistent with suppressed expression of cyclin E2, cyclin D1, and CDK2, blocking cell proliferation and inducing apoptosis[37]. Truncations of HDAC2 have been detected frequently in cancers[38] and knockouts of both HDAC1 and HDAC2 prompt TRAIL-induced apoptosis in chronic lymphocytic leukemia (CLL), indicating a level of cooperativity between these two isozymes[39]. Using mutant fibroblasts that are HDAC2-deficient, Zimmerman et al demonstrated a lack of response to insulin-like growth factors (IGFs) when compared to wild type cells, showing a potential link between HDACs and IGFs[40]. Mice models lacking HDAC1 and with a single HDAC2 allele developed a lethal pathology within 3 months, likely due to neoplastic transformation of immature T-cells[33]. Additionally, mutant mice with an inactive HDAC2 mutant exhibited a 25% decrease in overall body size and reduced cell number and thickness of intestinal mucosa[40].

Knockouts of HDAC3 in promyelocytic leukemia cells restore retinoic acid dependent gene expression, primarily due to loss of interactions between HDAC3, the nuclear corepressor NCoR, and PML-RARalpha fusion protein[41]. The best understood example of HDAC3 function is repression of retinoic acid and thyroid hormone receptors, which can modulate p53 expression[42]. HDAC3, along with HDAC1 and HDAC2, is often expressed in high levels in renal, colorectal, and gastric cancer[26,43]. High expression of

HDAC3 has also been observed in eight different pancreatic cancer cell lines and potentially generates a postinduction repression of p53, p27, and Bax genes through deacetylation of lysine 9 (K9) of histone H3[42]. Additionally, HDAC3 depletion in mouse liver upregulates lipogenic genes and causes histone hyperacetylation, leading to hepatostaetosis[44]. However, expression of inactive HDAC3 mutant proteins in these knockout mice almost completely rescues the metabolic and gene transcription alterations, suggesting that HDAC3 plays important non-deacetylase roles, such as protein-protein interaction signaling. Consistent with this, mice knockouts of the nuclear corepressor NCoR, an essential part of the HDAC3 deacetylase complex, exhibit metabolic and transcriptional effects resembling those of mice without hepatic HDAC3, demonstrating that interactions with NCoR are essential for the deacetylase-independent function of HDAC3[44]. Additionally, expression of HDAC1 and HDAC3 correlate with both estrogen and progesterone receptor expression and have been proposed as potential prognostic markers in breast cancer tumors[35].

HDAC8 is the best biochemically characterized HDAC isozyme to date[18,19,45,46]. HDAC8 is the only class I isozyme that is localized to both the cytoplasm and the nucleus and that is not observed in large, multiprotein complexes *in vivo*[47]. HDAC8 is overexpressed in childhood neuroblastoma[48] and T-cell lymphoma[25]. Knockouts of HDAC8 produce skull morphology and growth complications in mice models[13] and stop cell proliferation in lung, colon and cervical cancer cell lines[48]. Point mutations in HDAC8 have been discovered in child patients with symptoms similar to the Cornelia de Lange Syndrome (CdLS). Lack of deacetylation of SMC3 in the cohesin complex has been implicated as a contributor to this disease, inhibiting the cell cycle, disrupting proper

chromatid separation and causing debilitating mental and physical abnormalities[9].. Knockouts and inhibition of HDAC8 using HDACis have been shown to induce apoptosis in T-cell lymphoma and leukemia cell lines[25]. Using mice xenograft models of oncogene-amplified neuroblastoma, Rettig et al. demonstrated that selective inhibition of HDAC8 produces antineuroblastoma activity without significant toxicity and induces cell cycle arrest and differentiation both *in vivo* and *in vitro*[49]. Additionally, the combined treatment of HDACi and retinoic acid enhanced cell differentiation, demonstrating that inhibition of HDAC isozymes can be combined with differentiation-inducing agents to target tumors[49]. Currently, work on HDAC8 has focused on mass spectrometry and coimmunoprecipitation studies using the HDAC8 specific inhibitor PCI-34051, which have provided insight into potential protein substrates and interaction partners[30,50]. Recently, insight into the substrate selectivity and protein interaction partners have been gained by immunoprecipitation and treatment with an HDAC8 specific inhibitor followed by mass spectrometry[50]. However, the full spectrum of substrates have not been identified. Investigations of HDAC8 specificity are poised to provide additional insight into the biological function and protein-protein interactions of metal-dependent deacetylases.

Class II HDACs

Class II HDACs were discovered in the early 2000s[51,52]. These proteins are significantly larger than both class I and class IV HDACs due to N-terminal and C-terminal tails and domains attached to their canonical deacetylase domain. This class is subdivided into two subfamilies: Class IIa and IIb. Class IIa consists of HDAC 4, 5, 7, and 9, and class IIb is comprised of HDAC 6 and 10. These isozymes differ from class I HDACs in that the additional N-terminal domains interact with transcription factors to

target certain genes, such as the MEF2 proteins, a family of transcription factors that are key regulators in cellular differentiation[53]. Recruitment of class II HDACs by MEF2 proteins to various protein complexes can alter the protein acetylation landscape due to blocking interactions with acetylation complexes such as CREBBP/EP300 in non-Hodgkin's lymphoma[54,55]. Class II HDACs are localized to both the cytoplasm and the nucleus. Additionally, both upregulation and downregulation of these isozymes can have severe repercussions in various cancers.

Class IV HDACs

HDAC11, the most recently discovered isozyme, is the sole member of the class IV HDAC subfamily[22]. At 39 kDa, HDAC11 is the smallest isozyme. Sequence alignments suggest that HDAC11 is more closely aligned with class I HDACs (up to 28% sequence identity to HDAC8) than class II, with retention of highly conserved metal binding sites seen in other metal-dependent deacetylases. HDAC11 sequence alignments identify one significant sequence change, an aspartate (D101 in HDAC8) to asparagine, located in the flexible L2 loop, near the entrance to the active site tunnel[56].

HDAC11 expression is tissue specific, with the greatest expression occurring in the brain, heart, kidneys, skeletal muscle and testis[22]. Studies of murine brain development suggest a role for HDAC11 in the formation of mature oligodendrocytes[57]. Overexpression of HDAC11 in RAW264.7 cells is associated with a decrease in mRNA levels of the anti-inflammatory cytokine interleukin-10, indicating a possible role for HDAC11 in inflammatory and autoimmune diseases[58]. Furthermore, mRNA analysis uncovered a link between HDAC11 and cancer; mRNA levels for HDAC11 are in the top

1% of differentially overexpressed genes in ductal breast carcinoma when compared to healthy breast tissue[59]. Finally, the DNA replication factor Cdt1 is a potential HDAC11 substrate. Cdt1 is integral in recruiting mini-chromosome maintenance (MCM) helicase to DNA, which is required for DNA replication during the cell cycle. To maintain a single copy of DNA per cell, Cdt1 must be inhibited after loading MCM in the G1 phase[60]. Additionally, Cdt1 is an acetylated protein that coimmunoprecipitates with HDAC11[60]. Finally, HDAC11 knockout mice are viable, but they exhibit increased cell proliferation and secrete higher levels of IL-2, TNF and IFN-γ than wild type mice[61].

Mechanism and Inhibition of Metal-Dependent HDACs

All metal-dependent HDACs share a common deacetylase domain (Figure 1.3)[62]. Particularly, they possess a conserved pair of histidine residues along with a tyrosine deep within the active site tunnel, which are critical for activation and stabilization of the metal-water nucleophile and overall catalysis[46,63].

At the bottom of the HDAC active site tunnel, a divalent metal ion is coordinated by an Asp-Asp-His triad in a pentacoordinate, square pyramidal conformation along with a water molecule[46,63]. In crystal structures, the identity of the divalent metal ion is zinc; however, multiple divalent metals have been observed to activate HDAC8 catalysis *in vitro*, raising the question of the identity of the divalent metal *in vivo*[45]. Our work presents an extensive comparison of the reactivity of Fe^{2+} and Zn^{2+}-HDAC8 with various biologically relevant peptide substrates to gain insight into the identity of the *in vivo* divalent metal.

Mechanistic studies of HDAC8 have led to a proposed general acid/general base

catalytic mechanism (Figure 1.2)[18]. Upon binding to HDAC8, the carbonyl oxygen of the acetyl lysine moiety coordinates the active site metal ion. The metal-water is activated by His143 functioning as a general base to attack the carbonyl carbon of the acetyl moiety to form a tetrahedral oxyanion intermediate. This intermediate is stabilized through interactions with a conserved tyrosine (Tyr306), the divalent metal ion and a protonated His142. In a second step, the protonated His143 acts as a general acid, protonating the nitrogen of the lysine leaving group to facilitate break down of the tetrahedral intermediate to form acetate and lysine products[18].

Most HDAC inhibitors coordinate the divalent metal ion. Although an effective strategy, severe side effects have limited their use in the clinic. Three of the FDA-approved pan-HDAC inhibitors possess a hydroxamic acid (Vorinostat, Panobinostat and Belinostat) (Figure 1.4A – for Vorinostat) which has been demonstrated to chelate the active site divalent metal ion and target all metal-dependent HDACs. Thus, the need for isozyme-specific inhibitors has risen.

One isozyme-specific inhibitor has been developed for HDAC8 (PCI-34051) (Figure 1.5B). It has a K_i of 10 nM for HDAC8, and it is at least 200-fold more selective towards inhibition of HDAC8 compared to other HDACs[25], this inhibitor has proven to be crucial in identifying HDAC8 substrates[50].

A

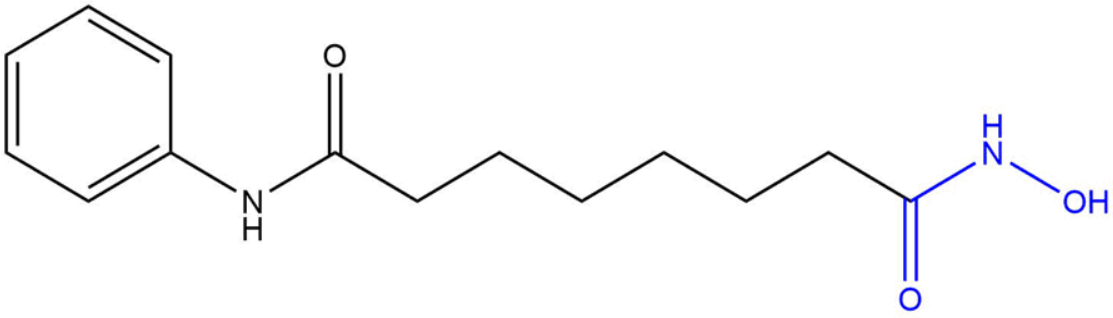

B

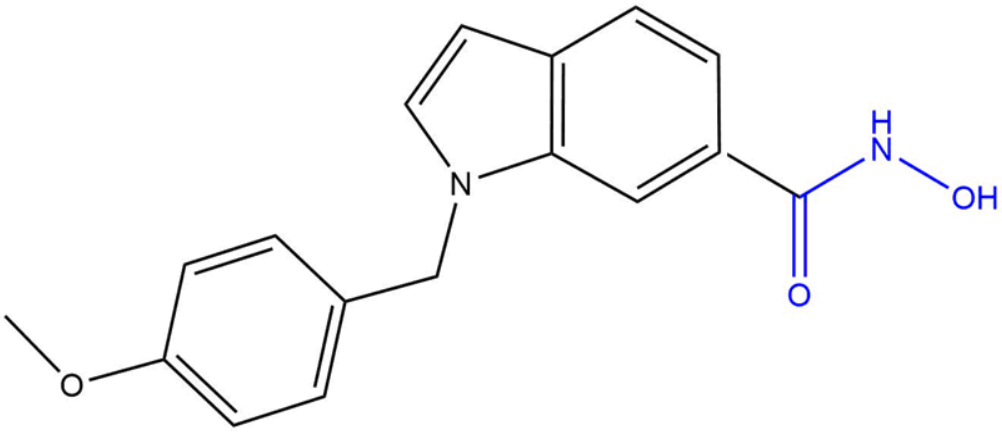

Figure 1.4: Hydroxamic acid inhibitors of metal dependent HDACs

A. The pan-HDAC inhibitor Vorinostat is a hydroxamic acid metal chelator, with a linker and a capping group. It is widely used in both research and as a drug to treat T-cell lymphoma.

B. The HDAC8 specific inhibitor PCI 34051. It has high specificity for inhibition of HDAC8 when compared to any other metal dependent HDAC8. It has been used to discover new HDAC8 substrates

Biological Significance of HDAC8

Despite the large array of current *in vitro* characterization, uncovering the biological role of HDAC8 *in vivo* has proven to be challenging. HDAC8 has been shown to be involved in a variety of diseases, from cancer to developmental disorders. *In vivo*, HDAC8 knockouts in mice have been shown to cause developmental issues due to alterations in skull morphology, followed by death[64].

Despite these observations, non-histone HDAC8 substrates remain as elusive targets. Current efforts have identified a small array of potential protein substrates using co-immunoprecipitation using HDAC-EGFP fusion proteins, stable isotope labeling of amino acids in cell culture (SILAC), followed by HDAC inhibitor dosing[30,50]. These studies have provided a snapshot of the versatility of roles that HDAC8 might play *in vivo*, as well as additional avenues to pursue for identifying new HDAC8 substrates. The work presented in this thesis presents an alternative, non-invasive system for identifying HDAC8-substrate interactions in cell lysates. This method could potentially be adapted to identify short-lived interacting substrates of other HDACs.

Potential *in vivo* HDAC8 Substrates

Current proposed substrates of HDAC8 include the estrogen-related receptor alpha (ERRα)[65], cAMP response binding protein (CREB)[66], AT-rich interactive domain-containing protein 1A (ARID1A)[50], cysteine-rich protein 2-binding protein (CSRP2BP)[50], and the structural maintenance of chromosomes 3 (SMC3)[9,50], among others.

Among the proposed substrates, the best characterized HDAC8-substrate is SMC3, a core component of the cohesin complex responsible for the proper separation

of sister chromatids during cell division[67]. SMC3 is acetylated during S phase and is promptly deacetylated during anaphase, after sister chromatid separation occurs as part of a checkpoint process (Figure 1.5)[67]. Studies have shown that HDAC8 is the deacetylase responsible for the deacetylation of SMC3 during anaphase[9]. Aberrant deacetylation due to SMC3 and/or HDAC8 mutations have been linked to approximately 10% of the cases of the Cornelia de Lange Syndrome (CdLS).

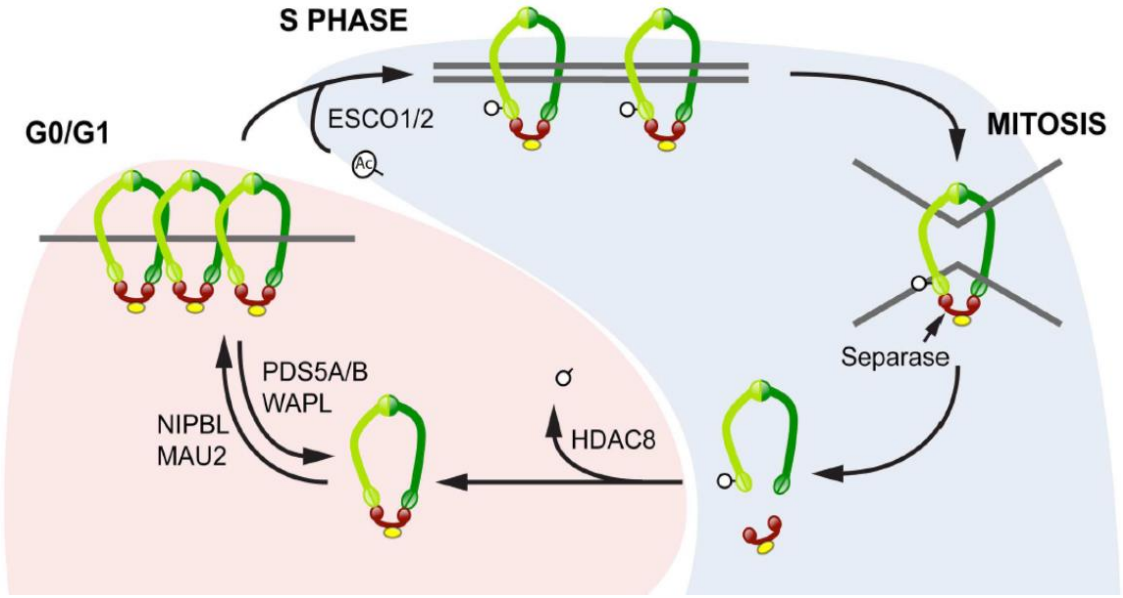

Figure 1.5: Regulation of the cohesin complex by HDAC8-mediated deacetylation of SMC3

Figure adapted from [67]. HDAC8-catalyzed deacetylation serves as a checkpoint for reassembly of the cohesin complex. A separase recognizes deacetylation of SMC3 and removes the RAD21 proteins from SMC1A and SMC3 followed by dissociation of the complex.

CdLS is a rare genetic disorder characterized by physical deformities and mental impairment. Multiple point mutations of HDAC8 have been discovered in infant CdLS patients since 2012[68]. Many of these mutations have been expressed in *E. coli*, with crystallographic studies (P91L, A188T, H180R, I243N, T311M, H334R, G320R, among others) and basic chemical characterization through circular dichroism of some mutants (H180R and G304R).[68] Additionally, many of these mutants displayed a noticeable decrease in HDAC8-catalyzed deacetylation using a commercially available methylcoumarin-bound substrate[68]. Finally, our laboratory has demonstrated that HDAC8 catalyzes deacetylation of an SMC3 peptide *in vitro*[50]. This thesis further explores changes in HDAC8-catalyzed deacetylation cause by each of these mutations.

Conclusions

Lysine acetylation/deacetylation is a dynamic, reversible post-translational modification with a defined role in histone modification and a growing pool of non-histone substrates that are critical for epigenetic regulation, DNA repair, cell cycle regulation and cancer growth and proliferation. The HDAC family of enzymes catalyzes deacetylation of both histone and non-histone proteins to maintain acetylation homeostasis that is critical for cell regulation and survival. Changes in acetylation patterns have become a key feature of various types of cancer and many of these acetylation level changes are due to increased expression and/or misregulation of HDACs. Due to the link between HDACs and cancer prognosis and survival, these enzymes have become an attractive target for drug development, as shown by the development and FDA-approval of pan-HDAC inhibitors and current development of novel immune-and oncolytic virus therapies. To further our understanding of the cellular function of HDACs, huge strides are currently

being made in discovering HDAC specific binding partners and substrates using a variety of methods, from gene knockouts and mass spectrometric-proteomic techniques to *in vivo* mammalian cell work. The current body of literature on HDACs has shed light on the multiple roles these enzymes perform in both transcriptional regulation and in protein-protein interactions, particularly with respect to their roles in disease, including multiple cancers, developmental disorders, and many others.

We predict that future work will incorporate varied approaches, such as mass spectrometry, co-immunoprecipitation, *in vivo* perturbation, *in vitro* functional studies, *etc.,* to advance our understanding of the cellular role of each isozyme. Understanding the specificity of each HDAC will provide further insight into their individual roles in the regulation of cellular pathways and various other disease states.

This thesis outlines the following investigations: an alternative method for identifying HDAC8 substrates in cell lysates using non-natural amino acid photo crosslinking and validation of these new substrates. An *in vitro* kinetic evaluation of HDAC8 point mutations found in the Cornelia de Lange Spectrum disorders and their effect on deacetylation, and the evaluation of HDAC8-catalyzed deacetylation using various divalent metal ions in order to determine the metal-dependent substrate specificity of HDAC8. Overall, the work presented in this thesis will provide insight into the substrate pool, regulation and role of HDAC8 in the cell.

Bibliography

(1) Parbin, S., Kar, S., Shilpi, A., Sengupta, D., Deb, M., Rath, S. K., and Patra, S. K. (2014) Histone deacetylases: a saga of perturbed acetylation homeostasis in cancer. *J. Histochem. Cytochem. 62*, 11–33.

(2) Verdin, E., and Ott, M. (2014) 50 years of protein acetylation: from gene regulation to epigenetics, metabolism and beyond. *Nat. Rev. Mol. Cell Biol. 16*, 258–64.

(3) Caron, C., Boyault, C., and Khochbin, S. (2005) Regulatory cross-talk between lysine acetylation and ubiquitination: role in the control of protein stability. *Bioessays 27*, 408–15.

(4) Glozak, M. A., Sengupta, N., Zhang, X., and Seto, E. (2005) Acetylation and deacetylation of non-histone proteins. *Gene 363*, 15–23.

(5) Khoury, G. A., Baliban, R. C., and Floudas, C. A. (2011) Proteome-wide post-translational modification statistics: frequency analysis and curation of the swiss-prot database. *Sci. Rep. 1*.

(6) Halkidou, K., Gaughan, L., Cook, S., Leung, H. Y., Neal, D. E., and Robson, C. N. (2004) Upregulation and nuclear recruitment of HDAC1 in hormone refractory prostate cancer. *Prostate 59*, 177–89.

(7) Zhang, Z., Yamashita, H., Toyama, T., Sugiura, H., Omoto, Y., Ando, Y., Mita, K., Hamaguchi, M., Hayashi, S. I., and Iwase, H. (2004) HDAC6 expression is correlated with better survival in breast cancer. *Clin. Cancer Res.*

(8) Wilson, A. J., Byun, D.-S., Popova, N., Murray, L. B., L'Italien, K., Sowa, Y., Arango, D., Velcich, A., Augenlicht, L. H., and Mariadason, J. M. (2006) Histone deacetylase 3 (HDAC3) and other class I HDACs regulate colon cell maturation and p21 expression and are deregulated in human colon cancer. *J. Biol. Chem. 281*, 13548–58.

(9) Deardorff, M. A., Bando, M., Nakato, R., Watrin, E., Itoh, T., Minamino, M., Saitoh, K., Komata, M., Katou, Y., Clark, D., Cole, K. E., De Baere, E., Decroos, C., Di Donato, N., Ernst, S., Francey, L. J., Gyftodimou, Y., Hirashima, K., Hullings, M., Ishikawa, Y., Jaulin, C., Kaur, M., Kiyono, T., Lombardi, P. M., Magnaghi-Jaulin, L., Mortier, G. R., Nozaki, N., Petersen, M. B., Seimiya, H., Siu, V. M., Suzuki, Y., Takagaki, K., Wilde, J. J., Willems, P. J., Prigent, C., Gillessen-Kaesbach, G., Christianson, D. W., Kaiser, F. J., Jackson, L. G., Hirota, T., Krantz, I. D., and Shirahige, K. (2012) HDAC8 mutations in Cornelia de Lange syndrome affect the cohesin acetylation cycle. *Nature 489*, 313–7.

(10) Jia, H., Morris, C. D., Williams, R. M., Loring, J. F., and Thomas, E. A. (2015) HDAC inhibition imparts beneficial transgenerational effects in Huntington's disease mice via altered DNA and histone methylation. *Proc. Natl. Acad. Sci. 112*, E56–E64.

(11) Khan, A. N. H., Magner, W. J., and Tomasi, T. B. (2007) An epigenetic vaccine model active in the prevention and treatment of melanoma. *J. Transl. Med. 5*, 64.

(12) Gallagher, S., Tiffen, J., and Hersey, P. (2015) Histone Modifications, Modifiers and

Readers in Melanoma Resistance to Targeted and Immune Therapy. *Cancers (Basel). 7*, 1959–1982.

(13) Haberland, M., Montgomery, R. L., and Olson, E. N. (2009) The many roles of histone deacetylases in development and physiology: implications for disease and therapy. *Nat. Rev. Genet. 10*, 32–42.

(14) Mottamal, M., Zheng, S., Huang, T. L., and Wang, G. (2015) Histone deacetylase inhibitors in clinical studies as templates for new anticancer agents. *Molecules 20*, 3898–941.

(15) Poole, R. M. (2014) Belinostat: first global approval. *Drugs 74*, 1543–54.

(16) Fenichel, M. P. (2015) FDA approves new agent for multiple myeloma. *J. Natl. Cancer Inst. 107*, djv165.

(17) Cao, K., Wang, G., Li, W., Zhang, L., Wang, R., Huang, Y., Du, L., Jiang, J., Wu, C., He, X., Roberts, A. I., Li, F., Rabson, A. B., Wang, Y., and Shi, Y. (2015) Histone deacetylase inhibitors prevent activation-induced cell death and promote anti-tumor immunity. *Oncogene 34*, 5960–70.

(18) Gantt, S. M. L., Decroos, C., Lee, M. S., Gullett, L. E., Bowman, C. M., Christianson, D. W., and Fierke, C. A. (2016) General Base-General Acid Catalysis in Human Histone Deacetylase 8. *Biochemistry*.

(19) Gantt, S. L., Joseph, C. G., and Fierke, C. A. (2009) Activation and Inhibition of Histone Deacetylase 8 by Monovalent Cations. *J. Biol. Chem. 285*, 6036–6043.

(20) Smith, B. C., and Denu, J. M. (2009) Chemical mechanisms of histone lysine and arginine modifications. *Biochim. Biophys. Acta 1789*, 45–57.

(21) Waltregny, D., Glénisson, W., Tran, S. L., North, B. J., Verdin, E., Colige, A., and Castronovo, V. (2005) Histone deacetylase HDAC8 associates with smooth muscle alpha-actin and is essential for smooth muscle cell contractility. *FASEB J. 19*, 966–8.

(22) Gao, L., Cueto, M. A., Asselbergs, F., and Atadja, P. (2002) Cloning and functional characterization of HDAC11, a novel member of the human histone deacetylase family. *J. Biol. Chem. 277*, 25748–55.

(23) Sullivan, E. D. (2016) Unlocking an HDAC Toolbox: Methods towards understanding isozyme-specific activity. University of Michigan.

(24) Spiegel, S., Milstien, S., and Grant, S. (2012) Endogenous modulators and pharmacological inhibitors of histone deacetylases in cancer therapy. *Oncogene 31*, 537–51.

(25) Balasubramanian, S., Ramos, J., Luo, W., Sirisawad, M., Verner, E., and Buggy, J. J. (2008) A novel histone deacetylase 8 (HDAC8)-specific inhibitor PCI-34051 induces apoptosis in T-cell lymphomas. *Leukemia 22*, 1026–34.

(26) Adams, H., Fritzsche, F. R., Dirnhofer, S., Kristiansen, G., and Tzankov, A. (2010) Class I histone deacetylases 1, 2 and 3 are highly expressed in classical Hodgkin's

lymphoma. *Expert Opin. Ther. Targets 14*, 577–84.

(27) Gao, L., and Alumkal, J. (2010) Epigenetic regulation of androgen receptor signaling in prostate cancer. *Epigenetics 5*, 100–4.

(28) Senese, S., Zaragoza, K., Minardi, S., Muradore, I., Ronzoni, S., Passafaro, A., Bernard, L., Draetta, G. F., Alcalay, M., Seiser, C., and Chiocca, S. (2007) Role for histone deacetylase 1 in human tumor cell proliferation. *Mol. Cell. Biol. 27*, 4784–95.

(29) Pulukuri, S. M. K., Gorantla, B., and Rao, J. S. (2007) Inhibition of histone deacetylase activity promotes invasion of human cancer cells through activation of urokinase plasminogen activator. *J. Biol. Chem. 282*, 35594–603.

(30) Joshi, P., Greco, T. M., Guise, A. J., Luo, Y., Yu, F., Nesvizhskii, A. I., and Cristea, I. M. (2013) The functional interactome landscape of the human histone deacetylase family. *Mol. Syst. Biol. 9*, 672.

(31) Santoro, F., Botrugno, O. A., Dal Zuffo, R., Pallavicini, I., Matthews, G. M., Cluse, L., Barozzi, I., Senese, S., Fornasari, L., Moretti, S., Altucci, L., Pelicci, P. G., Chiocca, S., Johnstone, R. W., and Minucci, S. (2013) A dual role for Hdac1: oncosuppressor in tumorigenesis, oncogene in tumor maintenance. *Blood 121*, 3459–68.

(32) Lagger, S., Meunier, D., Mikula, M., Brunmeir, R., Schlederer, M., Artaker, M., Pusch, O., Egger, G., Hagelkruys, A., Mikulits, W., Weitzer, G., Muellner, E. W., Susani, M., Kenner, L., and Seiser, C. (2010) Crucial function of histone deacetylase 1 for differentiation of teratomas in mice and humans. *EMBO J. 29*, 3992–4007.

(33) Dovey, O. M., Foster, C. T., Conte, N., Edwards, S. A., Edwards, J. M., Singh, R., Vassiliou, G., Bradley, A., and Cowley, S. M. (2013) Histone deacetylase 1 and 2 are essential for normal T-cell development and genomic stability in mice. *Blood 121*, 1335–44.

(34) Heideman, M. R., Wilting, R. H., Yanover, E., Velds, A., de Jong, J., Kerkhoven, R. M., Jacobs, H., Wessels, L. F., and Dannenberg, J.-H. (2013) Dosage-dependent tumor suppression by histone deacetylases 1 and 2 through regulation of c-Myc collaborating genes and p53 function. *Blood 121*, 2038–50.

(35) Yao, Y.-L., and Yang, W.-M. (2003) The metastasis-associated proteins 1 and 2 form distinct protein complexes with histone deacetylase activity. *J. Biol. Chem. 278*, 42560–8.

(36) Krusche, C. A., Wülfing, P., Kersting, C., Vloet, A., Böcker, W., Kiesel, L., Beier, H. M., and Alfer, J. (2005) Histone deacetylase-1 and -3 protein expression in human breast cancer: a tissue microarray analysis. *Breast Cancer Res. Treat. 90*, 15–23.

(37) Jung, K. H., Noh, J. H., Kim, J. K., Eun, J. W., Bae, H. J., Xie, H. J., Chang, Y. G., Kim, M. G., Park, H., Lee, J. Y., and Nam, S. W. (2012) HDAC2 overexpression confers oncogenic potential to human lung cancer cells by deregulating expression of apoptosis and cell cycle proteins. *J. Cell. Biochem. 113*, 2167–77.

(38) Ropero, S., Fraga, M. F., Ballestar, E., Hamelin, R., Yamamoto, H., Boix-Chornet, M., Caballero, R., Alaminos, M., Setien, F., Paz, M. F., Herranz, M., Palacios, J., Arango,

D., Orntoft, T. F., Aaltonen, L. A., Schwartz, S., and Esteller, M. (2006) A truncating mutation of HDAC2 in human cancers confers resistance to histone deacetylase inhibition. *Nat. Genet. 38*, 566–9.

(39) Inoue, S., Mai, A., Dyer, M. J. S., and Cohen, G. M. (2006) Inhibition of histone deacetylase class I but not class II is critical for the sensitization of leukemic cells to tumor necrosis factor-related apoptosis-inducing ligand-induced apoptosis. *Cancer Res. 66*, 6785–92.

(40) Zimmermann, S., Kiefer, F., Prudenziati, M., Spiller, C., Hansen, J., Floss, T., Wurst, W., Minucci, S., and Göttlicher, M. (2007) Reduced body size and decreased intestinal tumor rates in HDAC2-mutant mice. *Cancer Res. 67*, 9047–54.

(41) Atsumi, A., Tomita, A., Kiyoi, H., and Naoe, T. (2006) Histone deacetylase 3 (HDAC3) is recruited to target promoters by PML-RARalpha as a component of the N-CoR co-repressor complex to repress transcription in vivo. *Biochem. Biophys. Res. Commun. 345*, 1471–80.

(42) Jiao, F., Hu, H., Yuan, C., Jin, Z., Guo, Z., Wang, L., and Wang, L. (2014) Histone deacetylase 3 promotes pancreatic cancer cell proliferation, invasion and increases drug-resistance through histone modification of P27, P53 and Bax. *Int. J. Oncol. 45*, 1523–30.

(43) Fritzsche, F. R., Weichert, W., Röske, A., Gekeler, V., Beckers, T., Stephan, C., Jung, K., Scholman, K., Denkert, C., Dietel, M., and Kristiansen, G. (2008) Class I histone deacetylases 1, 2 and 3 are highly expressed in renal cell cancer. *BMC Cancer 8*, 381.

(44) Sun, Z., Feng, D., Fang, B., Mullican, S. E., You, S.-H., Lim, H.-W., Everett, L. J., Nabel, C. S., Li, Y., Selvakumaran, V., Won, K.-J., and Lazar, M. A. (2013) Deacetylase-independent function of HDAC3 in transcription and metabolism requires nuclear receptor corepressor. *Mol. Cell 52*, 769–82.

(45) Gantt, S. L., Gattis, S. G., and Fierke, C. A. (2006) Catalytic activity and inhibition of human histone deacetylase 8 is dependent on the identity of the active site metal ion. *Biochemistry 45*, 6170–8.

(46) Dowling, D. P., Gattis, S. G., Fierke, C. A., and Christianson, D. W. (2010) Structures of metal-substituted human histone deacetylase 8 provide mechanistic inferences on biological function . *Biochemistry 49*, 5048–56.

(47) Yang, X.-J., and Seto, E. (2008) The Rpd3/Hda1 family of lysine deacetylases: from bacteria and yeast to mice and men. *Nat. Rev. Mol. Cell Biol. 9*, 206–18.

(48) Oehme, I., Deubzer, H. E., Wegener, D., Pickert, D., Linke, J.-P., Hero, B., Kopp-Schneider, A., Westermann, F., Ulrich, S. M., von Deimling, A., Fischer, M., and Witt, O. (2009) Histone deacetylase 8 in neuroblastoma tumorigenesis. *Clin. Cancer Res. 15*, 91–9.

(49) Rettig, I., Koeneke, E., Trippel, F., Mueller, W. C., Burhenne, J., Kopp-Schneider, A., Fabian, J., Schober, A., Fernekorn, U., von Deimling, A., Deubzer, H. E., Milde, T., Witt, O., and Oehme, I. (2015) Selective inhibition of HDAC8 decreases neuroblastoma growth in vitro and in vivo and enhances retinoic acid-mediated differentiation. *Cell Death Dis. 6*,

e1657.

(50) Olson, D. E., Udeshi, N. D., Wolfson, N. A., Pitcairn, C. A., Sullivan, E. D., Jaffe, J. D., Svinkina, T., Natoli, T., Lu, X., Paulk, J., McCarren, P., Wagner, F. F., Barker, D., Howe, E., Lazzaro, F., Gale, J. P., Zhang, Y.-L., Subramanian, A., Fierke, C. A., Carr, S. A., and Holson, E. B. (2014) An unbiased approach to identify endogenous substrates of “histone” deacetylase 8. *ACS Chem. Biol. 9*, 2210–6.

(51) Grozinger, C. M., Hassig, C. A., and Schreiber, S. L. (1999) Three proteins define a class of human histone deacetylases related to yeast Hda1p. *Proc. Natl. Acad. Sci. U. S. A. 96*, 4868–73.

(52) Wang, A. H., Bertos, N. R., Vezmar, M., Pelletier, N., Crosato, M., Heng, H. H., Th’ng, J., Han, J., and Yang, X. J. (1999) HDAC4, a human histone deacetylase related to yeast HDA1, is a transcriptional corepressor. *Mol. Cell. Biol. 19*, 7816–27.

(53) Dequiedt, F., Kasler, H., Fischle, W., Kiermer, V., Weinstein, M., Herndier, B. G., and Verdin, E. (2003) HDAC7, a thymus-specific class II histone deacetylase, regulates Nur77 transcription and TCR-mediated apoptosis. *Immunity 18*, 687–98.

(54) Morin, R. D., Mendez-Lago, M., Mungall, A. J., Goya, R., Mungall, K. L., Corbett, R. D., Johnson, N. A., Severson, T. M., Chiu, R., Field, M., Jackman, S., Krzywinski, M., Scott, D. W., Trinh, D. L., Tamura-Wells, J., Li, S., Firme, M. R., Rogic, S., Griffith, M., Chan, S., Yakovenko, O., Meyer, I. M., Zhao, E. Y., Smailus, D., Moksa, M., Chittaranjan, S., Rimsza, L., Brooks-Wilson, A., Spinelli, J. J., Ben-Neriah, S., Meissner, B., Woolcock, B., Boyle, M., McDonald, H., Tam, A., Zhao, Y., Delaney, A., Zeng, T., Tse, K., Butterfield, Y., Birol, I., Holt, R., Schein, J., Horsman, D. E., Moore, R., Jones, S. J. M., Connors, J. M., Hirst, M., Gascoyne, R. D., and Marra, M. A. (2011) Frequent mutation of histone-modifying genes in non-Hodgkin lymphoma. *Nature 476*, 298–303.

(55) Han, A., He, J., Wu, Y., Liu, J. O., and Chen, L. (2005) Mechanism of recruitment of class II histone deacetylases by myocyte enhancer factor-2. *J. Mol. Biol. 345*, 91–102.

(56) Vannini, A., Volpari, C., Gallinari, P., Jones, P., Mattu, M., Carfí, A., De Francesco, R., Steinkühler, C., and Di Marco, S. (2007) Substrate binding to histone deacetylases as shown by the crystal structure of the HDAC8–substrate complex. *EMBO Rep. 8*, 879–884.

(57) Liu, H., Hu, Q., Kaufman, A., D’Ercole, A. J., and Ye, P. (2008) Developmental expression of histone deacetylase 11 in the murine brain. *J. Neurosci. Res. 86*, 537–43.

(58) Villagra, A., Cheng, F., Wang, H.-W., Suarez, I., Glozak, M., Maurin, M., Nguyen, D., Wright, K. L., Atadja, P. W., Bhalla, K., Pinilla-Ibarz, J., Seto, E., and Sotomayor, E. M. (2009) The histone deacetylase HDAC11 regulates the expression of interleukin 10 and immune tolerance. *Nat. Immunol. 10*, 92–100.

(59) Deubzer, H. E., Schier, M. C., Oehme, I., Lodrini, M., Haendler, B., Sommer, A., and Witt, O. (2013) HDAC11 is a novel drug target in carcinomas. *Int. J. Cancer 132*, 2200–2208.

(60) Glozak, M. A., and Seto, E. (2009) Acetylation/deacetylation modulates the stability

of DNA replication licensing factor Cdt1. *J. Biol. Chem. 284*, 11446–53.

(61) Woods, D., Woan, K., Wang, D., Yu, Y., Powers, J., Sahakian, E., Cheng, F., Wang, H., Rock-Klotz, J., Villagra, A., Pinilla-Ibarz, J., Yu, X.-Z., and Sotomayor, E. (2013) Histone deacetylase 11 is an epigenetic regulator of cytotoxic T-lymphocyte effector function and memory formation (P1404). *J. Immunol. 190*, 117.2.

(62) Gregoretti, I. V, Lee, Y.-M., and Goodson, H. V. (2004) Molecular evolution of the histone deacetylase family: functional implications of phylogenetic analysis. *J. Mol. Biol. 338*, 17–31.

(63) Dowling, D. P., Gantt, S. L., Gattis, S. G., Fierke, C. A., and Christianson, D. W. (2008) Structural studies of human histone deacetylase 8 and its site-specific variants complexed with substrate and inhibitors. *Biochemistry 47*, 13554–63.

(64) Haberland, M., Mokalled, M. H., Montgomery, R. L., and Olson, E. N. (2009) Epigenetic control of skull morphogenesis by histone deacetylase 8. *Genes Dev. 23*, 1625–1630.

(65) Wilson, B. J., Tremblay, A. M., Deblois, G., Sylvain-Drolet, G., and Giguère, V. (2010) An acetylation switch modulates the transcriptional activity of estrogen-related receptor alpha. *Mol. Endocrinol. 24*, 1349–1358.

(66) Gao, J., Siddoway, B., Huang, Q., and Xia, H. (2009) Inactivation of CREB mediated gene transcription by HDAC8 bound protein phosphatase. *Biochem. Biophys. Res. Commun. 379*, 1–5.

(67) Horsfield, J. A., Print, C. G., and Mönnich, M. (2012) Diverse Developmental Disorders from The One Ring: Distinct Molecular Pathways Underlie the Cohesinopathies. *Front. Genet. 3*, 171.

(68) Decroos, C., Christianson, N. H., Gullett, L. E., Bowman, C. M., Christianson, K. E., Deardorff, M. A., and Christianson, D. W. (2015) Biochemical and Structural Characterization of HDAC8 Mutants Associated with Cornelia de Lange Syndrome Spectrum Disorders. *Biochemistry 54*, 6501–6513.

Chapter 2

Identification of Novel HDAC8 Substrates Using Chemical Covalent Capture[‡,§]

Overview

Lysine acetylation is a reversible, dynamic post-translational modification that has been observed in a variety of processes such as chromatin remodeling[1], protein-protein interactions, protein stability and protein-DNA interactions, among others[2].There are two families of enzymes that regulate this reversible reaction: the lysine acetyltransferases (KATs), which are responsible for catalyzing the addition of the acetyl group from acetyl-CoA and the histone deacetylases (HDACs), which catalyze removal of the acetyl group. The HDAC family is divided into two groups: NAD-dependent sirtuins (class III) and metal-dependent deacetylases. Metal-dependent deacetylases can be further categorized into three subclasses: Class I (HDACs 1, 2, 3, and 8), class II (HDACs 4, 5, 6, 7, 9, and 10) and class IV (HDAC 11) based on their sequence homology to yeast orthologs[3]. Acetylation was first observed in histone tails[1]. However, recent experimental and computational studies have demonstrated that acetylation also occurs on non-histone

[‡] Reproduce, in part, from a manuscript in preparation: Lopez, J. E.; Haynes, S.; Majmudar, J.D.; Martin, B. R.; Fierke, C. A., Identification of novel HDAC8 substrates using Chemical Covalent Capture. *In preparation.*

[§] Jeffrey E. Lopez performed the HDAC8 mutant purifications, incorporation verification, activity testing, covalent capture assays, western blotting, proteomics stringency analysis, and full Michaelis-Menten kinetics of selected peptides screened and analyzed all the data. Sarah Haynes performed optimized proteomics analysis for each HDAC8 mutant. Jaimeen Majmudar performed and optimized the initial screens for proteomic analysis. Jeffrey E. Lopez, Sarah E. Haynes, Jaimeen D. Majmudar, Brent R. Martin and Carol A. Fierke designed the experiments and analyzed the data. Jeffrey E. Lopez, Sarah Haynes, Brent R. Martin, and Carol A. Fierke wrote the manuscript.

proteins[4], and identification of endogenous HDAC substrates is an important goal in the HDAC field.

Recent efforts have profiled the metal-dependent HDAC interactome via affinity purification proteomics, particularly using HDAC-eGFP fusion proteins combined with information on potential localization[5]. These data provide insight into stable protein-protein interactions of HDAC isozymes, either via direct contact or in a complex. However, they likely do not provide an accurate depiction of transient HDAC interactions and the fusion protein may potentially hinder interactions with larger binding partners and substrates[5]. Therefore, traditional immunoprecipitation methods have proven insufficient for the characterization of the complete cohort of native HDAC substrates. Since acetylation is a highly regulated and dynamic process, it is likely that many HDAC-substrate interactions are transient in nature and thus, there is a need to develop methods capable of capturing these HDAC-substrate interactions. Ideally, newly developed methods should require a small surface area to capture interactions while simultaneously being compatible with current mass spectrometry and proteomic approaches.

HDAC8, the best structurally characterized isozyme of the class I subfamily of deacetylases[6–8] and has been crystallized with a wide variety of ligands and peptides, yet the substrate pool for this isozyme remains largely unknown[9]. This makes HDAC8 an ideal enzyme for developing new methods for HDAC-substrate identification. To date, only two HDAC8 substrates had been identified and validated *in vivo*: estrogen-related receptor alpha (ERR-α), and the structural maintenance of chromosomes 3 (SMC3). ERR-α was identified as an HDAC8 substrate through *in vivo* co-transfection and *in vitro* radiolabeling and deacetylation assays[10]. SMC3 is part of the cohesin complex

responsible for the separation of sister chromatids in the cell, and it was identified as an HDAC8 substrate through the discovery that HDAC8 missense mutations and lack of SMC3 deacetylation are correlated in clinical patients. These mutations have been implicated in various phenotypes related to the Cornelia de Lange Spectrum disorders and has become the best validated *in vivo* HDAC8 substrate to date[11–13]. Finally, a recent SILAC study discovered several putative substrates using an HDAC8-specific inhibitor, namely AT-rich interactive domain-containing protein 1A (ARID1A), cysteine-rich protein2-binding protein (CSRP2BP), nuclear receptor coactivator 3 (NCOA3), among others[14].

Here, we report an alternative method for the identification of potential HDAC8 substrates using chemical covalent capture, where the photoreactive non-natural amino acid *p*-benzoyl-l-phenylalanine (Bpa) is used to capture protein-protein interactions, which are then analyzed using mass spectrometry. Non-natural amino acid incorporation has shown to efficiently trap protein-protein interactions with transcriptional activators *in vivo*[15]. We demonstrate that this approach also successfully captured transient HDAC8-protein interactions, identifying more than 100 proteins that interact with HDAC8. The majority of these proteins have been previously identified as being acetylated *in vivo.* We validated reactivity with HDAC8 of several of these potential substrates using small acetylated peptide mimics with an acetate coupled assay[16]. We demonstrated that these peptides possess catalytic activity higher than those measured for a peptide substrate based on an acetylated lysine on SMC3 (SMC3 K_{106}), the best validated HDAC8 substrate.

Materials and Methods

Materials.

Unless specified, chemicals and supplies were purchased from Fisher or Sigma. All chemicals were purchased at the highest quality available. Chromatography resins were purchased from GE Healthcare.

Expression of HDAC8-Bpa Mutants

Site-directed mutagenesis for amber codon incorporations (TAG) for Y100 (TAT), I94 (AAT) and F191 (TTT) of the pHD2-TEV-His HDAC8 plasmid were conducted using a QuikChange kit (Stratagene)[7]. Incorporation of desired mutations was confirmed by DNA sequencing (University of Michigan Sequencing Core). For incorporation of the non-natural amino acid, *p*-benzoyl-l-phenylalanine, into HDAC8, a vector (pEVOL) containing evolved *Methanocaldococcus jannaschii* aminoacyl-tRNA synthetases/suppressor tRNA pairs was purchased from AddGene[17]. Recombinant HDAC8-Bpa variants at positions Y100, I94 or F191 were expressed in BL21(DE3) *Escherichia coli* cells according to a previously published procedure[7], with small modifications. Briefly, cells were plated on LB media plates with 100 μg/mL ampicillin and 34 μg/mL chloramphenicol. Then a single colony was used to inoculate 50 mL cultures (2xYT media supplemented with 100 μg/mL ampicillin and 34 μg/mL chloramphenicol) that were grown overnight. These cultures were used to inoculate 4 liters of media per each mutant (2xYT media supplemented with 100 μg/mL ampicillin and 34 μg/mL chloramphenicol). Cells were grown at 37°C until OD_{600} reached 0.4 - 0.6, at which point the temperature was lowered to 20°C. After 1 hour, cells were induced by the addition of 0.5 mM isopropyl-β-D-thiogalactopyranoside

(IPTG), 0.2% w/v L-arabinose and 200 μM $ZnSO_4$, and grown overnight at 20°C. Cells were harvested by centrifugation (4000 x g, 15 min, 4°C). The cells were resuspended in buffer A (30 mM HEPES pH 8.0, 150 mM NaCl, 1 mM imidazole, 1 mM TCEP and 5 mM KCl with 1 protease inhibitor cocktail tablet per 50 mL of buffer (Roche Diagnostics)).

Purification of HDAC8-Bpa Variants.

Cells were lysed using a microfluidizer (Microfluidics) followed by centrifugation (27,000 x g, 45 min, 4°C). The cleared lysate was applied to $NiSO_4$-charged immobilized Sepharose fast flow metal affinity column and then eluted with a gradient of increasing imidazole concentration (25 - 200 mM imidazole in 30 mM HEPES pH 8.0, 150 mM NaCl. 1 mM TCEP and 5 mM KCl). HDAC8-Bpa mutants were then dialyzed overnight at 4°C against 25 mM MOPS pH 7.5, 1 mM EDTA, 1 mM TCEP and 5 mM KCl to remove any trace metals and then dialyzed again overnight at 4°C against 25 mM MOPS, pH 7.5, 1 mM TCEP and 5 mM KCl to ensure complete trace metal removal. HDAC8-Bpa mutants were concentrated to 150 - 300 μM and stored at -80°C. Bpa incorporation was verified by mass spectrometric analysis using an Agilent Q-TOF (Time-Of-Flight) HPLC-MS (University of Michigan)

Enzyme Activity Assay.

Before assaying, zinc was bound to the enzyme by incubation of apo-HDAC8-Bpa (10 μM) with atomic absorption zinc standard (Fluka) at a stoichiometric ratio on ice for 1 hour prior to dilution into the assay. The catalytic activity of HDAC8-Bpa variants was measured using the Fluor-de-Lys tetrapeptide assay substrate Ac-Arg-His-Lys(ac)-Lys(ac)-aminomethylcoumarin (Enzo Life Sciences). Deacetylation of the substrate by

HDAC8 is followed by the cleavage of the amide bond linking the C-terminal aminomethylcoumarin to the peptide backbone by a protease developer, resulting in a fluorescence shift. Activity assays were run at 30°C in assay buffer (25 mM HEPES pH 7.8, 137 mM NaCl, 3 mM KCl) that contained 100 μM peptide with 1 μM HDAC8-Bpa variant. The ratio of product fluorescence (ex. = 340 nm, em. = 450 nm) divided by the substrate fluorescence (ex. = 340 nm, em. = 380 nm) increases with product concentration. The initial rate was determined using the ratio of product formed over time. The catalytic efficiency ($k_{cat}/K_{M,app}$) was determined from dividing the initial rate by enzyme concentration.

Cell Culture and Treatment.

HEK293 cells (ATCC) were grown, expanded in DMEM medium from the same frozen vial stock and adhere into 75 cm^2 flasks in DMEM medium (~ 6 million cell/plate, 10 mL per plate). Prior to crosslinking, cells were detached by incubation with 0.05% Trypsin followed by neutralization with DMEM medium. The cells were sonicated (1-3 minutes, 10% duty cycle), centrifuged (17000 x g, 25 minutes) resuspended in 1 mL of phosphate buffer saline (PBS), aliquoted and stored at -80 °C.

Conjugation of Magnetic Beads.

Pierce™ Anti-6xHIS Epitope tag monoclonal antibodies (Thermo Scientific) (100 μg/mL) were coupled to M-270 epoxy Dynabeads (Invitrogen) using an optimized version of the suggested protocol. Briefly, magnetic beads (5 mg/pulldown) were washed twice with 1 mL of 0.1 M sodium phosphate buffer (pH 7.4) for a period of 10 minutes between washes. The buffer was removed and the beads resuspended with anti-6xHIS antibody

(100 µg of antibody/5 mg of beads) followed by addition of 0.1 M sodium phosphate buffer to bring the volume to 200 µL. After mixing, 100 µL of 3 M ammonium sulfate were added to bring the total volume to 300 µL. The beads were then incubated for 16-24 hours at 37°C. Finally, beads were washed with PBS prior to addition of the crosslinking samples.

HDAC8 Chemical Covalent Capture Assay.

HDAC8-Bpa variants were thawed and diluted in PBS (pH 7.4) to a concentration of 40 µM and kept on ice. 10 aliquots of HEK293 cells were thawed, resuspended and lysed in 800 µL of PBS using sonication and lysates were centrifuged (27,000 x g, 15 minutes, 4°C) to remove insoluble material. Cell lysate protein concentrations were measured using a bicinchoninic acid (BCA) protein assay (Thermo-Scientific)[18]. HDAC8-Bpa variant was mixed with HEK293 lysate to a final volume of 140 µL (HDAC8-Bpa = [5 µM]). Samples were incubated at 4°C for 15 minutes and then either irradiated using an ultraviolet light lamp (Thermo Scientific) at a wavelength of 365 nm (115 volts, 60 Hz) for 20-30 minutes or kept in the dark for the non-UV control samples. The crosslinked and non-crosslinked samples were then added to the beads and incubated for 1-2 hours with rotation at 4°C.

Western Blotting.

Samples from HEK293 lysates, UV-crosslinking assays and elutions from the Dynabeads were collected. Gel electrophoresis was performed using Mini-PROTEAN TGX 12% gels (Bio-Rad). Proteins were transferred to a nitrocellulose membrane and probed using anti-6xHIS epitome tag monoclonal antibodies (Fisher) and a mouse anti-HDAC8 monoclonal antibodies (Santa Cruz Biotech). The membrane was then probed

with either a secondary HRP-linked antibody and chemiluminescence induced by subsequent incubation with a HRP substrate (Santa Cruz Biotech) for the anti-6xHIS epitome tag antibody or by an anti-mouse Alexa Fluor® 633 antibody (Innovagen). Visualization was done using a C600 Series imager (Azure Biosystems) and visualized using ImageJ (NIH).

Proteomics.

Beads containing both HDAC8-Bpa crosslinked and non-crosslinked samples were washed twice with ice-cold PBS (pH 7.4) and resuspended in ice-cold 6 M urea. Protein samples were incubated with 10 mM dithiothreitol for 30 minutes at 37 ˚C followed by alkylation using 55 mM iodoacetamide for 30 minutes at 25˚C in the dark. Samples were diluted to 1 M urea using PBS and digested overnight by incubation with sequencing-grade Trypsin/Lys-C (Promega). Peptide samples were desalted using Oasis HLB Prime µElution C18 solid-phase extraction cartridges (Waters) following the manufacturer's protocol. Desalted peptides were reconstituted in water with 3% acetonitrile, 0.1% formic acid and 10 fmol/µL yeast alcohol dehydrogenase digest (Waters) as an internal standard. In triplicate, peptides were analyzed in positive mode on a Synapt G2-S HDMS traveling wave ion mobility time-of-flight (TOF) mass spectrometer (Waters). Reversed-phase liquid chromatography and data-independent acquisition were performed as previously described[19]. Peptide identification and label-free protein quantitation were performed with Progenesis QI for Proteomics 2.0.5 (Nonlinear Dynamics) against a database of the human proteome (downloaded from UniProt on February 2, 2016). Peptide and protein identifications were made using the following criteria: tryptic cleavage rules with one missed cleavage allowed,

carbamidomethyl cysteine as a fixed modification and methionine oxidation as a variable modification, a minimum of two identified fragment ions per peptide and a minimum of five fragments per protein, and at least two identified peptides per protein. The global false discovery rate (FDR) for protein identification was set at 1% using a reversed database. Peptide identifications with a calculated mass error greater than 10 ppm were not considered. Fold-change, p-value (equation 2.1) and number of unique peptides were used to rank the confidence of hits.

$$t = \frac{\bar{x}_1 - \bar{x}_2}{\sqrt{\frac{s_1^2}{n_1} + \frac{s_2^2}{n_2}}} \qquad (Equation\ 2.1)$$

Peptide Identification and Screening of Acetyl Lysine Positions.

Proteins identified through peptide fragments were screened for potential acetylated lysine positions using PhosphoSite Plus. These acetylated lysine positions were then evaluated using the Rosetta Flex-Pep-Bind structure-based protocol tailored to HDAC8[20]. Acetylated lysine residues with the highest overall algorithm score were considered as the best candidates for *in vitro* peptide testing. A library of 58 peptides based on identified proteins from all of the HDAC8-Bpa mutant crosslink experiments was purchased. Peptides varied in length to enhance water solubility using a peptide solubility calculator provided by Innovagen[21].

HDAC8-Peptide Activity.

Desalted peptides (>75% purity) were purchased from Synthetic Biomolecules with an acetylated N-terminus, an amidated C-terminus and a single acetylated lysine. Peptides were resuspended in water unless otherwise specified. Peptide concentrations were measured using a micro-bicinchoninic acid (micro-BCA) protein assay (Thermo-Scientific). Recombinant wild-type HDAC8 was purified from *E. coli*[7]. HDAC8 assays were performed using an enzyme-coupled assay to measure acetate production[16]. Reactions were performed using a standard HDAC reaction buffer (25 mM HEPES pH 7.8, 137 mM NaCl, 3 mM KCl at 30°C). Reactions measuring deacetylation of acetylated peptides (12.5 - 100 μM) were initiated by the addition of recombinant Zn(II)-HDAC8 (1 μM). The reactions were quenched with 10% HCl, and the acetate product, as reflected by an increase in NADH fluorescence, was measured at 5 time points (up to 50 min) and used to calculate the initial rates. Steady state kinetic parameters *(k_{cat}, K_M,* and *k_{cat}/K_M)* were calculated by fitting either the Michaelis-Menten equation or a line, where deemed appropriate, to the substrate concentration dependence of the initial rate.

Results and Discussion

Site-directed incorporation of Bpa identifies a variety of HDAC8 interactions.

To facilitate covalent capture, incorporation of a non-natural amino acid photo-crosslinker was carried out using amber stop codon nonsense suppression in *E. coli*[17]. To trap interactions based on protein proximity, all mutations were designed such that the incorporated Bpa is expected to be solvent and surface exposed. Furthermore, positions for incorporation were chosen based on their distance to the active site, and preliminary

data of using covalent capture with Rpd3, the yeast ortholog of HDAC8[22]. Ultimately, Bpa was incorporated at three positions: Y100, I94 and F191 (Figure 2.1A). Substitutions of Bpa at these three sites decreased values of *k*cat/K_M for deacetylation of the Fluor-de-Lys coumarin-labeled tetrapeptide by values of 2-fold (Y100) to 7-fold (I94)

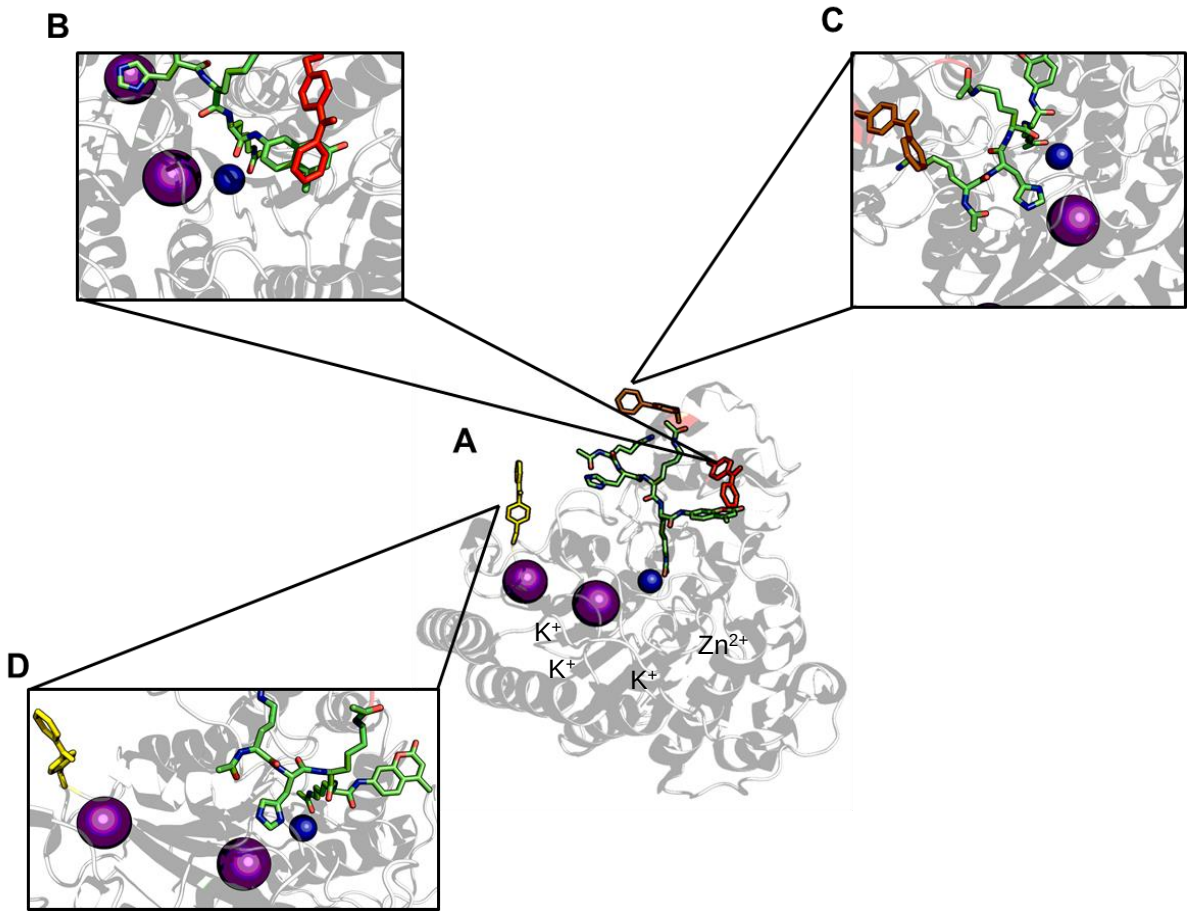

Figure 2.1: HDAC8 Bpa mutations

(A) Incorporation positions of Bpa on HDAC8. Positions were chosen based on proximity to the tethered peptide that is bound. (B) Y100 - this residue substitution is in close proximity to the active site binding surface and appears to interact with the bound peptide. (C) I94 - this residue substitution is located in the L2 loop, a region hypothesized to aid in the binding of peptide substrate to the active site surface. (D) F191 - this residue substitution is located 20 ˚A away from the active site metal and was used to explore potential, non-active binding site interactions of proteins with HDAC8. PDB: 2V5W

Specifically, Y100 was selected as a site for Bpa incorporation to capture substrates due to: an immediate proximity to the active site tunnel with potential interactions with the methylcoumarin moiety (Figure 2.1B). The methylcoumarin-HDAC interaction has demonstrated a modest effect of enhancement on overall catalytic turnover[6] consistent with our measurements of the activity of the Y100Bpa variant. Crosslinking with I94 was of interest because it is positioned on the L2 loop of HDAC8, a primarily disordered loop in the crystal structures HDAC8•peptide complexes which has been proposed to aid in substrate binding and release[6,9,23,24] (Figure 2.1C). This substitution had the largest effect on catalytic activity. Finally, F191 is located 24 A° away from the active site tunnel (Figure 2.1D). This position was selected as a control to try to distinguish between protein substrates and protein interaction partners. Identification of proteins that interact with HDAC8 at sites other than the active site will provide insight into protein binding partners that could affect HDAC8 function and specificity. Incorporation of Bpa at these three, independent positions resulted in the covalent capture of previously unidentified protein substrates that provide insight into the HDAC8 protein substrate pool and the role of HDAC8 in cellular homeostasis.

For the covalent capture experiments, HDAC8-Bpa variants were incubated with HEK293 lysate, irradiated using an ultraviolet light lamp (+UV samples), immunoprecipitated, proteolyzed and the crosslinked proteins identified by LC-MS/MS analysis of peptides (Figure 2.2). Control samples were prepared identically without irradiation (-UV samples).

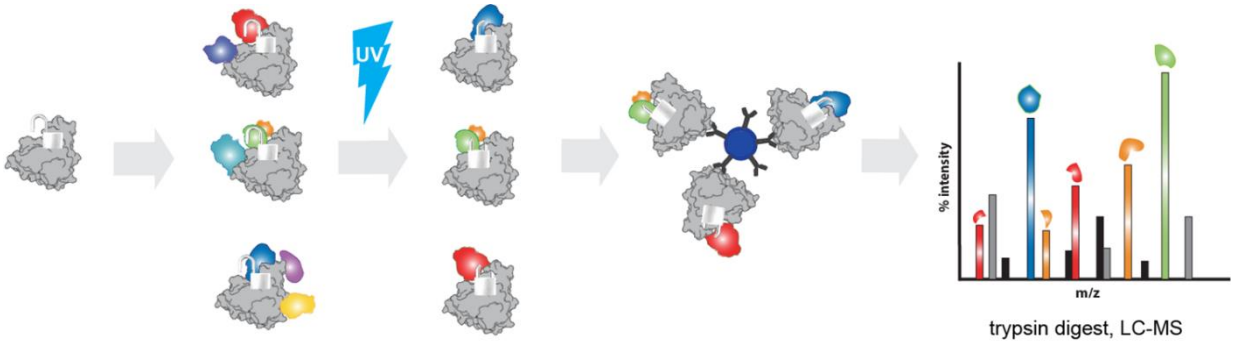

Figure 2.2: Scheme of Chemical Covalent Capture using HDAC8.

Recombinant HDAC8-Bpa mutants were added to HEK293 lysate and incubated on ice. Potential HDAC8-substrate interactions were covalently captured by activating Bpa using UV light. Conjugation to an α-6HIS antibody coupled to magnetic beads was done immediately post-covalent capture. Co-immunoprecipitation and verification via Western Blots were done simultaneously, followed by mass spectrometry and proteomic analysis in order to identify new HDAC8 substrates.

We verified covalent capture for each mutant by western blot (Figure 2.3). We used a mouse anti-HDAC8 monoclonal antibody as a primary antibody (Santa Cruz Biotech) followed by an anti-mouse Alexa Fluor® 633 antibody (Innovagen). We saw that irradiated samples possess multiple, heavier molecular weight bands above the recombinant HDAC8-Bpa bands, indicating the covalent capture of higher molecular weight proteins. The resulting data set led to identification of a large number of unique proteins (Table 2.2 and Figure 2.5). HDAC8 with a Bpa substitution at Y100 captured the largest number of different proteins (452), likely due to the proximity to the active site tunnel. Fewer proteins were identified for the I94Bpa variant (123), possibly due to the decreased catalytic activity. Finally, the F191Bpa variant yielded the fewest number of unique proteins captured (45) out of all three variants, suggesting both that less proteins interact with this region of HDAC8.

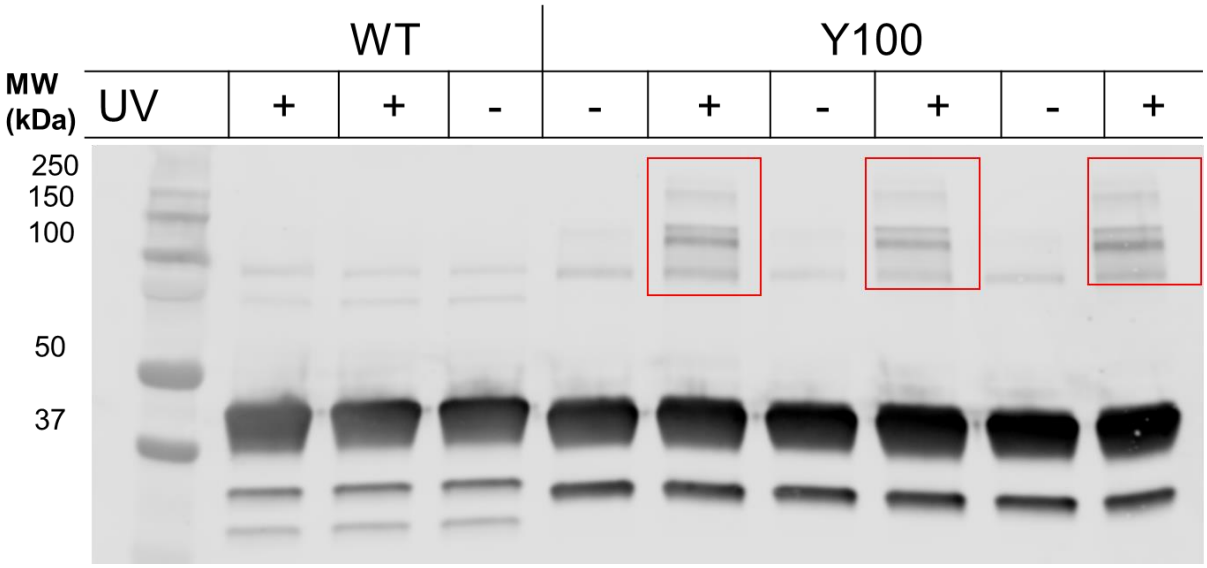

Figure 2.3: HDAC8-Bpa covalent capture western blot

Western blot of recombinant HDAC8-Bpa mutants with HEK293 lysate after UV exposure. The membrane was blotted with an anti-HDAC8 monoclonal antibody and an anti-mouse Alexa Fluor® 633 secondary antibody. We observed higher molecular weight bands in UV exposed samples, suggesting that covalent capture occurred in these samples. Western blots were performed in triplicate.

The resulting data sets for -UV (N = 3 biological replicates) and +UV (N = 3 biological replicates) samples were compiled and the identified proteins for each HDAC8-Bpa variant were subject to stringent cutoffs per the following criteria (Figure 2.4): (i) proteins showed an overall fold enrichment (+UV/-UV) of ≥ 2.5-fold for; (ii) a *t*-test between UV and non-UV treated data sets for each protein generated a *p*-value of ≤ 0.05; and (iii) at least two peptide fragments per protein were identified. These stringency cutoffs significantly reduce (by 3- to 22-fold) the number of specific HDAC8-protein interactions identified for all three mutants, with the largest differential being the p-value score. Furthermore, the increased stringency severely reduced the number of proteins identified that crosslinked to more than one of the Bpa variants, suggesting that some of

the initially identified proteins in these categories made nonspecific interactions. It is possible that some protein substrates that have long-lived, stable interactions with HDAC8, such as those identified in previous proteomic studies[5,14], were deleted using these cutoffs if they are abundant in both +UV and -UV samples. In particular, two substrates that form stable complexes with HDAC8, namely ERR-α and SMC3, were identified in the original pool of proteins for the Y100Bpa variant but were removed by the cutoffs as the +UV/-UV ratio was not larger than 2.5.

These criteria identified new potential protein substrates based on their capture efficiency, statistical fidelity and enrichment. The Y100Bpa exhibited the highest number of proteins after undergoing stringent cutoffs, and ≥ 90% of proteins captured by this mutant exhibit multiple acetylation sites based on the Phosphosite Plus database. These results suggest that the proteins that formed crosslinks with Y100Bpa are likely substrates. This covalent capture proteomics reveal a vast network of previously identified interacting proteins of HDAC8 as well as a large subset of newly identified interacting proteins (Appendix A).

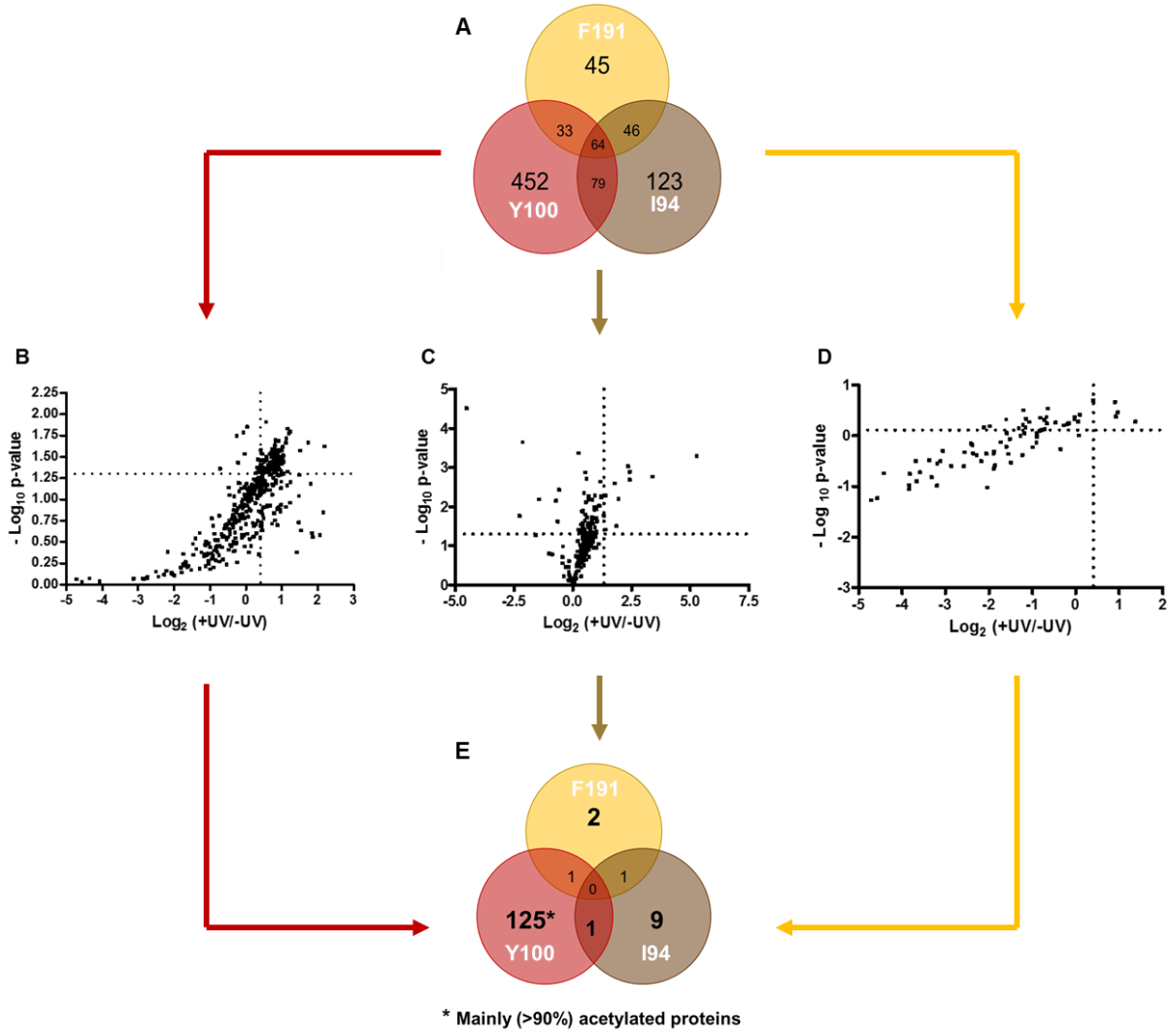

Figure 2.4: Evaluation and stringency cutoffs of HDAC8 Chemical Covalent Capture

(A) Total enrichment of proteins covalently captured with each HDAC8-Bpa mutants along with common proteins between all mutants. (B-D) Volcano plots of Y100Bpa, I94Bpa and F191Bpa; each mutant was subject to the same stringency cutoffs: fold enrichment (+UV/-UV) ≥ 2.5, p-value of ≤ 0.05 and a minimum of two peptide IDs per protein ID. (E) Enrichment after stringency for each HDAC8-Bpa variant. The Y100Bpa exhibited the highest number of proteins after stringent cutoffs,and ≥ 90% of proteins captured by this mutant exhibit multiple acetylation sites based on the Phosphosite Plus database.

HDAC8 testing reveals high turnover of *novel* peptide substrates.

To further investigate whether the identified proteins are likely HDAC8 substrates we measured the reactivity of HDAC8 with peptides containing acetylated lysine residues taken from the 135 proteins that remained after applying our stringency cutoffs (Table 2.1).

Table 2.1 - Proteins identified through HDAC8 covalent capture after cutoffs

Protein ID	UV/No UV FC	p-value (UV/No UV)	# peptides ID
SYAC	24.311	0.024	2
PGAM4	7.266	0.027	5
SYEP	5.163	0.016	4
H14	4.968	0.017	5
COPA	4.577	0.020	8
SYQ	4.544	0.022	2
LARP1	4.254	0.037	4
PDLI1	4.206	0.031	3
ACTN2	4.191	0.032	11
DHX9	4.158	0.024	5
RL7A	4.131	0.050	10
ESYT1	4.095	0.036	6
LPPRC	4.093	0.032	18
HSP72	4.065	0.027	53
PSA	4.031	0.039	23
ITB1	4.025	0.038	7
CAPR1	4.002	0.033	5
LRC47	3.976	0.047	2
MSH2	3.960	0.036	3
TIF1B	3.939	0.036	21
CDK1	3.937	0.052	5
EIF3B	3.929	0.027	7
VPS35	3.924	0.026	4
UBA1	3.879	0.036	46
DPP3	3.779	0.027	9
RENT1	3.766	0.026	10
NCAP	3.766	0.044	2
HS90B	3.758	0.037	87
SFPQ	3.757	0.035	13
ACTN1	3.736	0.021	16

ENPL	3.724	0.038	51
KINH	3.713	0.027	19
C1TC	3.704	0.033	36
HNRL1	3.702	0.040	2
RBBP7	3.662	0.045	4
MCM6	3.649	0.042	10
PARP1	3.639	0.031	32
EZRI	3.622	0.030	26
HS105	3.619	0.033	19
PSMD2	3.616	0.034	8
TPIS	3.609	0.026	21
CLH1	3.597	0.027	45
ACLY	3.584	0.036	20
GANAB	3.562	0.031	27
P5CS	3.556	0.037	11
EIF3C	3.528	0.045	9
AT1A1	3.508	0.034	19
CAND1	3.507	0.026	24
DDB1	3.484	0.028	5
CPSF6	3.477	0.021	6
CSDE1	3.473	0.033	5
HSPB1	3.462	0.060	3
1433B	3.456	0.065	10
IPO7	3.451	0.027	3
PSD12	3.451	0.020	5
ACON	3.440	0.048	3
ACTN4	3.422	0.032	35
EF2	3.402	0.040	93
HNRPU	3.396	0.045	22
COPB2	3.395	0.023	9
ADH1YEAST	3.382	0.048	59
TERA	3.380	0.044	34
HXK1	3.367	0.026	6
AINX	3.361	0.044	3
XRCC5	3.359	0.033	20
STRAP	3.343	0.047	4
TNPO1	3.340	0.043	8
SAE2	3.324	0.036	4
MCM7	3.319	0.030	12
SND1	3.314	0.042	17
VINC	3.299	0.034	40
GLRX3	3.267	0.028	11
HS90A	3.266	0.037	92

GBLP	3.253	0.070	6
LAP2B	3.252	0.042	8
MYH9	3.248	0.028	63
MYH14	3.234	0.044	16
MCM5	3.201	0.036	11
VDAC1	3.194	0.029	10
ACOT9	3.169	0.026	7
SF01	3.148	0.028	7
DHX15	3.140	0.041	6
STX11	3.137	0.029	4
MIC60	3.129	0.038	8
IPYR	3.127	0.039	6
DHE3	3.123	0.032	12
COPG1	3.104	0.044	8
AXA2L	3.099	0.052	21
U5S1	3.070	0.043	18
PDIP2	3.052	0.029	2
EF1B	3.050	0.045	2
NUCL	3.044	0.043	43
AIP	3.017	0.040	3
DDX17	3.009	0.040	29
RIR1	2.996	0.037	10
FUS	2.954	0.047	5
PRDX1	2.905	0.040	4
UBQL1	2.880	0.046	2
NSUN2	2.868	0.033	9
FUBP1	2.854	0.035	13
IMB1	2.852	0.044	25
PHB2	2.843	0.032	18
ACTZ	2.804	0.012	5
ROA1	2.776	0.046	7
EIF3A	2.740	0.044	24
STAU1	2.732	0.049	4
PYGL	2.720	0.044	8
FETUA	2.701	0.043	8
SETP9	2.688	0.037	5
G3PT	2.679	0.000	2
HSP74	2.672	0.044	22
PCBP1	2.662	0.035	11
GDIA	2.633	0.043	11
SRSF7	2.615	0.030	2
RL8	2.595	0.048	15
BACH	2.595	0.035	4

ANXA2	2.570	0.040	25
HS74L	2.547	0.046	10
LDHC	2.544	0.044	3
PRS10	2.539	0.027	3
KCRB	2.504	0.035	15
TBB2A	2.503	0.040	55
HUS1B	39.205	0.001	2
ADT1	10.596	0.002	7
S10A9	5.431	0.001	5
TXLNA	5.421	0.002	4
VDAC1;VDAC3	5.178	0.001	6
HS71L	3.914	0.007	5
COX41	3.654	0.032	2
RL3	3.486	0.003	18
PHB	2.678	0.040	10
PLMN	2.664	0.005	5
ROA1;RA1L2	3.911	0.001	3
IL6	3.745	0.005	3
TIAR	2.507	0.000	3

We used the HDAC8 Flex-Pep-Bind algorithm[20] to score potential binding and activity with each of the acetylated lysine residues identified in Phosphosite Plus database for each protein. We then purchased fifty-eight (58) short, synthetic peptides corresponding to the acetylated lysine sites with the highest algorithm score and the largest fold change (+UV/-UV ratio). The reactivity of zinc-bound HDAC8 with all water soluble potential peptide substrates (38 peptides) was measured using an acetate-coupled assay[16] with at least two concentrations of substrate (50, 100 μM or more) (Table 2.2). These data reveal that 30% of the peptides tested have values of $k_{cat}/K_M > 30\ M^{-1}s^{-1}$.

Table 2.2 - HDAC8 deacetylation screen of protein-based peptide substrates

Protein ID	UV/No UV ratio	Peptide score	Peptide sequence	$k_{cat}/K_{M\ (app)}$ ($M^{-1}s^{-1}$)
ACLY	3.95	-20.5	DHKQ(K-Ac)FYWGHK	220
HSP90AB1	4.15	-20.8	YK(K-Ac)FYE	155
HSP90AA1	3.59	-20.8	YK(K-Ac)FYE	155
ITGB1	4.44	-20.1	TL(K-Ac)FKR	70
PFKP	4.11	-18.3	HRIP(K-Ac)EQW	56
TUBA1A	5.2	-19.8	DH(K-Ac)FDL	40
PDLIM1	4.06	-14.6	GG(K-Ac)DFE	33
LARP1	4.65	-22.2	YV(K-Ac)RRR	33*
TRIM28	4.35	-17.3	RMF(K-Ac)QFNK	32
SLC25A4	10.59	-19.4	ET(K-Ac)YRW	30
UPF1	4.13	-16.3	RYKGDLAPLW(K-Ac)GIGHVIKVPD	30
COPA	5.05	N/A	DY(K-Ac)IKV	23
AARS	24.31	-17.6	FF(K-Ac)RNE	21*
SEC24C	4.72	-18.6	MH(K-Ac)EIR	21*
SFPQ	4.14	-19.5	EF(K-Ac)RLF	18*
VDAC1	3.43	-18	FF(K-Ac)GAW	17*
ACTIN1	4.13	-16.9	YG(K-Ac)LRK	17*
HIST1H1E	5.16	-18.2	AAL(K-ac)KAL	16*
KIF5B	4.07	-16.8	YE(K-Ac)EKE	16*
NPEPPS	4.45	-17.2	PE(K-Ac)KRP	15*
MSH2	4.37	-19.2	RIIL(K-Ac)ASRH	15*
VPS35	4.34	-15.8	GG(K-Ac)RVM	15*
EiF3B	4.33	-17.5	GE(K-Ac)FKQ	15*
CPNE3	3.44	-16.3	FH(K-Ac)QTSD	14*
QARS	4.54	-17.2	EPEPGF(K-Ac)RLAWGQ	12*
HSP90B1	4.11	-18.1	SQ(K-Ac)KTF	11*
MTHFD1	4.08	-15.9	TD(K-Ac)ALFNR	11*
PARP1	4	-18.6	LS(K-Ac)KSK	11*
PCBP1	2.66	-15.8	HG(K-Ac)EVG	10*
RPL3	3.48	-19.3	PL(K-Ac)KDR	8*
CAPRIN1	4.41	N/A	TY(K-Ac)VLK	8*
DPP3	4.17	N/A	AH(K-Ac)RGS	8*
EPRS	5.69	-18.1	EF(K-Ac)HPQ	7*
S100A9	5.43	-19.5	AH(K-Ac)KSH	5*
HSP90A1L	3.91	-18.7	EF(K-Ac)RKH	5*
HDLBP	7.84	N/A	KSQH(K-Ac)YVIPK	3*
ESYT1	4.51	-16.5	KGT(K-Ac)HLS	3*
UBA1	4.28	-18.5	VS(K-Ac)RKL	2*

***only tested as one concentration with HDAC8**

We then tested the peptides with k_{cat}/K_M values higher than 30 $M^{-1}s^{-1}$ using various peptide concentrations. In fact, eight peptides have k_{cat}/K_M values for deacetylation of acetylated peptides that are comparable to or faster than the values for SMC3-based peptides[14] (Figure 2.5B) where SMC3 is the best validated *in vivo* HDAC8 substrate. This set included peptides from proteins identified in previous proteomic studies as HDAC8-specific or pan-HDAC interacting proteins, including heat shock protein 90 (HSP90AB1)[25], tubulin 1-alpha (TUBA1A)[26] and transcription intermediary factor beta (TRIM28)[27]. Excitingly, this analysis also validated new putative HDAC8 protein substrates such as ATP-citrate lyase (ACLY), integrin beta-1 (ITGB1), 6-phosphofructokinase (PFKP), PDZ and LIM domain protein 1 (PDLIM1), and the regulator of nonsense transcripts (UPF1). The highly reactive peptides from ACLY (240 ± 55 $M^{-1}s^{-1}$), ITGB1 (435 ± 150 $M^{-1}s^{-1}$), UPF1 (350 ± 130 $M^{-1}s^{-1}$) and PFKP (106 ± 48 $M^{-1}s^{-1}$) suggest that these proteins are particularly interesting to study further as biological substrates of HDAC8.

The HDAC8-catalyzed deacetylation of peptides from proteins previously observed in proteomic studies and novel proteins provide evidence that this covalent capture approach can be used to identify novel deacetylase targets. Additionally, the Y100 amino acid is conserved in multiple metal-dependent deacetylases (i.e. HDAC6, HDAC7 and HDAC10) so that this experiment could be repeated with little optimization for these isozymes. Many of the putative HDAC8 substrates are involved in a wide variety

of cellular processes, such as metabolism, cell differentiation and DNA repair suggesting that HDAC8 could have different roles depending on its cellular localization (Figure 2.5A).

A

Peptide Deacetylation Assay (in vitro)					
Protein	**Ac-Sequence-NH_2**	**Position of Ac**	**k_{cat}/K_M (M^{-1} s^{-1})**	**Localization**	**Function**
HSP90AB1	YKK$_{ac}$FYE	K428	120 ± 40	Cytoplasm/Nucleus	Protein Folding
ACLY	DHKQK$_{ac}$FYWGHK	K540	240 ± 55	Cytoplasm	Metabolism
TUBA1A	DHK$_{ac}$FDL	K394	60 ± 13	Cytoplasm/Nucleus	Mitosis
ITGB1	TLK$_{ac}$FKR	K134	435 ± 150	Cytoplasm/Membrane	Cell Differentiation and Adhesion
PFKP	HRIPK$_{ac}$EQW	K747	128 ± 110	Cytoplasm/Nucleus	Metabolism
UPF1	RYKGDLAPLWK$_{ac}$GIGHVIKVPD	K386	350 ± 130	Nucleus	DNA Repair
TRIM28	RMFK$_{ac}$QFNK	K770	70 ± 3	Nucleus	DNA Repair
PDLIM1	GGK$_{ac}$DFE	K22	106 ± 48	Cytoplasm/Cytoskeleton	Oxidative Stress
SMC3*	**RVIGAKK$_{ac}$DQY**	**K106**	**63 ± 11**	**Nucleus**	**Mitosis**

B

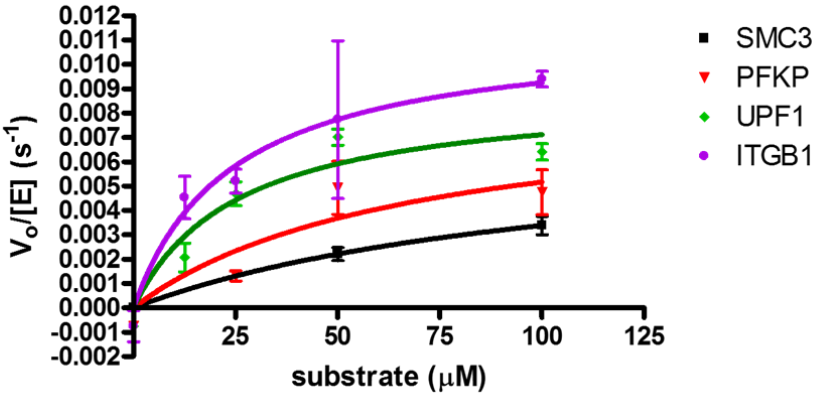

Figure 2.5: Representative putative substrates and peptide testing

(A) Localization, function and steady state parameters for the deacetylation of synthetic acetylated peptides corresponding to a subset of identified HDAC8 substrates. Reactions were catalyzed by Zn^{2+}-HDAC8. (B) Dependence of Zn^{2+}-HDAC8 catalyzed deacetylation on the concentration of PFKP, UPF1 and ITGB1 peptides and compared against an SMC3 synthetic peptide. The Michaelis-Menten equation is fit to the data.

Interestingly, some of these proteins, namely TUBA1A, ITGB1 and PDLIM1 are found in both the cytoplasm and bound to the cytoskeleton of the cell. HDAC8 has been visualized bound to the actin cytoskeleton in human smooth muscle cells and along siRNA knockouts of HDAC8 that have shown that they can significantly alter the cellular cytoskeleton[26] and has been hypothesized to regulate actin dynamics and cytoskeleton interactions through protein complex formation with HSP20, myosin heavy chain and cofilin[26, 28, 29]. However, neither HSP20 or cofilin have been observed as HDAC8 targets, and myosin associates better with HDAC8 in a non-acetylated form, suggesting that it is not an HDAC8 substrate[29]. The covalent capture results suggest that TUBA1A, ITGB1 and PDLIM1 might be the cytoskeletal targets of HDAC8. Additionally, our data suggests that HSP90 is a putative HDAC8 substrate. HSP90 has been proposed to play a role in modulating actin dynamics[30,25], thus making it another potential target for HDAC8 in the cytoskeleton. Consistent with this, a bacteria two-hybrid experiment indicated that HDAC8 interacts with HOP1, an adaptor protein linking HSP70 and HSP90[31].

The covalent capture and peptide reactivity data suggest that HDAC8 activity could regulate nonsense-mediated decay of mRNAs by catalyzing deacetylation of UPF1. UPF1 is recruited to mRNAs upon translation termination and plays a role in replication-dependent histone mRNA degradation[32,33]. Although UPF1 complex formation is regulated by phosphorylation, it is possible that HDAC8-catalyzed deacetylation regulates UPF1 function at certain times of the cell cycle, as hypothesized with SMC3 during mitosis[11].

Unexpectedly, these data suggest that HDAC8 might also act as a potential regulator of glycolysis, fatty acid biosynthesis and metabolites that are associated with

cancer (oncometabolite). Two of the proteins discovered in our screen, PFKP and ACLY, are involved in cell energy production and storage, respectively. PFKP is responsible for the first committed step in glycolysis, the phosphorylation of D-fructose 6-phosphate to fructose 1,6-bisphosphate while ACLY is responsible for converting citrate to acetyl-CoA, linking multiple metabolic and biosynthetic processes[34,35]. We hypothesize that metal dependent HDACs might play a larger role in cellular metabolic regulation than previously thought.

Finally, and consistent with previous *in vitro* peptide studies[24,36], it appears that a common motif for HDAC8 catalysis is the presence of aromatic residues, mainly phenylalanine and tyrosine, near the acetyllysine. Of the eight peptides with highest reactivity, six contain a phenylalanine at the -1 or -2 position. This motif might increase either binding affinity or reactivity, possibly similar to the observed interactions with the -1 coumarin moiety visualized in the HDAC8-peptide crystal structures[23,37,38]. The appearance of an aromatic residue downstream of the acetyllysine might be an indication of a biological substrate.

Conclusions

Overall, we have identified new potential HDAC8 substrates using chemical covalent capture coupled with proteomics and *in vitro* peptide validation. The protein-based peptides tested possess comparable deacetylation rates to an SMC3 peptide mimic, the best *in vivo* validated HDAC8 protein substrate. These newly identified proteins possess a diverse array of both nuclear and cytosolic functions; including cell regulation and homeostasis, chromatin and DNA remodeling and cell cytoskeleton regulation;

suggesting that HDAC8 might have a role in various cellular processes not investigated previously. This alternative approach provides a new strategy that could be useful for the identification of other HDAC isozyme substrates and provide a better understanding of how each HDAC is regulated through each of their specific and non-specific transient and long-lived interactions**.**

Bibliography

(1) Parbin, S., Kar, S., Shilpi, A., Sengupta, D., Deb, M., Rath, S. K., and Patra, S. K. (2014) Histone deacetylases: a saga of perturbed acetylation homeostasis in cancer. *J. Histochem. Cytochem. 62*, 11–33.

(2) Glozak, M. A., Sengupta, N., Zhang, X., and Seto, E. (2005) Acetylation and deacetylation of non-histone proteins. *Gene 363*, 15–23.

(3) Haberland, M., Montgomery, R. L., and Olson, E. N. (2009) The many roles of histone deacetylases in development and physiology: implications for disease and therapy. *Nat. Rev. Genet. 10*, 32–42.

(4) Khoury, G. A., Baliban, R. C., and Floudas, C. A. (2011) Proteome-wide post-translational modification statistics: frequency analysis and curation of the swiss-prot database. *Sci. Rep. 1*.

(5) Joshi, P., Greco, T. M., Guise, A. J., Luo, Y., Yu, F., Nesvizhskii, A. I., and Cristea, I. M. (2013) The functional interactome landscape of the human histone deacetylase family. *Mol. Syst. Biol. 9*, 672.

(6) Dowling, D. P., Gantt, S. L., Gattis, S. G., Fierke, C. A., and Christianson, D. W. (2008) Structural studies of human histone deacetylase 8 and its site-specific variants complexed with substrate and inhibitors. *Biochemistry 47*, 13554–63.

(7) Gantt, S. L., Gattis, S. G., and Fierke, C. A. (2006) Catalytic activity and inhibition of human histone deacetylase 8 is dependent on the identity of the active site metal ion. *Biochemistry 45*, 6170–8.

(8) Gantt, S. M. L., Decroos, C., Lee, M. S., Gullett, L. E., Bowman, C. M., Christianson, D. W., and Fierke, C. A. (2016) General Base-General Acid Catalysis in Human Histone Deacetylase 8. *Biochemistry*.

(9) Wolfson, N. A., Ann Pitcairn, C., and Fierke, C. A. (2013) HDAC8 substrates: Histones and beyond. *Biopolymers 99*, 112–26.

(10) Wilson, B. J., Tremblay, A. M., Deblois, G., Sylvain-Drolet, G., and Giguère, V. (2010) An acetylation switch modulates the transcriptional activity of estrogen-related receptor alpha. *Mol. Endocrinol. 24*, 1349–1358.

(11) Deardorff, M. A., Bando, M., Nakato, R., Watrin, E., Itoh, T., Minamino, M., Saitoh, K., Komata, M., Katou, Y., Clark, D., Cole, K. E., De Baere, E., Decroos, C., Di Donato, N., Ernst, S., Francey, L. J., Gyftodimou, Y., Hirashima, K., Hullings, M., Ishikawa, Y., Jaulin, C., Kaur, M., Kiyono, T., Lombardi, P. M., Magnaghi-Jaulin, L., Mortier, G. R., Nozaki, N., Petersen, M. B., Seimiya, H., Siu, V. M., Suzuki, Y., Takagaki, K., Wilde, J. J., Willems, P. J., Prigent, C., Gillessen-Kaesbach, G., Christianson, D. W., Kaiser, F. J., Jackson, L. G., Hirota, T., Krantz, I. D., and Shirahige, K. (2012) HDAC8 mutations in Cornelia de Lange syndrome affect the cohesin acetylation cycle. *Nature 489*, 313–7.

(12) Decroos, C., Christianson, N. H., Gullett, L. E., Bowman, C. M., Christianson, K. E.,

Deardorff, M. A., and Christianson, D. W. (2015) Biochemical and Structural Characterization of HDAC8 Mutants Associated with Cornelia de Lange Syndrome Spectrum Disorders. *Biochemistry 54*, 6501–6513.

(13) Decroos, C., Bowman, C. M., Moser, J. A. S., Christianson, K. E., Deardorff, M. A., and Christianson, D. W. (2014) Compromised structure and function of HDAC8 mutants identified in Cornelia de Lange Syndrome spectrum disorders. *ACS Chem. Biol. 9*, 2157–2164.

(14) Olson, D. E., Udeshi, N. D., Wolfson, N. A., Pitcairn, C. A., Sullivan, E. D., Jaffe, J. D., Svinkina, T., Natoli, T., Lu, X., Paulk, J., McCarren, P., Wagner, F. F., Barker, D., Howe, E., Lazzaro, F., Gale, J. P., Zhang, Y.-L., Subramanian, A., Fierke, C. A., Carr, S. A., and Holson, E. B. (2014) An unbiased approach to identify endogenous substrates of “histone” deacetylase 8. *ACS Chem. Biol. 9*, 2210–6.

(15) Dugan, A., Majmudar, C. Y., Pricer, R., Niessen, S., Lancia, J. K., Fung, H. Y.-H., Cravatt, B. F., and Mapp, A. K. (2016) Discovery of Enzymatic Targets of Transcriptional Activators via in Vivo Covalent Chemical Capture. *J. Am. Chem. Soc. 138*, 12629–35.

(16) Wolfson, N. A., Pitcairn, C. A., Sullivan, E. D., Joseph, C. G., and Fierke, C. A. (2014) An enzyme-coupled assay measuring acetate production for profiling histone deacetylase specificity. *Anal. Biochem. 456*, 61–69.

(17) Young, T. S., Ahmad, I., Yin, J. A., and Schultz, P. G. (2010) An Enhanced System for Unnatural Amino Acid Mutagenesis in E. coli. *J. Mol. Biol. 395*, 361–374.

(18) Smith, P. K., Krohn, R. I., Hermanson, G. T., Mallia, A. K., Gartner, F. H., Provenzano, M. D., Fujimoto, E. K., Goeke, N. M., Olson, B. J., and Klenk, D. C. (1985) Measurement of protein using bicinchoninic acid. *Anal. Biochem. 150*, 76–85.

(19) Hernandez, J. L., Davda, D., Majmudar, J. D., Won, S. J., Prakash, A., Choi, A. I., and Martin, B. R. (2016) Correlated S-palmitoylation profiling of Snail-induced epithelial to mesenchymal transition. *Mol. Biosyst. 12*, 1799–808.

(20) Alam, N., Zimmerman, L., Wolfson, N. A., Joseph, C. G., Fierke, C. A., and Schueler-Furman, O. (2016) Structure-Based Identification of HDAC8 Non-histone Substrates. *Structure 24*, 458–68.

(21) Innovagen. InC. Peptide solubility calculator.

(22) Wolfson, N. A., Lancia, J. K., Mapp, A. K., and Fierke, C. A. (2012) Unpublished data.

(23) Dowling, D. P., Gattis, S. G., Fierke, C. A., and Christianson, D. W. (2010) Structures of metal-substituted human histone deacetylase 8 provide mechanistic inferences on biological function . *Biochemistry 49*, 5048–56.

(24) Alam, N., Zimmerman, L., Wolfson, N. A., Joseph, C. G., Fierke, C. A., and Schueler-Furman, O. (2016) Structure-Based Identification of HDAC8 Non-histone Substrates. *Structure 24*, 458–468.

(25) Taiyab, A., and Rao, C. M. (2011) HSP90 modulates actin dynamics: inhibition of HSP90 leads to decreased cell motility and impairs invasion. *Biochim. Biophys. Acta*

1813, 213–21.

(26) Waltregny, D., Glénisson, W., Tran, S. L., North, B. J., Verdin, E., Colige, A., and Castronovo, V. (2005) Histone deacetylase HDAC8 associates with smooth muscle alpha-actin and is essential for smooth muscle cell contractility. *FASEB J. 19*, 966–8.

(27) Schultz, D. C., Friedman, J. R., and Rauscher, F. J. (2001) Targeting histone deacetylase complexes via KRAB-zinc finger proteins: the PHD and bromodomains of KAP-1 form a cooperative unit that recruits a novel isoform of the Mi-2alpha subunit of NuRD. *Genes Dev. 15*, 428–43.

(28) Waltregny, D., de Leval, L., Glénisson, W., Ly Tran, S., North, B. J., Bellahcène, A., Weidle, U., Verdin, E., and Castronovo, V. (2004) Expression of Histone Deacetylase 8, a Class I Histone Deacetylase, Is Restricted to Cells Showing Smooth Muscle Differentiation in Normal Human Tissues. *Am. J. Pathol. 165*, 553–564.

(29) Karolczak-Bayatti, M., Sweeney, M., Cheng, J., Edey, L., Robson, S. C., Ulrich, S. M., Treumann, A., Taggart, M. J., and Europe-Finner, G. N. (2011) Acetylation of Heat Shock Protein 20 (Hsp20) Regulates Human Myometrial Activity. *J. Biol. Chem. 286*, 34346–34355.

(30) Nishida, E., Koyasu, S., Sakai, H., and Yahara, I. (1986) Calmodulin-regulated binding of the 90-kDa heat shock protein to actin filaments. *J. Biol. Chem. 261*, 16033–16036.

(31) Lee, H., Sengupta, N., Villagra, A., Rezai-Zadeh, N., and Seto, E. (2006) Histone Deacetylase 8 Safeguards the Human Ever-Shorter Telomeres 1B (hEST1B) Protein from Ubiquitin-Mediated Degradation. *Mol. Cell. Biol. 26*, 5259–5269.

(32) Franks, T. M., Singh, G., and Lykke-Andersen, J. (2010) Upf1 ATPase-Dependent mRNP Disassembly Is Required for Completion of Nonsense- Mediated mRNA Decay. *Cell 143*, 938–950.

(33) Lykke-Andersen, J., Shu, M.-D., and Steitz, J. A. (2000) Human Upf Proteins Target an mRNA for Nonsense-Mediated Decay When Bound Downstream of a Termination Codon. *Cell 103*, 1121–1131.

(34) Hellinga, H. W., and Evans, P. R. (1987) Mutations in the active site of Escherichia coli phosphofructokinase. *Nature 327*, 437–439.

(35) ELSHOURBAGY, N. A., NEAR, J. C., KMETZ, P. J., WELLS, T. N. C., GROOT, P. H. E., SAXTY, B. A., HUGHES, S. A., FRANKLIN, M., and GLOGER, I. S. (1992) Cloning and expression of a human ATP-citrate lyase cDNA. *Eur. J. Biochem. 204*, 491–499.

(36) Gurard-Levin, Z. A., and Mrksich, M. (2008) The activity of HDAC8 depends on local and distal sequences of its peptide substrates. *Biochemistry 47*, 6242–50.

(37) Vannini, A., Volpari, C., Gallinari, P., Jones, P., Mattu, M., Carfí, A., De Francesco, R., Steinkühler, C., and Di Marco, S. (2007) Substrate binding to histone deacetylases as shown by the crystal structure of the HDAC8–substrate complex. *EMBO Rep. 8*, 879–884.

(38) Vannini, A., Volpari, C., Filocamo, G., Casavola, E. C., Brunetti, M., Renzoni, D., Chakravarty, P., Paolini, C., De Francesco, R., Gallinari, P., Steinkühler, C., and Di Marco, S. (2004) Crystal structure of a eukaryotic zinc-dependent histone deacetylase, human HDAC8, complexed with a hydroxamic acid inhibitor. *Proc. Natl. Acad. Sci. U. S. A. 101*, 15064–9.

Chapter 3

Effects of Cornelia de Lange Spectrum Mutations on HDAC8 Catalysis

Overview

Protein acetylation is an important, reversible post-translational modification that affects protein-DNA interactions, protein stability and protein-protein interactions[1]. Lysine acetyltransferases (KATs) catalyze the addition of an acetyl moiety to lysine residues and histone deacetylases (HDACs) catalyze removal of this group. The balance of activity from these two families of enzymes regulate the acetylation state of proteins involved in many cellular roles[2]. Aberrant acetylation, along with differential expression of various HDACs, has been observed in a variety of disease states[3–7]. Thus, it is important to discover not only the specificity of each HDAC isozyme, but also their downstream effects during the progression of diseases.

HDAC8, a class I isozyme, has been biochemically characterized in vitro[8–10]. However, its current cellular role is still under investigation. Identification of HDAC8 substrates has proven difficult at least partly due to lack of improved assay methods for measuring HDAC activity and substrate promiscuity between other HDACs.

Recent proteomic studies utilizing mass spectrometric approaches[11,12] have provided evidence for multiple potential HDAC8 substrates[12–14]. One of the best validated HDAC8 substrates discovered through these studies is the structural maintenance of

chromosomes 3 (SMC3)[6]. SMC3 is a component of the cohesin complex, which is a highly regulated multi-protein assembly that ensures cohesion and proper separation of sister chromatids during the cell cycle. The complex consists of four components: SMC1A, SMC3, RAD21 and STAG[15], which form a quaternary ring-like structure that is capable of encasing two sister chromatids at a time (Figure 3.1)[15,16]. SMC1A and SMC3 each contain a long, antiparallel coiled-coil that separates their hinge and ATPase domains. SMC1A and SMC3 associate through these hinge and ATPase domains and this complex is stabilized through the binding of RAD21. The last protein in the complex, STAG1/2, binds RAD21, further stabilizing the overall complex.

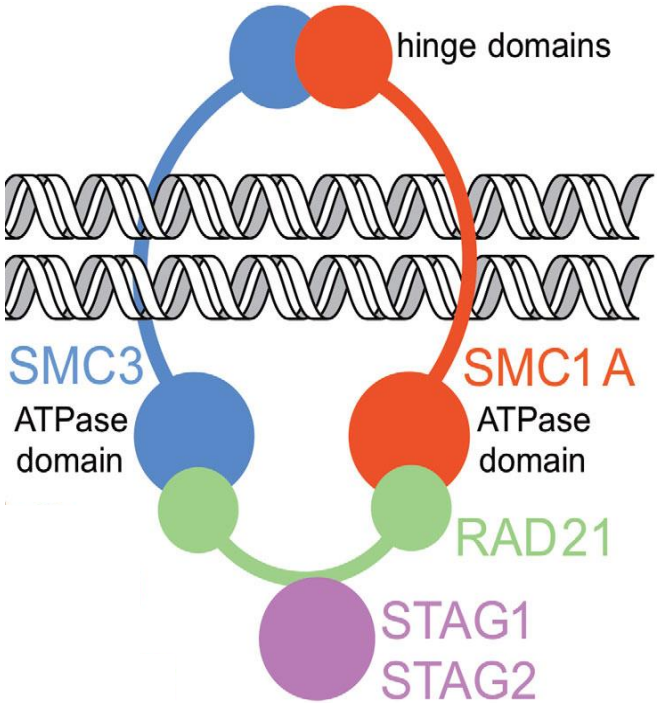

Figure 3.1 – Quaternary structure of the cohesin complex

Figure adapted from 33. The cohesin complex consists of four protein elements that encase sister chromatids during cell division: SMC1A, SMC3, RAD21 and STAG1/2. Post-translational modifications, such as acetylation, are important for the regulation and assembly of this quaternary complex.

Mutations in the genes that encode these core proteins have given rise to Cornelia de Lange spectrum (CdLS) disorders. CdLS disorders, also referred to as cohesinopathies, encompass a wide range of phenotypes characterized by skull and limb abnormalities, stunted physical growth, and mental disabilities typically coupled with cardiovascular and nervous system problems[17,18,19]. The prevalence of CdLS is very low, at an estimate of 1 – 2 individuals per 100,000 births[20].

It was recently discovered that additional proteins outside the cohesin complex, including HDAC8, play a critical role in regulating its function. Misregulation of these proteins can also lead to CdLS phenotypes[6]. Evidence suggests that cohesion of sister chromatids occurs in tandem with the acetylation of SMC3 at residues K105 and K106 catalyzed by the lysine acetyltransferases ESCO1 and ESCO2[21]. The acetylation of these residues blocks activity of one of the ATPase sites in the complex that normally facilitates ring opening[22]. Dissociation of the complex is initiated during the prophase and finalized during the anaphase[15]. The opening of the cohesin ring is required for the proper separation of sister chromatids. Current evidence suggests that HDAC8 catalyzes the deacetylation of K105 and K106 in SMC3, leading to dissociation of the complex.

To date, a total of 16 missense mutations have been identified in the gene encoding for HDAC8 in patients with CdLS conditions[6]. Many of these mutations have resulted in partial or complete loss of *in vitro* deacetylase activity. Ten of these HDAC8 mutants have been biochemically characterized with three dimensional crystal structures, thermostability measurements and basic biochemical assays using a methylcoumarin peptide[23,24].

In this study, we investigate the effects of three HDAC8 mutants (P91L, I243N, T311M) with varying deacetylase activities to further analyze the functional effects of the mutations including secondary structure, divalent metal ion affinity and catalytic activity using an SMC3-based peptide.

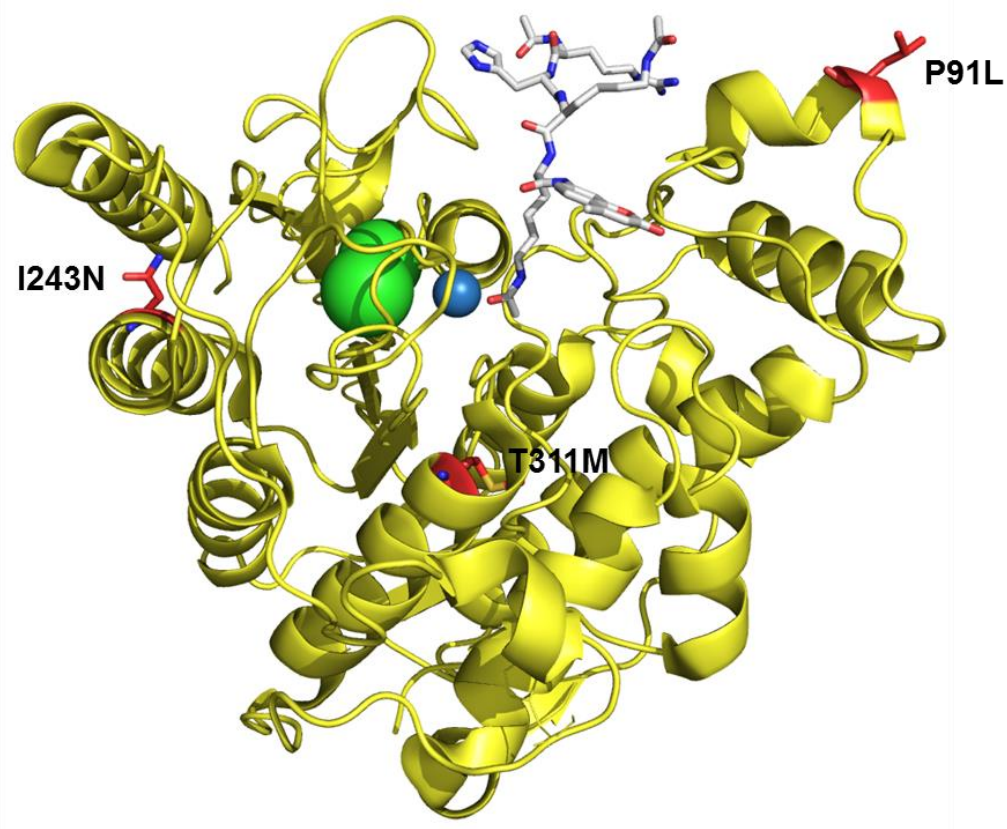

Figure 3.2 – Selected HDAC8 CdLS mutations

Single HDAC8 mutations used in this study are shown on the tertiary structure of HDAC8. These point mutations (PDB: 2v5w) were selected due to their previously reported wide range of effects on HDAC8 activity previously published[23,24].

Materials and Methods

Materials

Unless specified, chemicals and supplies were purchased from Sigma. All chemicals were purchased at the highest quality available. Chromatography resins were purchased from GE Healthcare.

HDAC8 Purification

Both HDAC8 WT and CdLS mutants (P91L, I243N and T311M) were prepared using the following method, modified from (8). HDAC8 mutants were constructed using PCR-based site directed mutagenesis to replace the wild-type (WT) codon at: Pro91 (CCG) with the codon for Leu (CTG); Ile243 (ATT) with the codon for Asn (AAC); and Thr311 (ACC) with the codon for Met (AUG). HDAC8-TEV-His6 was transformed into BL21-DE3 Z-competent cells, grown on LB/ampicilin media plates and then inoculated into 2xYT media supplemented with 100 µg/mL of ampicillin at 37°C at 170 RPM until OD_{600} = 0.4 - 0.7. The temperature was then decreased to 20°C for 45 – 60 minutes, followed by induction with isopropyl β-D-1-thiogalactopyranoside (IPTG) (0.5 mM) and addition of $ZnSO_4$ (0.2 mM). Cells were harvested 15 - 16 hours post-induction by centrifugation (4000 x g, 15 minutes, 4°C) and the pellets were resuspended in HDAC8 buffer A (30 mM HEPES pH 8.0, 150 mM NaCl, 1 mM imidazole, 1 mM TCEP, 5mM KCl) supplemented with a complete protease inhibitor cocktail tablet (Roche). Cell were lysed using a microfluidizer (Microfluidics) followed by centrifugation (27,000 x g, 45 minutes, 4°C). The cleared lysate was loaded onto a Ni^{2+}-charged chelating sepharose (GE Healthcare) gravity column equilibrated with HDAC8 buffer A. The column was washed

with 20 mM imidazole in buffer A and HDAC8 was eluted in a linear gradient using buffer B (30 mM HEPES pH 8.0, 150 mM NaCl, 200 mM imidazole, 1 mM TCEP, 5 mM KCl). The His6 tag was cleaved by addition of 1 mg/mL His6-tagged TEV protease during an overnight dialysis using HDAC8 buffer A without imidazole at 4°C. A second, stepwise-elution Ni^{2+}-charged column was used to separate HDAC8 from TEV protease. HDAC8 was eluted in the flow through and 20 mM imidazole step gradients. HDAC8 was concentrated in 10k or 30k MWCO Amicon Ultra centrifugal concentrators and dialyzed to remove metal using metal-free reagents (25 mM MOPS pH 7.5, 1 mM TCEP, 5 mM KCl and 1 mM EDTA). This was followed by multiple dialyses (25 mM MOPS pH 7.5, 1 mM TCEP, 5 mM KCl) to remove EDTA. HDAC8 was then aliquoted, flash frozen in liquid nitrogen and stored at -80°C. Concentration was measured by absorbance at 280 nm using the extinction coefficient of 52,120 $M^{-1}cm^{-1}$, which was determined previously[8].

HDAC8 CdLS activity with a Methylcoumarin labeled peptide

The catalytic activities of HDAC8 WT and CdLS mutants were measured using the Fluor de Lys tetrapeptide assay substrate Ac-Arg-His-Lys(ac)-Lys(ac)-aminomethylcoumarin (Enzo Life Sciences). Deacetylation of the substrate by HDAC8 is followed by the cleavage of the amino bond linking the C-terminal methylcoumarin to the peptide backbone catalyzed by trypsin, resulting in a fluorescence shift between the deacetylated product (ex. = 430 nm, em. = 450 nm) and the remaining substrate (ex. = 340 nm, em. = 380 nm). Fe^{2+} and Zn^{2+} were bound to apo-HDAC8 (10 μM) by incubation in a ratio of 5:1 and 1:1 metal: HDAC8, respectively, on ice for 1 hour prior to dilution into the assay. Activity assays were performed at 25°C in HDAC8 assay buffer (25 mM HEPES pH 7.8, 137 mM NaCl, 3 mM KCl). Zn^{2+}-HDAC8 CdLS mutants (1 μM) were measured

using 50 μM substrate and Fe^{2+}-HDAC8 CdLS mutants (1 μM) were measured using 100 μM substrate. The data were fit using a linear equation and k_{cat}/K_M was calculated from these data assuming a linear dependence on substrate concentration, as previously demonstrated for WT-HDAC8[8].

Measurement of Circular Dichroism (CD) of HDAC8 CdLS Mutants

The secondary structure for each HDAC8 CdLS mutant was measured using circular dichroism. HDAC8 CdLS mutants were reconstituted (5 μM) as apo-HDAC8 or at a molar ratio of 1:1 with Zn^{2+} in HDAC8 assay buffer (25 mM HEPES, pH 7.8, 137 mM NaCl, 3 mM KCl) for 1 hour on ice. CD measurements were carried out at a concentration of 5 μM for each mutant and performed using a JASCO J-1500 CD Spectrophotometer with a 0.1 cm path length cell. Spectra were acquired at 25 ℃ using a bandwidth of 2 nm, a scan rate of 100 nm/min and averaging spectra over 61 continuous scans.

Measurement of Metal (Zn^{2+}/Fe^{2+}) dissociation constants (K_D^{Me}) of CdLS Mutants

The affinities of HDAC8 CdLS mutants for Zn^{2+} and Fe^{2+} were measured using changes in anisotropy by coupling the binding of fluorescein-labeled suberoylanilide hydroxamic acid (fl-SAHA) to metal binding[25]. Fl-SAHA has a comparable binding affinity to both Zn^{2+}-HDAC8 and Fe^{2+}HDAC8 when compared to SAHA, thus we can monitor HDAC8 metal binding based on the concentrations of metal found in solution. These reactions were carried out in 1x assay buffer containing 50 nM fl-SAHA. Fluorescence anisotropy assays were performed in a half-area black 96-well microplate by monitoring the anisotropy signal of fluorescein (λ_{ex} = 485 nm and λ_{em} = 535 nm) using a TECAN plate reader. For metal affinity measurements, apo-HDAC8 WT and mutants (1 – 10 μM) were

incubated with 1 mM nitrolotriacetic acid (NTA), 137 mM NaCl, 3 mM KCl, 10 mM MOPS pH 7)[26], and either 0 – 0.5 mM Zn_{total} (0 – 3.3 nM Zn_{free}) or 0 – 950 μM Fe_{total} (0 – 2.6 μM Fe^{2+}_{free}) as calculated by MINEQL. The assay mixtures were incubated for 1 hour on ice in the anaerobic glove box for Fe^{2+} measurements and incubated for 10 – 30 minutes at RT for Zn^{2+} measurements, followed by addition of fl-SAHA and a 10-minute equilibration at 25 ˚C before measuring anisotropy signal. Zn^{2+} and Fe^{2+} K_D values were obtained by fitting a binding isotherm to the dependence of anisotropy on the concentration of free metal. Equation 3.1. which describes the change in anisotropy based on the concentration of metal bound, was fit to the curves.

$$\frac{FP}{\Delta FP} = \frac{X}{K_D * X} \qquad (Equation\ 3.1)$$

HDAC8 CdLS activity with a non-methylcoumarin SMC3 K_{106} based peptide.

SMC3 10-mer (Ac-RVIGAKK_{ac}DQY-NH_2) peptide (Synthetic Biomolecules) was purchased at > 95% purity and with an acetylated lysine corresponding to K_{106}. CdLS mutants were reconstituted with either Zn^{2+} or Fe^{2+} as described previously[8] with small modifications. Apo-HDAC8 (10 μM) was reconstituted with stoichiometric Zn^{2+} (Fluka) in peptide assay buffer (20-25 mM HEPES pH 8, 137 mM NaCl, 3 mM KCl) and incubated for 1 hour on ice. For Fe^{2+}-HDAC8, apo-HDAC8 was equilibrated on ice in an anaerobic glove box (Coy Laboratory Products) for one hour prior to reconstitution. Solid $FeCl_2$ (Sigma), L(+)-ascorbic acid (Fluka), and peptide assay buffer were equilibrated in the anaerobic chamber at least overnight before using. Fe^{2+} (100 μM) in 5 mM ascorbate and assay buffer was prepared daily. Fe^{2+}-HDAC8 (10 μM) was reconstituted anaerobically by incubating with 5-fold excess Fe^{2+} in assay buffer and 2.5 mM ascorbate for 1 hour in

a 0 – 4°C CoolBox (Biocision). Fe^{2+}-HDAC8 assays were performed anaerobically. The enzyme-coupled assay was performed as described[27]. Fe^{2+} and Zn^{2+}-HDAC8 CdLS mutants and peptides in assay buffer were independently equilibrated at 30 °C for 15 minutes prior to reaction initiation. Reactions were initiated by the addition of enzyme (WT and P91L = 1 μM, I243N = 5 μM and T311M = 2 μM) to various concentrations of SMC3 K_{106} peptide (0 – 300 μM). Time points were quenched with 10% hydrochloric acid (HCl), flash frozen in liquid nitrogen, and stored at -80°C. Assay workup was performed as described[27]. Assay standards were prepared using acetic acid (Ricca Chemical Company). After thawing, time points were neutralized with 6% sodium bicarbonate ($NaHCO_3$), and centrifuged (16,000 x g, 1 minute), and added to equilibrated coupled enzyme solution in a 96-well plate (Corning #3686) and incubated for 30 minutes prior to reading. The fluorescence of the resulting NADH was measured (ex. = 340 nm, em. = 460 nm). Either the Michaelis-Menten equation (MM) or a line was used to calculate kinetic parameters ($k_{cat,}$ K_M and k_{cat}/K_M). Initial rates were calculated from the concentration of acetate as a function of time and dependence on the initial ratio on the peptide concentration.

Results

HDAC8 CdLS catalysis using a methylcoumarin peptide

To define the catalytic function of these residues (P91L, I243N and T311M) in HDAC8 that are mutated in CdLS patients, we measured the catalytic activity of HDAC8 WT and CdLS mutants with either bound Fe^{2+} or Zn^{2+} using the Fluor de Lys (FdL) assay. The kinetic parameter ($k_{cat}/K_{M,\ app}$) was determined from a linear fit of the dependence of the initial rate of product formation on the concentration of substrate.

HDAC8 P91L was the most active of the measured mutants (>70-80% of WT activity) with both bound Fe^{2+} and Zn^{2+} (Table 3.1), consistent with previously published data[24] for the Zn^{2+} enzyme. The I243N mutation has a larger effect on catalytic turnover, with only 10% residual activity remaining with either Fe^{2+} or Zn^{2+} when compared to WT (Table 3.1). Surprisingly, this was the only HDAC8 mutant not consistent to previous data for the Zn^{2+} enzyme[23], which demonstrated 40% residual activity. Interestingly, the T311M mutation has the largest effect on catalysis, with overall residual activity of less than 5% for either bound divalent metals when compared to WT (Table 3.1).

Table 3.1 – Catalytic efficiency of Zn^{2+} and Fe^{2+} bound HDAC8 CdLS mutants

HDAC8 variant	Zn^{2+} k_{cat}/K_M (M^{-1} s^{-1})	Zn^{2+} % relative activity	Fe^{2+} k_{cat}/K_M (M^{-1} s^{-1})	Fe^{2+} % relative activity
WT	800 ± 40	100 ± 5	2000 ± 180	100 ± 9
P91L	590 ± 25	74 ± 3	1340 ± 20	67 ± 1.5
I243N	30 ± 5	4 ± 0.6	90 ± 10	4.5 ± 0.5
T311M	8 ± 2	1 ± 0.25	8 ± 1	0.4 ± 0.05

CD measurements of HDAC8 CdLS mutants

Circular dichroism measures the overall secondary structure of proteins. Our measurements showed that the mutants' spectra are nearly identical to that of WT-HDAC8, suggesting retention of secondary structure, despite the loss of activity (Figure 3.3). All spectra were evaluated using BeStSel (Beta Structure Selection) secondary structure prediction program for CD[28]. All of the CdLS mutant spectra retained similar secondary structure calculations as WT-HDAC8, with ~15% α-helicity, ~30-35% β-sheet and ~35% random coil character. These data indicate that none of the mutations cause large disruptions in the overall protein structure. Thus, it is possible that the catalytic activity of HDAC8 CdLS mutants is altered by small rearrangements rather than major structural changes. It is possible that these HDAC8 mutant proteins could still bind to substrates and interacting proteins but do not catalyze deacetylation.

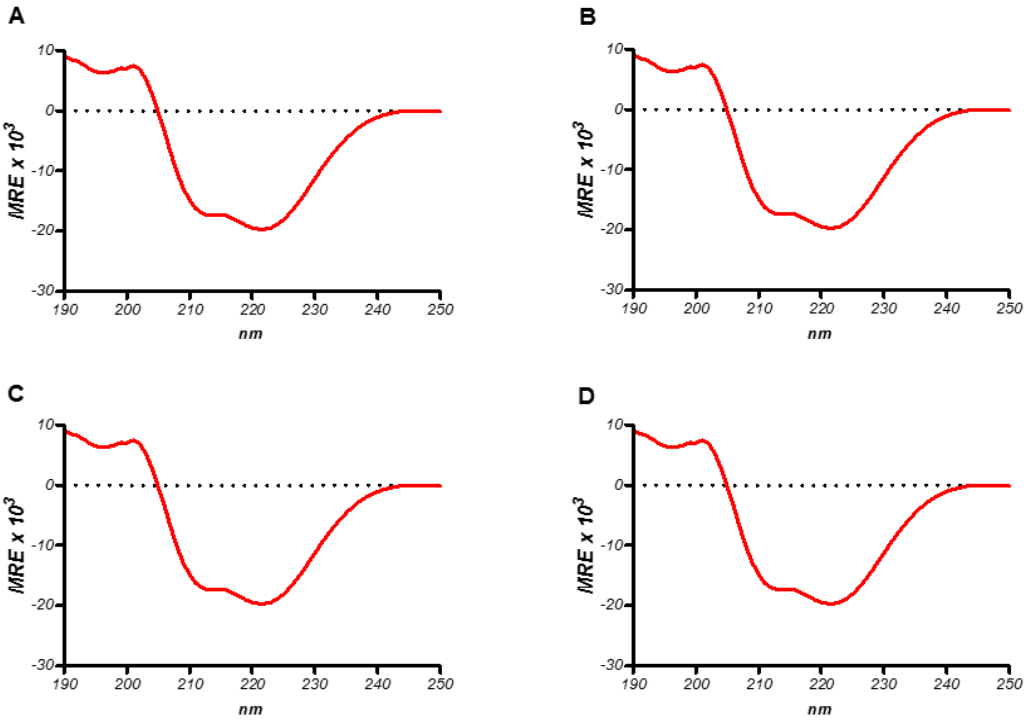

Figure 3.3 – CD spectra of HDAC8 WT and CdLS mutants

CD spectra of WT (A), P91L (B), I243N (C), and T311M (D) as apo enzyme (black) and Zn^{2+}-bound enzyme (red). The spectra reflecting the overall structure remains unmodified between all mutants. These spectra were used to predict secondary structure using the BeStSel prediction program.

Measurements of divalent metal binding affinity of CdLS mutants

Given that these mutations do not affect the overall structure but instead alter the activity of both Zn^{2+} and Fe^{2+}-HDAC8, we tested the importance of each of these mutants in determining metal selectivity by measuring the dissociation constant (K_D) for both Zn^{2+} and Fe^{2+} in HDAC8. For these experiments, apo-HDAC8 was equilibrated with various concentrations of free metal ions in NTA-buffered solutions. The amount of metal bound HDAC8 was determined by the binding of fl-SAHA, which preferentially binds to metallated HDAC8[25]. Fluorescence anisotropy displays a hyperbolic dependence on free metal concentration (Figure 3.4). To verify the accuracy of this method, we measured the affinity of WT HDAC8 for metal and obtained similar results to previously reported data[25].

Metal affinity was measured for each CdLS mutant with both Zn^{2+} and Fe^{2+}-NTA buffered solutions. P91L displayed identical divalent metal binding affinities as compared to WT HDAC8 (Table 3.2 and Figure 3.5). This led us to the hypothesis that the effect of this mutation on catalysis is mostly due to perturbation of binding loops, which can affect both substrate binding and product release. The two other mutants, I243N and T311M, displayed altered affinities. Both mutants have similar (within 2-fold) binding affinities for Fe^{2+} when compared to WT HDAC8, however, Zn^{2+} affinity was decreased by at least 10^3-fold (Table 3.2).

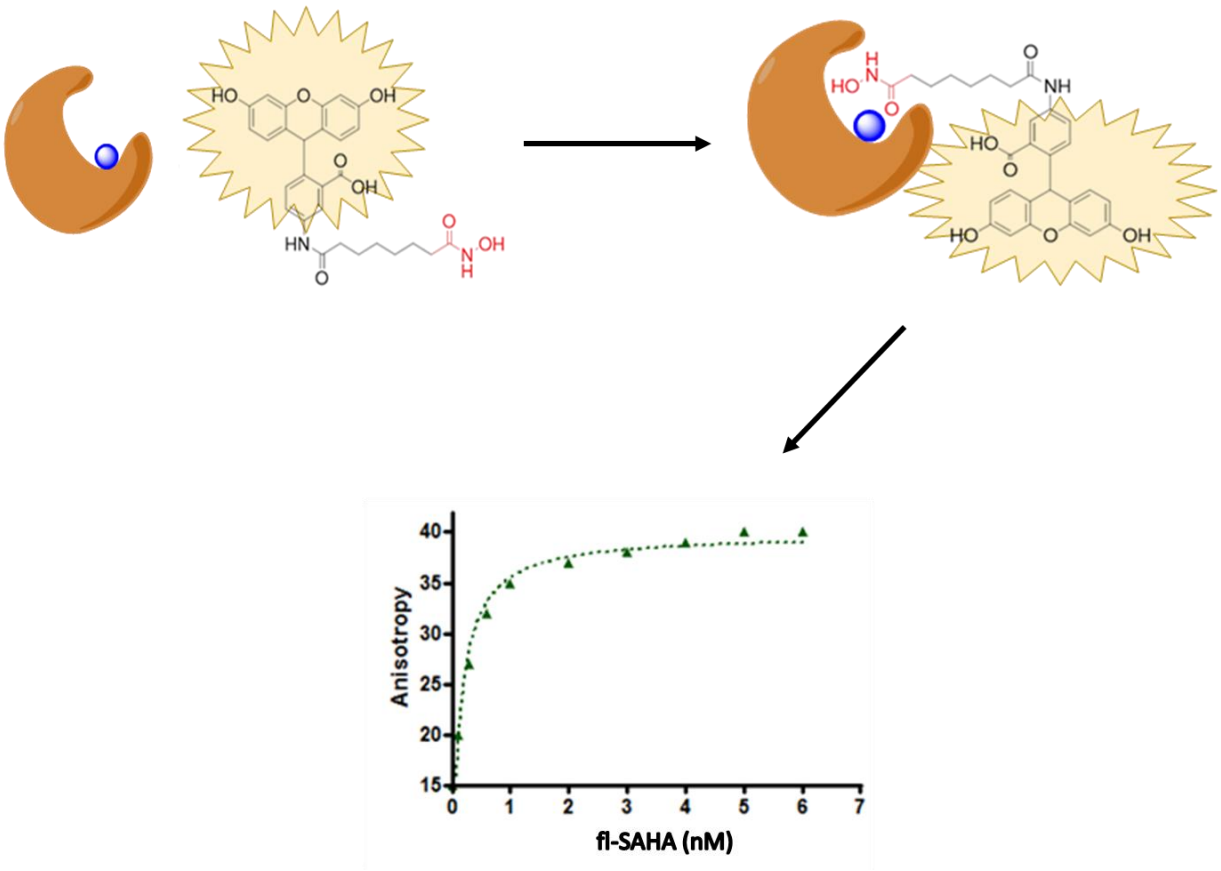

Figure 3.4 – HDAC8 metal binding affinity scheme using fl-SAHA

General scheme for HDAC8 divalent metal binding. Fluorescein-SAHA (fl-SAHA) binds with high affinity to metal bound HDAC8, allowing for coupling of metal binding to fl-SAHA as indicated by changing fluorescence anisotropy. Apo-HDAC8 does not binding fl-SAHA while any metal-reconstituted HDAC8 species will display a change in anisotropy.

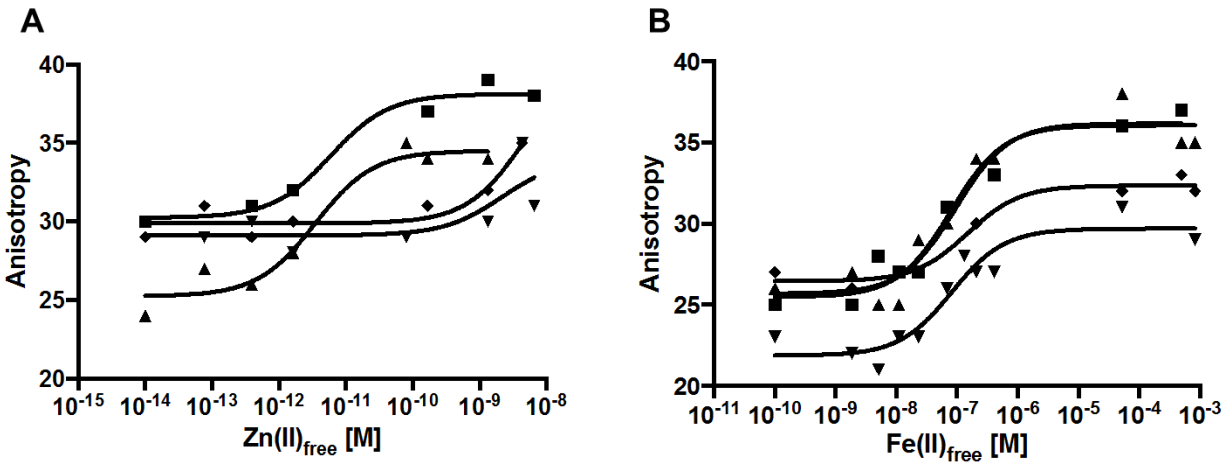

Figure 3.5 – Metal binding affinities of HDAC8 CdLS mutants

Measurement of metal binding affinities for (A) Zn^{2+}-bound and (B) Fe^{2+}-bound WT-HDAC8 (■), P91L (▲), I243N (▼) and T311M (♦). Measurements were done using NTA-buffered metal solutions in the presence of fl-SAHA. A binding isotherm is fit to the data (Equation 3.1)

Table 3.2 – Metal (Zn^{2+}/Fe^{2+}) affinities of HDAC8 CdLS mutants

HDAC8 variant	Zn^{2+} K_D (pM)	Fe^{2+} K_D (pM)
WT	6 ± 4	95,000 ± 40,000
P91L	4 ± 2	80,000 ± 35,000
I243N	≥ 3000	80,000 ± 35,000
T311M	≥ 4000	150,000 ± 60,000

HDAC8 CdLS activity using an SMC3 mimic peptide

To date, all *in vitro* activity assays with CdLS mutants have been done using the FdL peptide[6,23,24]. We sought to test each HDAC8 CdLS mutant with a biologically relevant peptide, SMC3 10-mer, to obtain insight into possible effects of SMC3 deacetylation. To measure deacetylation, we used an enzyme-coupled assay that measures the stoichiometric exchange of acetate product to NADH using fluorescence[27]. Assays were performed with both Zn^{2+} and Fe^{2+}- HDAC8 CdLS mutants under multiple turnover conditions and the dependence of the initial rates of deacetylation were used to calculate catalytic efficiencies. The dependence of the initial rate on the peptide concentration for WT and all CdLS mutants are shown in Figure 3.6. The catalytic efficiencies (k_{cat}/K_M) for CdLS mutants ranged from < 5 $M^{-1}s^{-1}$ for the Zn^{2+} enzyme and < 5 – 100 $M^{-1}s^{-1}$ for the Fe^{2+} enzyme (Table 3.3).

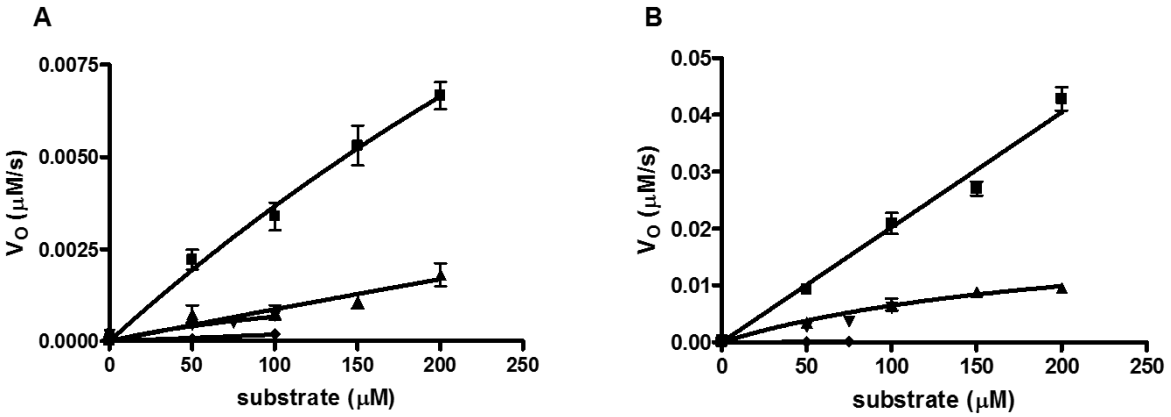

Figure 3.6 – Catalytic efficiencies of HDAC8 CdLS mutants on an SMC3 mimic peptide.

Deacetylation of an SMC3 10-mer peptide (50 – 200 μM) catalyzed by (A) Zn^{2+} and (B) Fe^{2+} bound WT HDAC8 (■), P91L (▲), I243N (▼) and T311M (♦). Reactions were initiated by the addition of enzyme (1 – 5 μM) to peptide in 20-25 mM HEPES pH 8, 137 mM NaCl, 3 mM KCl at 30°C. Reactions were quenched at various times and the acetate concentration produced was determined using an enzyme coupled assay. Data was collected for up to 4 hours per reaction and the initial rates were calculated from a linear fit to the time dependence. The Michaelis-Menten equation or a line were used to fit the concentration dependence of the initial rates to calculate kinetic parameters.

Table 3.3 – Catalytic efficiency of HDAC8 CdLS mutants using an SMC3 mimic peptide

HDAC8 variant	Zn^{2+} k_{cat}/K_M (M^{-1} s^{-1})	Zn^{2+} SMC3 % deacetylation	Fe^{2+} k_{cat}/K_M (M^{-1} s^{-1})	Fe^{2+} SMC3 % deacetylation
WT	40 ± 2	100 ± 5	235 ± 40	100 ± 17
P91L	6 ± 1	15 ± 2.5	95 ± 13	40 ± 5
I243N	< 5	< 15	11 ± 1	5 ± 0.4
T311M	< 5	< 15	< 5	< 5

Our data demonstrates an overall decrease in SMC3 deacetylase activity for all CdLS mutants when compared to WT-HDAC8. It is worth noting that SMC3 deacetylation and FdL peptide percent deacetylation is comparable for most mutants, except for P91L, which displays a slower deacetylation of the SMC3 peptide in comparison to FdL peptide deacetylation.

Discussion

HDAC8 has recently been associated with Cornelia de Lange Spectrum Disorders (CdLS) through the use of RNA interference-based screening and monitoring loss of HDAC8 activity using an HDAC8-specific inhibitor[6], making it one of the first validated HDAC8 substrates. Nearly all the mutations identified in HDAC8 associated to CdLS are in randomly distributed regions and not near the active site as predicted. Interestingly, some of these mutations affect HDAC8 catalysis in a variety of ways. This study provides insight into the chemistry and the variety of effects that some of these mutations have on HDAC8 catalysis, which in turn can be used to understand how the overall structure of HDAC8 plays a role in deacetylation.

P91 residue is located in the L2 loop, which flanks one section of the active site surface and has been proposed to aid in the binding of both substrates and inhibitors by its positioning in crystallographic studies[10,29,30]. It has been hypothesized that the L2 loop is essential in peptide-substrate binding due to this intrinsic flexibility[29,30]. In our study, we observe that the P91L HDAC8 mutation behaves most similarly to WT-HDAC8, however, it displays the largest change in deacetylation between the FdL peptide and the SMC3

peptide. We hypothesize that P91L effect on activity is mainly due to decreased peptide-substrate affinity and/or peptide-product release.

The I243 residue is located in helix F, approximately 20 Å from the divalent metal ion binding site[31]. Mutation of isoleucine to asparagine introduces a polar residue into an otherwise nonpolar helix, which may destabilize the structure near a monovalent metal binding site. Previous studies have demonstrated that HDAC8 activity is modulated by monovalent metal ion binding[10]. Binding of potassium (K^+) to the monovalent site activates catalytic activity in a time-dependent manner[10]. We hypothesize that mutations near this site could either significantly decrease K^+ binding to the site and inhibit activation or allow K^+ binding without activation. The unexpected effect of this mutation is that it does not affect the affinity of Fe^{2+}. Our data provides evidence that deacetylation of both FdL and SMC3 peptides is slow with either Zn^{2+}-bound and Fe^{2+}-bound HDAC8, and Fe^{2+} binding affinity remains similar to WT-HDAC8 while Zn^{2+} is decreased by at least 10^3-fold. We hypothesize that there could be a difference between HDAC8 metalloforms that this mutation could potentially alter, we discuss this difference and a potential transient mechanism in-depth in chapter five.

The T311M mutation is located in the H2 helix, approximately 10 Å from the divalent metal ion active site. Decroos and collaborators have demonstrated that this mutation causes a shift in the conformation of Arg37, a “gatekeeper” residue of the acetate release channel[23]. This shift breaks the hydrogen bonds with the backbones of Gly303 and Gly305 compromising product release. Additionally, crystallographic data shows that the shift of Arg37 causes the L1 loop (Leu31-Pro35) to reorganize. This loop has been shown to influence substrate binding through a substrate-enzyme hydrogen

bond with Lys33[29,30]. Our data shows that this mutant is the most detrimental towards catalysis using both the FdL and SMC3 peptides with either Zn^{2+} or Fe^{2+}-bound HDAC8. We hypothesize that the T311M mutation affects both the L1 and L2 loop indirectly by disrupting hydrogen bond interactions within HDAC8, affecting both peptide-substrate binding and product release.

Conclusions

Overall, our work provides insight into the kinetic and catalytic effects of CdLS point mutations on HDAC8. We demonstrated that the P91L mutation affects overall substrate release through disruptions of the L2 loop region, which is important for both substrate binding and product release. The I243N and T311M mutations affect the divalent metal ion binding site by affecting the internal bonding network of HDAC8 while still retaining its overall secondary structure, as supported by simulation studies[23,24]. We also provide the first evidence of SMC3 peptide deacetylation by the P91L and I243N mutants. Additionally, with their retained structure, these mutants could be further functionalize using crosslinking probes and click chemistry to identify HDAC8-substrate interactions *in vivo*. Further characterization of the other 13 CdLS mutants will be needed to highlight the role of each mutant on SMC3 deacetylation and their extended downstream effects on CdLS-like diseases.

Bibliography

(1) Glozak, M. A., Sengupta, N., Zhang, X., and Seto, E. (2005) Acetylation and deacetylation of non-histone proteins. *Gene 363*, 15–23.

(2) Norris, K. L., Lee, J.-Y., and Yao, T.-P. (2009) Acetylation Goes Global: The Emergence of Acetylation Biology. *Sci. Signal. 2*, pe76-pe76.

(3) Halkidou, K., Gaughan, L., Cook, S., Leung, H. Y., Neal, D. E., and Robson, C. N. (2004) Upregulation and nuclear recruitment of HDAC1 in hormone refractory prostate cancer. *Prostate 59*, 177–89.

(4) Zhang, Z., Yamashita, H., Toyama, T., Sugiura, H., Omoto, Y., Ando, Y., Mita, K., Hamaguchi, M., Hayashi, S. I., and Iwase, H. (2004) HDAC6 expression is correlated with better survival in breast cancer. *Clin. Cancer Res.*

(5) Wilson, A. J., Byun, D.-S., Nasser, S., Murray, L. B., Ayyanar, K., Arango, D., Figueroa, M., Melnick, A., Kao, G. D., Augenlicht, L. H., and Mariadason, J. M. (2008) HDAC4 promotes growth of colon cancer cells via repression of p21. *Mol. Biol. Cell 19*, 4062–75.

(6) Deardorff, M. A., Bando, M., Nakato, R., Watrin, E., Itoh, T., Minamino, M., Saitoh, K., Komata, M., Katou, Y., Clark, D., Cole, K. E., De Baere, E., Decroos, C., Di Donato, N., Ernst, S., Francey, L. J., Gyftodimou, Y., Hirashima, K., Hullings, M., Ishikawa, Y., Jaulin, C., Kaur, M., Kiyono, T., Lombardi, P. M., Magnaghi-Jaulin, L., Mortier, G. R., Nozaki, N., Petersen, M. B., Seimiya, H., Siu, V. M., Suzuki, Y., Takagaki, K., Wilde, J. J., Willems, P. J., Prigent, C., Gillessen-Kaesbach, G., Christianson, D. W., Kaiser, F. J., Jackson, L. G., Hirota, T., Krantz, I. D., and Shirahige, K. (2012) HDAC8 mutations in Cornelia de Lange syndrome affect the cohesin acetylation cycle. *Nature 489*, 313–7.

(7) Gregoretti, I. V, Lee, Y.-M., and Goodson, H. V. (2004) Molecular evolution of the histone deacetylase family: functional implications of phylogenetic analysis. *J. Mol. Biol. 338*, 17–31.

(8) Gantt, S. L., Gattis, S. G., and Fierke, C. A. (2006) Catalytic activity and inhibition of human histone deacetylase 8 is dependent on the identity of the active site metal ion. *Biochemistry 45*, 6170–8.

(9) Gantt, S. M. L., Decroos, C., Lee, M. S., Gullett, L. E., Bowman, C. M., Christianson, D. W., and Fierke, C. A. (2016) General Base-General Acid Catalysis in Human Histone Deacetylase 8. *Biochemistry*.

(10) Gantt, S. L., Joseph, C. G., and Fierke, C. A. (2009) Activation and Inhibition of Histone Deacetylase 8 by Monovalent Cations. *J. Biol. Chem. 285*, 6036–6043.

(11) Joshi, P., Greco, T. M., Guise, A. J., Luo, Y., Yu, F., Nesvizhskii, A. I., and Cristea, I. M. (2013) The functional interactome landscape of the human histone deacetylase family. *Mol. Syst. Biol. 9*, 672.

(12) Olson, D. E., Udeshi, N. D., Wolfson, N. A., Pitcairn, C. A., Sullivan, E. D., Jaffe, J.

D., Svinkina, T., Natoli, T., Lu, X., Paulk, J., McCarren, P., Wagner, F. F., Barker, D., Howe, E., Lazzaro, F., Gale, J. P., Zhang, Y.-L., Subramanian, A., Fierke, C. A., Carr, S. A., and Holson, E. B. (2014) An unbiased approach to identify endogenous substrates of “histone” deacetylase 8. *ACS Chem. Biol. 9*, 2210–6.

(13) Gao, J., Siddoway, B., Huang, Q., and Xia, H. (2009) Inactivation of CREB mediated gene transcription by HDAC8 bound protein phosphatase. *Biochem. Biophys. Res. Commun. 379*, 1–5.

(14) Wilson, B. J., Tremblay, A. M., Deblois, G., Sylvain-Drolet, G., and Giguère, V. (2010) An acetylation switch modulates the transcriptional activity of estrogen-related receptor alpha. *Mol. Endocrinol. 24*, 1349–1358.

(15) Nasmyth, K., and Haering, C. H. (2009) Cohesin: Its Roles and Mechanisms. *Annu. Rev. Genet. 43*, 525–558.

(16) Horsfield, J. A., Print, C. G., and Mönnich, M. (2012) Diverse Developmental Disorders from The One Ring: Distinct Molecular Pathways Underlie the Cohesinopathies. *Front. Genet. 3*, 171.

(17) Liu, J., and Baynam, G. (2010) Cornelia de Lange syndrome. *Adv. Exp. Med. Biol. 685*, 111–23.

(18) Liu, J., and Krantz, I. (2009) Cornelia de Lange syndrome, cohesin, and beyond. *Clin. Genet. 76*, 303–314.

(19) Dorsett, D., and Krantz, I. D. (2009) On the Molecular Etiology of Cornelia de Lange Syndrome. *Ann. N. Y. Acad. Sci. 1151*, 22–37.

(20) Barisic, I., Tokic, V., Loane, M., Bianchi, F., Calzolari, E., Garne, E., Wellesley, D., and Dolk, H. (2008) Descriptive epidemiology of Cornelia de Lange syndrome in Europe. *Am. J. Med. Genet. Part A 146A*, 51–59.

(21) Beckouët, F., Hu, B., Roig, M. B., Sutani, T., Komata, M., Uluocak, P., Katis, V. L., Shirahige, K., Nasmyth, K., Wang, Y., and al., et. (2010) An Smc3 acetylation cycle is essential for establishment of sister chromatid cohesion. *Mol. Cell 39*, 689–99.

(22) Beckouët, F., Srinivasan, M., Roig, M. B., Chan, K.-L., Scheinost, J. C., Batty, P., Hu, B., Petela, N., Gligoris, T., Smith, A. C., Strmecki, L., Rowland, B. D., and Nasmyth, K. (2016) Releasing Activity Disengages Cohesin’s Smc3/Scc1 Interface in a Process Blocked by Acetylation. *Mol. Cell 61*, 563–574.

(23) Decroos, C., Bowman, C. M., Moser, J. A. S., Christianson, K. E., Deardorff, M. A., and Christianson, D. W. (2014) Compromised structure and function of HDAC8 mutants identified in Cornelia de Lange Syndrome spectrum disorders. *ACS Chem. Biol. 9*, 2157–2164.

(24) Decroos, C., Christianson, N. H., Gullett, L. E., Bowman, C. M., Christianson, K. E., Deardorff, M. A., and Christianson, D. W. (2015) Biochemical and Structural Characterization of HDAC8 Mutants Associated with Cornelia de Lange Syndrome Spectrum Disorders. *Biochemistry 54*, 6501–6513.

(25) Kim, B., Pithadia, A. S., and Fierke, C. A. (2015) Kinetics and thermodynamics of metal-binding to histone deacetylase 8. *Protein Sci. 24*, 354–365.

(26) Keith A. McCall‡, § and, and Carol A. Fierke*, ǁ. (2004) Probing Determinants of the Metal Ion Selectivity in Carbonic Anhydrase Using Mutagenesis†.

(27) Wolfson, N. A., Pitcairn, C. A., Sullivan, E. D., Joseph, C. G., and Fierke, C. A. (2014) An enzyme-coupled assay measuring acetate production for profiling histone deacetylase specificity. *Anal. Biochem. 456*, 61–69.

(28) Micsonai, A., Wien, F., Kernya, L., Lee, Y.-H., Goto, Y., Réfrégiers, M., and Kardos, J. (2015) Accurate secondary structure prediction and fold recognition for circular dichroism spectroscopy. *Proc. Natl. Acad. Sci. 112*, E3095–E3103.

(29) Vannini, A., Volpari, C., Filocamo, G., Casavola, E. C., Brunetti, M., Renzoni, D., Chakravarty, P., Paolini, C., De Francesco, R., Gallinari, P., Steinkühler, C., and Di Marco, S. (2004) Crystal structure of a eukaryotic zinc-dependent histone deacetylase, human HDAC8, complexed with a hydroxamic acid inhibitor. *Proc. Natl. Acad. Sci. U. S. A. 101*, 15064–9.

(30) Dowling, D. P., Gantt, S. L., Gattis, S. G., Fierke, C. A., and Christianson, D. W. (2008) Structural studies of human histone deacetylase 8 and its site-specific variants complexed with substrate and inhibitors. *Biochemistry 47*, 13554–63.

(31) Somoza, J. R., Skene, R. J., Katz, B. A., Mol, C., Ho, J. D., Jennings, A. J., Luong, C., Arvai, A., Buggy, J. J., Chi, E., Tang, J., Sang, B.-C., Verner, E., Wynands, R., Leahy, E. M., Dougan, D. R., Snell, G., Navre, M., Knuth, M. W., Swanson, R. V, McRee, D. E., and Tari, L. W. (2004) Structural snapshots of human HDAC8 provide insights into the class I histone deacetylases. *Structure 12*, 1325–34.

(32) Dowling, D. P., Gattis, S. G., Fierke, C. A., and Christianson, D. W. (2010) Structures of metal-substituted human histone deacetylase 8 provide mechanistic inferences on biological function . *Biochemistry 49*, 5048–56.

(33) Deardorff, M. A., Porter, N. J., and Christianson, D. W. (2016) Structural aspects of HDAC8 mechanism and dysfunction in Cornelia de Lange syndrome spectrum disorders. *Protein Sci. 25*, 1965–1976.

Chapter 4

Metal Switching Specificity: A Novel Regulatory Mechanism for HDAC8[**,††]

Overview

Protein lysine acetylation is an enzymatically reversible post-translational modification (PTM). Acetylation is catalyzed by twenty lysine acetyl transferases (KATs) and eighteen lysine deacetylases, including both metal-dependent histone deacetylases (HDACs) and the NAD^+ dependent sirtuins (SIRTs). HDACs and SIRTs catalyze deacetylation through hydrolysis of the acetyl moiety[1]. The balance of the enzymatic activities of both lysine deacetylases (HDACs and SIRTs) and KATs regulate the acetylation states of both histone proteins and non-histone proteins involved in many different cellular processes[2]. These enzyme families control the acetylation state of >6000 acetylated sites in the mammalian proteome[3], and it is therefore important to understand the mechanism by which each isozyme is specifically regulated[4,5]. HDACs are medically relevant enzymes because aberrant acetylation has been implicated in several disease states. Elucidating the determinants of substrate specificity and regulation of each HDAC

[**] Reproduced, in part, from a manuscript in preparation: Pitcairn, C. A., Lopez, J. E., Joseph, C. G., Scholle, M. D., Mrksich, M., Fierke, C. A., Metal switching specificity: A novel regulatory mechanism for HDAC8. *In Preparation*

[††] Caleb G. Joseph performed the SAMDI high-throughput screen, Carol Ann Pitcairn performed the initial peptide screen assays, Jeffrey E. Lopez performed full Michaelis-Menten kinetics of all peptides screened, Michael D. Scholle performed the MALDI mass spectrometry, Milan Mrksich and Carol A. Fierke designed the SAMDI experiments. Caleb G. Joseph, Carol Ann Pitcairn, Jeffrey E. Lopez and Carol A. Fierke analyzed the data. Carol Ann Pitcairn, Jeffrey E. Lopez, Caleb G. Joseph, and Carol A. Fierke wrote the manuscript.

isozyme is important for understanding the regulatory mechanisms of acetylation/deacetylation in the cell and for designing isozyme selectivity in therapeutics.

HDAC8 is a class I isozyme and a metal dependent HDAC. HDAC8 is well understood biochemically, but its cellular role and regulation require further investigation. It is primarily expressed in human smooth muscle cells and is the only class I isozyme that can be found in both the nucleus and the cytoplasm[6,7]. The precise HDAC8 substrate set remain largely undefined, but predicted HDAC8 substrates include the nuclear structural maintenance of chromosomes 3 (SMC3)[8], core histone proteins[9], cAMP response binding protein (CREB)[10], the cysteine-rich protein 2-binding protein (CSRP2BP)[11], and the estrogen-related receptor alpha (ERRα)[12,13] among others. HDAC8 was originally proposed to be a zinc-dependent metalloenzyme since zinc co-purified with the enzyme and was observed in the first HDAC8 crystal structure[14]. However, several divalent metal ions can activate the enzyme. The k_{cat}/K_M trend of catalysis for metal-substituted HDAC8 is $Co^{2+} > Fe^{2+} > Zn^{2+} > Ni^{2+} > Mn^{2+}$[15]. In contrast to Zn^{2+}, the activity of Fe^{2+}-HDAC8 decreases when exposed to oxygen[15]. Furthermore, the trend of the inhibition constant, K_i, of the FDA-approved pan-HDAC inhibitor suberoylanilide hydroxamic acid (SAHA) is $Co^{2+} < Fe^{2+} < Zn^{2+}$[16], inversely proportional to that of k_{cat}/K_M. The fact that the enzyme can be activated by different divalent metal ions leads to the suggestion that HDAC8 activity *in vivo* may be regulated by the identity of the active site metal ion.

Crystal structures of HDAC8 have not been able to explain the metal-dependent differences in activation and inhibition. Structures of Fe^{2+}- Co^{2+}- and Zn^{2+}-HDAC8 bound to hydroxamic acid inhibitors show a common pentacoordinate, square pyramidal

geometry for all metal-substituted forms[16]. However, these structures are only a snapshot and cannot show dynamic conformational changes and interactions that might occur when a peptide substrate is bound to the enzyme. Additionally, the hydroxamic acid inhibitor could potentially stabilize the active site metal coordination state in the fixed conformation observed in the various crystal structures, regardless of the identity of the bound divalent metal ion.

Based on these observations, the affinity of HDAC8 for each divalent metal and the readily available metal concentrations, HDAC8 could be activated by either Zn^{2+} or Fe^{2+} *in vivo*. Under normal conditions, readily exchangeable Zn^{2+} concentrations is lower than Fe^{2+} in cells; exchangeable Zn^{2+} concentration ranges from 5 pM – 2 nM while predictions of the Fe^{2+} concentration ranges from 200 nM – 12 μM[17–19]. However, the concentrations of zinc in cells can increase significantly, such as under conditions of oxidative stress[17] or after telophase arrest[20]. HDAC8 has a 10^6-fold higher affinity for Zn^{2+} compared to Fe^{2+}, at 5 ± 1 pM and 0.2 ± 0.1 μM, respectively[15,16,21]. Additionally, HDAC8 is not activated by Fe^{3+}. HDAC8 expressed in bacteria binds and is activated by Fe^{2+}[15]. Furthermore, HDAC activity in mammalian cell lysates is oxygen sensitive, consistent with Fe^{2+} dependent activity[15,16]. Immunopurified HDAC8 in HeLa cells demonstrates oxygen-sensitive activity[22]. Together, these data suggest that iron may play a role in cellular HDAC8 activation and demonstrates the importance of determining which metals activate and regulate HDAC8 activity *in vivo*.

Prompted by the difference in divalent metal-dependent deacetylase activity and the observed HDAC8 oxygen sensitivity in cell lysates, we investigated whether the identity of the catalytic divalent metal ion affects the substrate selectivity of HDAC8-

catalyzed deacetylation *in vitro*. Here we show that the divalent metal ion (Zn^{2+} or Fe^{2+}) in the active site alters both the activity and the peptide substrate selectivity of HDAC8. Based on these data, we hypothesize that *in vivo* metal switching could regulate both the activity and selectivity of HDAC8. For metal switching, we propose that HDAC8 is bound to Fe^{2+} in cells, however, when the Zn^{2+} concentration increases the active site metal ion is replaced to form Zn^{2+}-HDAC8. This work suggests a new mechanism by which peptide specificity and deacetylase activity of HDAC8 may be regulated *in vivo*.

Materials and Methods

Metal free HEPES, NaCl, KCl, and NaOH were purchased from Sigma, and TCEP (tris(2-carboxylethyl)phosphine) was purchased from GoldBio. All other reagents were purchased from Fisher unless otherwise specified.

HDAC8 Purification

HDAC8 was prepared using the following method, modified from ([15]). HDAC8-TEV-His6 was transformed into BL21-DE3 Z-competent cells and grown in 2xYT media supplemented with 100 µg/mL of ampicillin at 37°C with shaking at 170 RPM until OD_{600} = 0.4 - 0.7. The temperature was then decreased to 20°C for 45 – 60 minutes, followed by induction with isopropyl β-D-1-thiogalactopyranoside (IPTG) (0.5 mM) and addition of $ZnSO_4$ (0.2 mM). Cells were harvested 15-16 hours post-induction by centrifugation (4000 x g, 15 – 20 minutes, 4°C) and resuspended in HDAC8 resuspension buffer (30 mM HEPES pH 7.8-8.0, 150 mM NaCl, 5 mM KCl, 1 mM imidazole, and 1 mM TCEP) supplemented with a complete protease inhibitor cocktail tablet (Roche). Cells were lysed

by microfluidizer (Microfluidics), followed by nucleic acid precipitation with polyethyleneimine (pH 7.9) and followed by centrifugation (27,000 x g, 45 minutes, 4˚C). HDAC8 was loaded onto a Ni^{2+}-charged chelating sepharose (GE Healthcare) gravity column equilibrated with HDAC8 purification buffer (30 mM HEPES pH 8, 150 mM NaCl, 5 mM KCl, 1 mM TCEP and 1 mM imidazole). The column was washed with 20 mM imidazole purification buffer and HDAC8 was eluted using a linear gradient (25 – 250 mM imidazole). The His6 tag was cleaved using His6-tagged TEV protease during an overnight dialysis against HDAC8 purification buffer without imidazole. A second, stepwise-elution Ni^{2+}-charged column was used to separate HDAC8 from TEV protease. HDAC8 eluted in the flowthrough and 20 mM imidazole steps. HDAC8 was concentrated in 10k or 30k MWCO Amicon Ultra centrifugal concentrators and dialyzed against metal free buffer A (25 mM MOPS pH 7.5, 1 mM TCEP, 5 mM KCl and 1 mM EDTA) followed by several dialyses against metal free buffer B (25 mM MOPS pH 7.5, 1 mM TCEP, 5 mM KCl). For MALDI deacetylation assays, a PD-10 desalting column (GE Healthcare) in either PD-10 buffer A (25 mM HEPES pH 7.4 – 7.8, 150 mM NaCl, 3 mM KCl, 1 mM TCEP) or PD-10 buffer B (25 mM MOPS pH 7.5, 1 mM TCEP) was used to remove residual EDTA. HDAC8 was aliquoted, flash frozen in liquid nitrogen, and stored at -80˚C. Concentration was measured by absorbance at 280 nm using the extinction coefficient of 52,120 $M^{-1}cm^{-1}$, which was determined previously[15]. ICP-MS confirmed less than 10% Zn^{2+} present in the final enzyme sample.

High-throughput SAMDI mass spectrometry deacetylation assays

Selectivity screens were performed using Self-Assembled Monolayers for MALDI-TOF Mass Spectrometry (SAMDI). The SAMDI assays were performed as previously

published[23–26]. Peptides of varying sequence were transferred to an array plate containing 384 gold islands, each with a monolayer presenting a maleimide group at a density of 10% against a background of tri(ethylene glycol) groups. In this way, the peptides were immobilized through reaction of the side chain of the terminal cysteine residue with maleimide while the glycol groups prevent non-specific adsorption of proteins onto the monolayer. The peptide array was incubated with HDAC8 by distributing 3 μL portions of a solution (0.5 μM enzyme, 25 mM Tris pH 8.0, 147 mM KCl, 3mM NaCl) using a 12-channel pipette. Solutions were kept at 37°C for 30 minutes followed by stopping the reaction by rinsing the array plate with ethanol. Separate controls were performed using ICP-MS to measure metal bound to HDAC8 after incubation with the SAMDI plates. Separate controls were performed using ICP-MS to measure metal contamination in HDAC8 reactions from several SAMDI plates. Zn^{2+} contamination ranged between 0.3 – 0.6 μM in the control assays tested.

Enzyme-coupled assay for in solution non-methylcoumarin peptides

Peptides (Peptide 2.0 and/or Synthetic Biomolecules) were synthesized with acetylated N-termini and carboxamide C-termini. Zn^{2+}-HDAC8 and Fe^{2+}-HDAC8 were reconstituted as described[15]. Apo-HDAC8 (10 μM) was reconstituted with stoichiometric Zn^{2+} (Fluka) in peptide assay buffer (25 mM HEPES pH 8, 137 mM NaCl, 3 mM KCl) and incubated for 1 hour on ice. For Fe^{2+}-HDAC8, apo-HDAC8 was equilibrated in an anaerobic glove box (Coy Laboratory Products) for one hour prior to reconstitution. Solid $FeCl_2$ (Sigma), L(+)-ascorbic acid (Fluka), and peptide assay buffer were equilibrated in the anaerobic chamber at least overnight. Fe^{2+} (100 μM) in 5 mM ascorbate and assay buffer was prepared daily. Fe^{2+}-HDAC8 (10 μM) was reconstituted anaerobically with 5-

fold excess Fe^{2+} in assay buffer and 2.5 mM ascorbate for 1 hour in a 0 – 4°C CoolBox (Biocision). Assays were performed aerobically on ice within 2 hours, the effective working time for ascorbic acid to preserve Fe^{2+} activity[27]. The enzyme-coupled assay was performed as described[28]. Fe^{2+}- and Zn^{2+}-HDAC8 and peptides in assay buffer were equilibrated at 30°C for 15 minutes prior to reaction initiation. Reactions were initiated by the addition of enzyme (1 μM) to various concentrations of substrates (25 – 400 μM). Time points were quenched with 10% hydrochloric acid (HCl), flash frozen in liquid nitrogen, and stored at -80°C. Assay workup was performed as described[28]. Standards were prepared using acetic acid (Ricca Chemical Company). After thawing, time points were neutralized with 6% sodium bicarbonate ($NaHCO_3$), centrifuged (16,000 x g, 1 minute), and added to an equilibrated coupled enzyme solution in a 96-well plate (Corning #3686). The fluorescence of the resulting NADH was measured (ex. = 340 nm, em. = 460 nm) and the initial rate was calculated from the time dependence of NADH appearance. Michaelis-Menten parameters (MM) or a line was fit to the concentration dependence of the initial rate to calculate kinetic parameters ($k_{cat,}$ K_M and k_{cat}/K_M).

Assay for measuring methylcoumarin-labeled peptides

Peptides containing a methylcoumarin-bound C-terminus were measured using the Fluor de Lys (FdL) assay (Enzo Life Sciences) conditions. Deacetylation of the substrates by HDAC8 is followed by cleavage of the amino bond linking the C-terminal methylcoumarin to the peptide backbone catalyzed by trypsin, resulting in a fluorescence shift between the deacetylated product (ex. = 340 nm, em. = 450 nm) and the remaining substrate (ex. = 340 nm, em. = 380 nm). Fe^{2+}- and Zn^{2+}-HDAC8 were reconstituted and equilibrated as described previously. Reactions were initiated by the addition of enzyme

(1 μM) to various concentrations of substrates (25 – 200 μM). Time points were quenched by the addition of trichostatin A (TSA) and trypsin developer. The initial rate was calculated from the time dependence of the changes in fluorescence. Michaelis-Menten parameters (MM) or a line was fit to the concentration dependence of the initial rate to calculate kinetic parameters (k_{cat}, K_M and k_{cat}/K_M).

Results and Discussion

Mass spectrometry screen

To identify potential differences in selectivity with different active site metals bound to HDAC8, we screened HDAC8 reactivity with a 361-peptide array using self-assembled monolayers for matrix assisted laser desorption/ionization time-of-flight mass spectrometry (SAMDI) assays[24]. The peptides were of the form $GXK_{Ac}ZGC$, where the flanking residues X and Z were varied across nineteen amino acids (all natural residues excluding cysteine). After incubation with HDAC8, the monolayers were analyzed by matrix-assisted laser desorption-ionization mass spectrometry to observe the substrate and product of the reaction from their masses (Figure 4.1). The fraction deacetylation of each peptide was determined by the ratio of the deacetylated peak area to the sum of the peak areas for the substrate and product.

We prepared HDAC8 reconstituted with Fe^{2+} or Zn^{2+} and incubated each of these enzyme forms with the peptide array. In both cases, we observed deacetylation of multiple substrates. For Zn^{2+}-HDAC8, 172 of the peptides showed no significant reactivity (<3% deacetylation), 72 peptides showed moderate reactivity (3 – 15% deacetylation) and 117 peptides showed high reactivity (>15% deacetylation). Similarly, for Fe^{2+}-HDAC8, 139 of

the peptides showed no significant activity, 62 peptides showed moderate activity and 160 peptides showed high activity. Overall, the number of active peptides was higher for Fe^{2+}-HDAC8 (222 peptides) than for Zn^{2+}-HDAC8 (189 peptides). Deacetylation heat maps were generated for both Zn^{2+}- (Figure 4.1A) and Fe^{2+}-HDAC8 (Figure 4.1B). These assays suggested general peptide sequence specificity trends for HDAC8. One particular trend showed that all but three peptides containing an aromatic residue (Phe) at the Z position were deacetylated efficiently by both Zn^{2+}- and Fe^{2+}-HDAC8, while a methionine in the Z position was largely unfavorable to both enzyme forms and was observed in many of the non-substrate peptides. Therefore, these data demonstrated that HDAC8 substrate selectivity depends on the immediate sequence surrounding the acetyl lysine, consistent with previous results[25,29].

To examine differences in relative activity between the two metal forms of the enzyme, we generated a selectivity map that displays the ratio of Zn^{2+}-HDAC8 to Fe^{2+}-HDAC8 product conversion (Figure 4.1C). This heat map demonstrates that the substrate selectivity of HDAC8 depends on the identity of the bound divalent metal ion. In the screen, Zn^{2+}-HDAC8 had higher reactivity (relative product conversion was greater than 7-fold) than Fe^{2+}-HDAC8 for approximately 10% of the peptides and Fe^{2+}-HDAC8 deacetylated 13% of the peptides to a greater extent (by a factor of at least 7-fold) than Zn^{2+}-HDAC8. Many peptides displayed similar reactivity; 31% of peptides were comparably deacetylated by both enzyme forms and 46% of peptides demonstrated negligible deacetylation by both enzyme forms. Overall, these data showed that HDAC8 substrate selectivity is altered by the identity of the active site metal ion as well as the immediate sequence surrounding the acetyl lysine substrate.

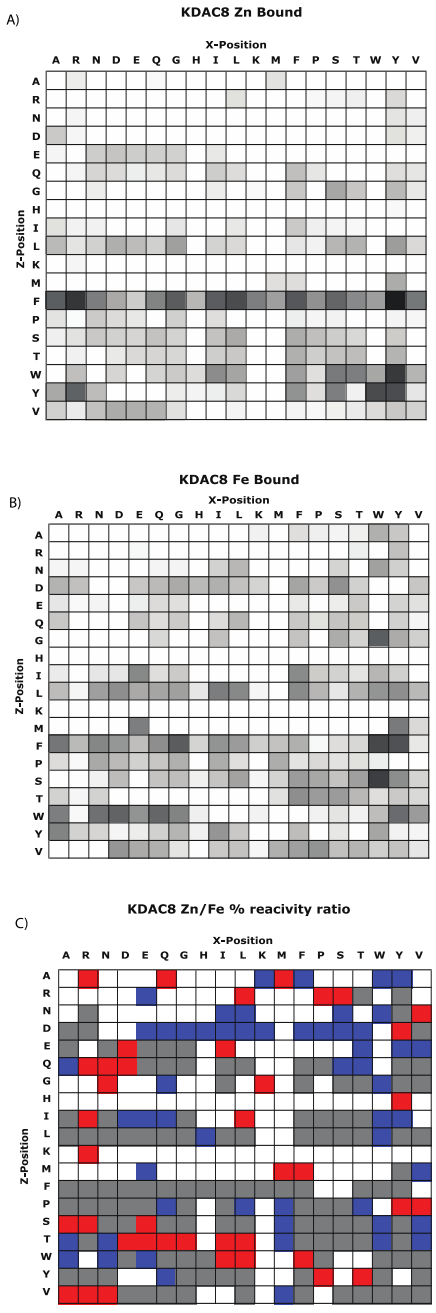

Figure 4.1: HDAC8 metal specificity peptide screen

The selectivity of (A) Zn^{2+}- and (B) Fe^{2+}-bound HDAC8 was evaluated by incubating each enzyme form with an array of 361 immobilized peptides of sequence $GXK_{AC}ZGC$. The extent of deacetylation of each peptide is shown in grey scale. (C) A heat map indicating alterations in peptide selectivity dependent on the metal ion bound to HDAC8 was generated by taking the ratio of Zn^{2+}-HDAC8 to Fe^{2+}-HDAC8 product conversion. Peptides with a ratio that is greater than seven-fold (Zn^{2+}-HDAC8 selective) are shown in blue and peptides with a ratio < 0.14 Fe^{2+}-HDAC8 (Fe^{2+}-HDAC8 selective) are shown in red. Peptides that were deacetylated by both metalloenzyme forms are shown in grey and non-substrate peptides for both enzyme forms are shown in white.

Kinetic assays *with in vitro* protein-based peptide substrates

To further investigate the differences in peptide selectivity due to the identity of the divalent metal bound, we measured kinetic parameters for reactivity with peptide substrates. We selected peptides (Table 4.1) based on biologically relevant putative *in vivo* substrates as predicted by proteomic and computational methods[11,30], and measured HDAC8-catalyzed deacetylation under steady-state conditions. We compared k_{cat}/K_M (catalytic efficiency) values for Fe^{2+}- and Zn^{2+}-HDAC8.

To determine HDAC8 reactivity, we used an enzyme-coupled deacetylation assay that measures the stoichiometry of acetate formation to NADH using changes in fluorescence. Additionally, we measured deacetylation of methylcoumarin-bound peptides as a benchmark for Fe^{2+}/Zn^{2+} selectivity, as previously described[15]. Both stopped assays were performed using Zn^{2+} or Fe^{2+}-HDAC8 under multiple turnover conditions to measure the initial rates of peptide deacetylation. The k_{cat}/K_M values were calculated from the dependence of the initial rates on the substrate concentration, as shown for both non-coumarin (Figure 4.2) and coumarin-bound (Figure 4.3) peptides. The catalytic efficiencies for the peptides ranged from 2 – 500 $M^{-1}s^{-1}$ for Zn^{2+}-HDAC8 and 3 – 6000 $M^{-1}s^{-1}$ for Fe^{2+}-HDAC8. The specificity constant for Fe^{2+}-HDAC8 was higher for most peptides tested, however, the ratio of the k_{cat}/K_M values for the two metalloenzyme forms varied significantly, as predicted from the original immobilized peptide screen. The ratios of Fe^{2+}/Zn^{2+}-HDAC8 k_{cat}/K_M values ranged from 0.3 to 16

Table 4.1 – Metal dependence of HDAC8 substrate specificity for non-coumarin and coumarin bound peptides[a]

Abbreviation	Protein name	Peptide sequence	Fe^{2+}-HDAC8 k_{cat}/K_M ($M^{-1}s^{-1}$)	Zn^{2+}-HDAC8 k_{cat}/K_M ($M^{-1}s^{-1}$)	Fe^{2+}/Zn^{2+} ratio[b]
H3K9 7-mer	Histone H3	TARK$_{ac}$STG	170 ± 30	45 ± 3	4 ± 1
H3K9 13-mer	Histone H3	TKQTARK$_{ac}$STGGKA	290 ± 20	50 ± 5	6 ± 1
LARP1	La-related protein 1	LGK$_{ac}$FRR	1080 ± 160	130 ± 40	8 ± 3
SMC3 9-mer	Structural Maintenance of Chromosomes 3	RVIGAK$_{ac}$DQ	242 ± 67	15 ± 5	16 ± 7
SMC3 10-mer	Structural Maintenance of Chromosomes 3	RVIGAK$_{ac}$DQY	220 ± 40	36 ± 2	6 ± 1
CREB94	cAMP responsive element-binding protein	CKDLK$_{ac}$RLFS	8 ± 1	2 ± 0.5	4 ± 1
CSRP2BP	Cysteine-rich protein 2-binding protein	STPVK$_{ac}$FISR	660 ± 110	40 ± 11	17 ± 5
THRAP3	Thyroid hormone receptor-associated protein 3	LGDGK$_{ac}$MKS	3 ± 0.5	9 ± 1	0.3 ± 0.06
HDAC8 p53 FdL	Cellular tumor antigen 53	RHK$_{ac}$K$_{ac}$-coumarin	2300 ± 160[c]	800 ± 50[c]	3 ± 0.2
SIRT1 FdL	Cellular tumor antigen 53	RHKK$_{ac}$-coumarin	6150 ± 760	410 ± 30	15 ± 2
Boc-Lys	Boc-protected acetyllysine	Boc-K$_{ac}$-coumarin	890 ± 160	290 ± 30	3 ± 1

[a] Peptides were acetylated on the N-terminus with C-terminal amides (except for coumarin peptides)
Unless noted, k_{cat}/K_M values were calculated from the initial rates of 25 – 400 µM peptide and 1µM HDAC8 in assay buffer (25 mM HEPES pH 8, 137 mM NaCl, 3 mM KCl) at 30°C.

[b] The error in the Fe^{2+}/Zn^{2+} ratio was propagated using the equation $\partial R = R \times \sqrt{\left(\left(\frac{\partial Fe}{Fe}\right)^2 + \left(\frac{\partial Zn}{Zn}\right)^2\right)}$, where ∂ is overall error, R is the ratio of Fe^{2+}/Zn^{2+} and Fe and Zn are the k_{cat}/K_M values.

[c] Values were taken from (14)

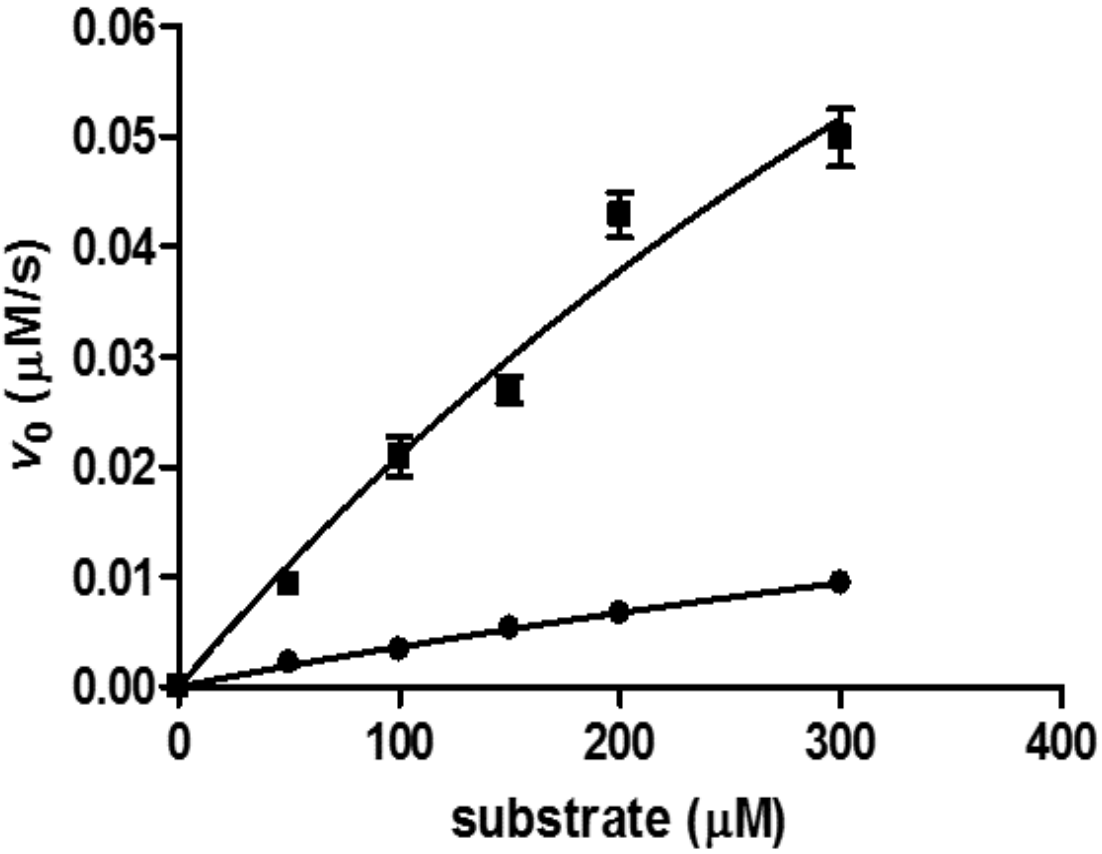

Figure 4.2: Representative data of metal-dependent reactivity of HDAC8 with a non-methylcoumarin labeled peptide

Dependence of the initial rates for Zn^{2+}-HDAC8- (●) and Fe^{2+}-HDAC8- (■) catalyzed deacetylation on the concentration of a SMC3-derived 10-mer peptide (50 – 300 μM). Reactions were initiated by addition of enzyme (1 μM) in 25 mM HEPES pH 8, 137 mM NaCl, 3 mM KCl at 30°C. After quenching the reaction, acetate product was coupled to the formation of NADH, as measured by fluorescence. The Michaelis-Menten equation was fit to the data.

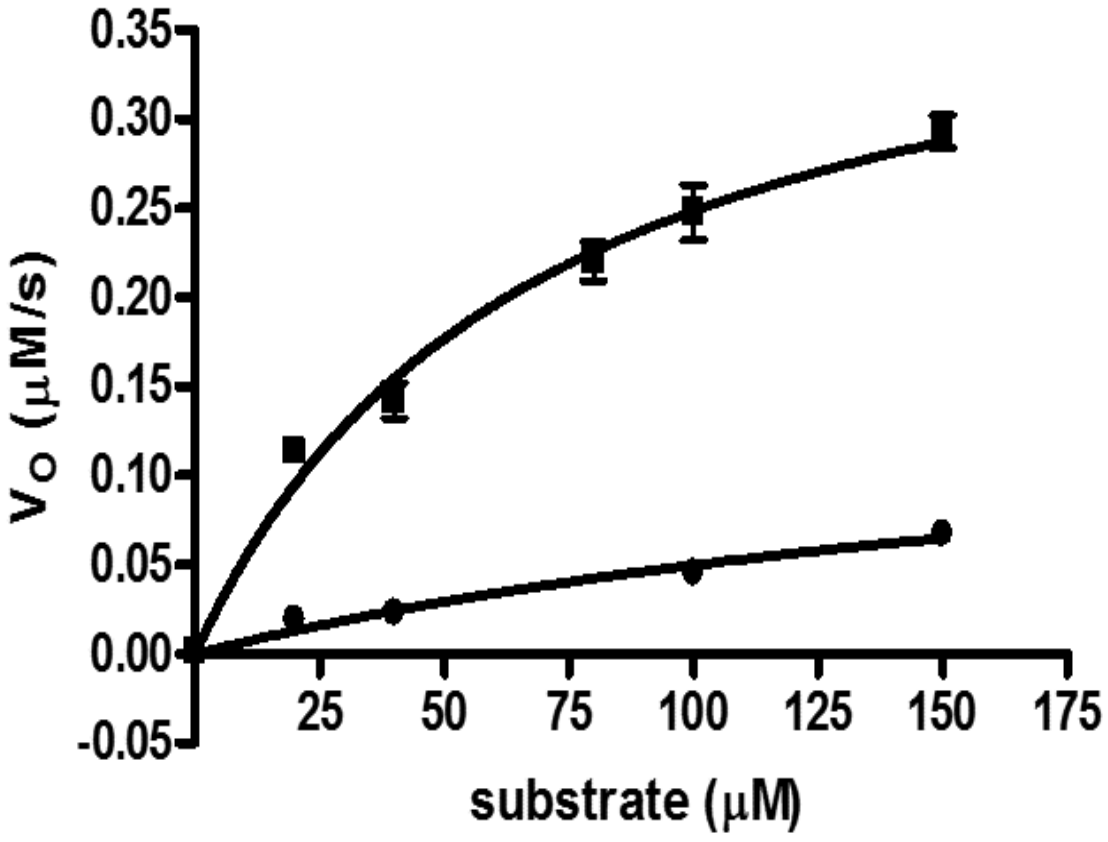

Figure 4.3: Representative data of metal-dependent reactivity of HDAC8 with a methylcoumarin labeled peptide

Dependence of the initial rates for Zn^{2+}-HDAC8- (●) and Fe^{2+}-HDAC8- (■) catalyzed deacetylation on the concentration of a SIRT1 C-terminal methylcoumarin peptide (20 – 150 μM). Reactions were initiated by addition of enzyme (1 μM) in 25 mM HEPES pH 8, 137 mM NaCl, 3 mM KCl at 30°C. After quenching the reaction, free methylcoumarin was monitored through fluorescence using the commercially available Fluor de Lys developer conditions. The Michaelis-Menten equation was fit to the data.

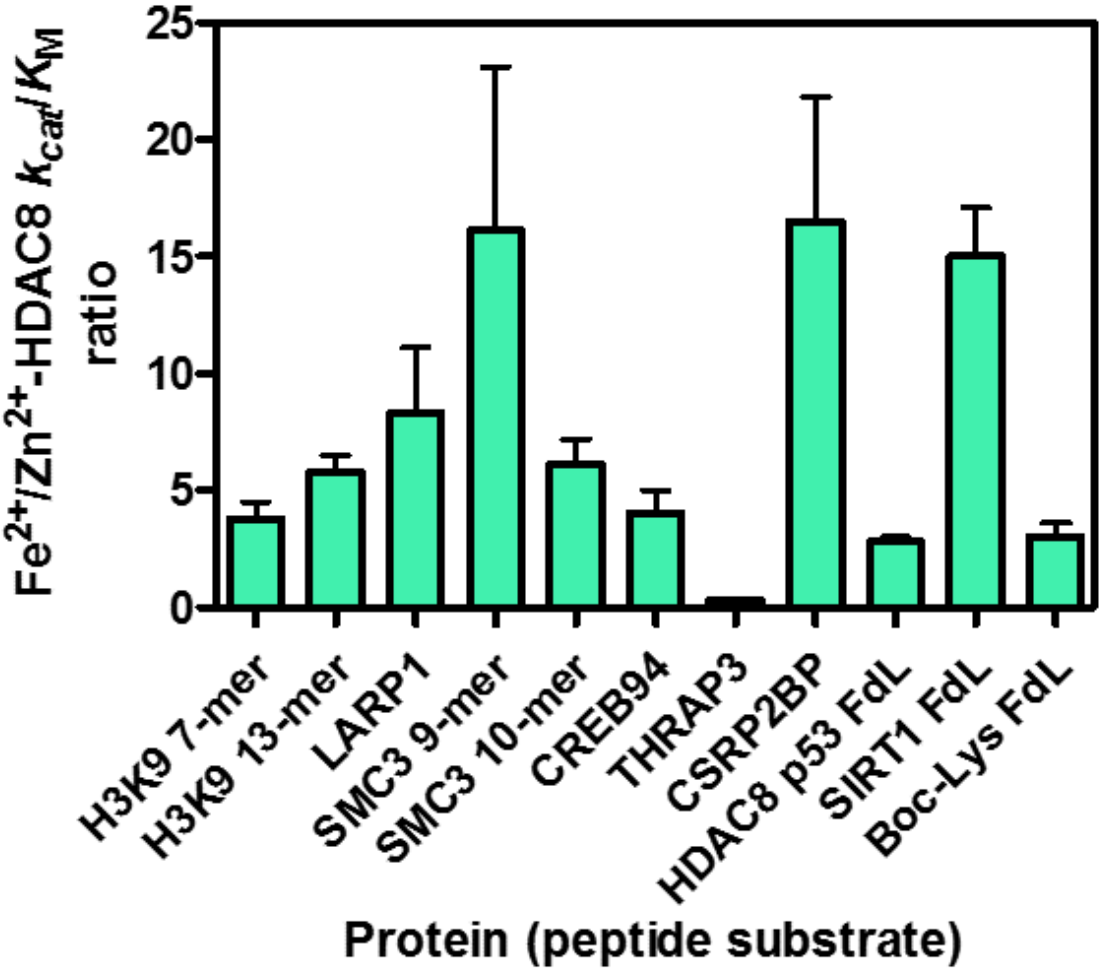

Figure 4.4: Ratio of k_{cat}/K_M values catalyzed by Fe^{2+}/Zn^{2+} HDAC8 for various peptide substrates

The values of k_{cat}/K_M were calculated from the dependence of the initial rates on the peptide concentration (25 – 400 μM) catalyzed by 1 μM HDAC8 in assay buffer. The ratios of the k_{cat}/K_M values for Fe^{2+}-HDAC8 / Zn^{2+}-HDAC8 are shown. The error was calculated using the equation listed in the legend of Table 4.1.

For the peptides measured, the k_{cat}/K_M values Fe^{2+}-HDAC8 are higher than values for Zn^{2+}-HDAC8 for all except one peptide (THRAP3). The ratios of the k_{cat}/K_M values catalyzed by Fe^{2+}-/Zn^{2+} HDAC8 vary from 0.3 to 17 (Table 4.1) further demonstrating that substrate selectivity is dependent on the identity of the active site metal ion. For the non-coumarin peptides, the increased selectivity ratio generally correlates with an increase in the value of k_{cat}/K_M for reaction of a peptide with Fe^{2+}-HDAC8 with the exception of the LARP1 peptide. In fact, there is a linear correlation between Fe/Zn selectivity ratio and Fe^{2+}-HDAC catalyzed k_{cat}/K_M values (removing the LARP1 peptide data) with R = 0.8. This suggests that the differential reactivity for the majority of peptides is mainly explained by an increased reactivity with Fe^{2+}-HDAC8 relative to Zn^{2+}-HDAC8. Therefore, these data suggest alterations in the structure or dynamics of the Fe^{2+}-substituted HDAC8 that lead to enhanced interactions with peptides that increase binding affinity and/or reactivity of the catalytic metal-bound water nucleophile. From crystal structures, we know that the HDAC8 divalent metal ion active site is in a square planar coordination[15,16,31]. However, these crystal structures have hydroxamic acid inhibitors bound and we think it is possible that these inhibitors restrict the conformations that the active site metal ion can adapt. We propose that Fe^{2+}-HDAC8 can adopt other coordination motifs in the absence of bound inhibitors, such as a trigonal bipyramidal conformation, and this flexibility can accommodate and catalyze deacetylation of more diverse substrates than Zn^{2+}-HDAC8.

The reactivity data (Table 4.1) suggest several potential determinants of the metal-dependent HDAC8 substrate selectivity. The first potential determinant is peptide length. For the peptides based on Histone H3, an increase in peptide length from 7 to 13 amino acids resulted in an increase in the Fe^{2+}/Zn^{2+} ratio, due to an increase in the k_{cat}/K_M value

for Fe^{2+}-HDAC8 only. This result suggests that additional HDAC8-substrate interactions can occur with the Fe^{2+}-enzyme that affect substrate binding affinity or deacetylation activity. We hypothesize that interactions outside of short peptide sequences (i.e. long range interactions) are important for enhancing HDAC8 substrate specificity[25]. However, peptide length alone is not likely an important determinant of metal-dependent selectivity as there is no correlation between the selectivity ratio and peptide length (R = 0.06).

The Flex-Pep-Bind analysis of peptide selectivity of HDAC8 suggests that the three upstream and two downstream side chains flanking the acetyllysine as well as the conformation of the peptide substrate are important for peptide recognition by Zn^{2+}-HDAC8[29]. Based on this model, the main determinant of the metal dependent selectivity ratio is likely due to varied interactions with specific peptide side chains. The SMC3 peptides provide a clear illustration of this effect since they vary only by the presence or absence of a tyrosine residue at the +3 position. In this case, addition of the +3 Tyr residue increased the activity of Zn^{2+}-HDAC8 by 2-fold, while the Fe^{2+}-HDAC8 activity remained constant, thereby decreasing the Fe^{2+}/Zn^{2+} ratio from 16 (9-mer) to 6 (10-mer). It is possible that Zn^{2+}-HDAC8 forms stable interactions with +3 aromatic residues that are not needed for Fe^{2+}-HDAC8.

Furthermore, the residues flanking the acetyllysine moiety could be particularly important for metal-dependent HDAC8-substrate recognition. Both peptides with +1 Phe residues (LARP1 and CSRP2BP) are Fe^{2+}-specific substrates with Fe^{2+}/Zn^{2+} ratios 8 and 16, respectively. These data suggest that a Phe at the +1 position enhances reactivity with Fe^{2+}-HDAC8. However this is not the only determinant of the metal-dependent selectivity as the SMC3 9-mer has a Fe^{2+}/Zn^{2+} ratio of 16 but has an Asp at the +1

position. Additionally, the data suggest that a Met residue at the +1 position may decrease reactivity as low activity was observed with the peptides in the screen (Figure 4.1). Furthermore, THRAP3 has a +1 Met residue and reacts slowly with both enzyme forms. The +1 Met residue may interfere with local HDAC8-substrate interactions and decrease the stability of the enzyme-substrate complex. These data suggest that while the +1 (Z) and -1 (X) positions are important determinants of the metal-dependent substrate selectivity, the residues at other local sites also alter selectivity. This avenue remains to be investigated further.

Finally, data from the methylcoumarin labeled peptides suggests that a -1 K_{ac} could present a detriment to HDAC8-catalyzed deacetylation. Both SIRT1 and HDAC8 FdL substrates are based on a small p53 peptide, with the only difference between the two being that both lysines are acetylated in the HDAC8 FdL substrate while only the terminal lysine adjacent to the methylcoumarin is acetylated in the SIRT1 substrate. Even though these peptides have the most sequence similarity, the Fe^{2+}/Zn^{2+} ratios exhibit the biggest differential between these two peptides, with ratios of 3 and 15, respectively, for the p53 FdL and SIRT FdL substrates. These data suggest that HDAC8-catalyzed deacetylation is altered by acetylation and, possibly, other PTMs, near the target acetyllysine.

The data presented reveal that HDAC8 substrate selectivity may depend on the identity of the bound divalent metal ion. Although many peptides have comparable reactivity with both Fe^{2+}- and Zn^{2+}-HDAC8, other peptides have significantly higher reactivity with the iron-bound enzyme. The data suggest that peptide sequence, length and local interactions with residues flanking the acetyl lysine moiety are synergistic in determining the metal-dependent selectivity of HDAC8. Furthermore, these data predict

that in cells either metallated form of HDAC8 has deacetylase activity and that manipulating the identity of the divalent metal bound could possibly alter the pool of reactive protein substrates.

Remarkably, the ratio of the Fe^{2+} and Zn^{2+}-HDAC8 activities varies greatly depending on the sequence of the substrate peptide. Our laboratory has previously shown that Fe^{2+}-HDAC8 haa a higher k_{cat}/K_M value than Zn^{2+}-HDAC8 for a commercial methyl-coumarin labeled peptide[15] (Table 4.1), Here we demonstrate that even for short 6-mer peptides, which interact only with the active site and substrate binding surface directly near the active site, there are drastic differences in specificity based on the divalent metal ion. A constant Fe^{2+}/Zn^{2+} ratio for all peptides tested would have suggested that changing the identity of the divalent metal ion was a method to modulate overall cellular deacetylation. However, the substrate-dependent variation in the Fe^{2+}/Zn^{2+} ratio indicates a more complicated mechanism of regulation that involves altering both the activity and selectivity of HDAC8 which is predicted to lead to differential changes in cellular acetylation.

The structural basis for the metal-dependent substrate specificity remains undefined. Crystal structures of HDAC8 indicate that the substrate binding site is primarily composed of flexible loops which can accommodate a range of substrates but can also influence the enzyme's specificity[13,28,32–34]. Furthermore, the residues that coordinate the active site divalent metal ion are positioned by these loops. Intrinsic properties of the divalent metal ion, including Lewis acidity and size, could influence the structure and dynamics of the loop regions and alter the binding interface presented to substrates. Altering the active site metal coordination is expected to propagate structural changes to

the peptide binding site via the residues in the hydrophobic shell around the metal ligands[35].

The metal-dependent selectivity of HDAC8 may be important for regulating levels of acetylated proteins in the cell, particularly because relative concentrations of Zn^{2+} and Fe^{2+} fluctuate with changing cellular conditions[20,36]. For example, cellular zinc is tightly buffered but the concentration of exchangeable Zn^{2+} is increased under redox stress as cellular zinc ligands are oxidized and release Zn^{2+}.[37] Zn^{2+} concentrations can increase from picomolar (pM) to nanomolar levels (nM) under oxidative stress[37]. The dependence of readily exchangeable Fe^{2+} concentration on the redox state is unclear, likely due to the limits of detection and differentiation from Fe^{3+}. We have previously shown that the metal-dependent bacterial deacetylase LpxC binds either Zn^{2+} or Fe^{2+} in *E. coli* based on the relative abundance of these metals in the growth conditions, and that the metal cofactor bound to LpxC readily switches from Fe^{2+} to Zn^{2+} under aerobic conditions *in vitro*[38]. A similar mechanistic model may occur for metal-dependent HDACs. One scenario is that Fe^{2+}-HDAC8 (K_D = 0.2 ± 0.1 μM)[21] is the predominant species under basal conditions with low exchangeable Zn^{2+} concentrations, but upon an increased exchangeable Zn^{2+} concentration, HDAC8 exchange bound Fe^{2+} for the higher affinity Zn^{2+} (K_D = 5 ± 1 pM)[21], maintaining HDAC8 activation but altering the activity level and substrate selectivity.

Our peptide data present a universal trend of greater catalytic efficiency for the Fe^{2+}-bound enzyme among the longer, more physiologically relevant peptides and supports our initial screen where we saw a significant difference between peptide specificity for both metalloforms, These data are consistent with the hypothesis that the enzyme is activated, at least in part, by Fe^{2+} in the cell. Furthermore, it is possible that

the peptides with a high ratio of Fe^{2+}/Zn^{2+} activity may represent *in vivo* substrates while peptides with a near stoichiometric ratio may be nonspecific substrates. This is bolstered by the fact that the two highest Fe^{2+}/Zn^{2+} ratios (SMC3 9-mer and CSRP2BP) correspond to proteins recently identified as potential HDAC8 substrates in a proteomic screen[11].

Conclusions

Overall, this work is the first to demonstrate that the substrate selectivity of a metal-dependent HDAC varies with the identity of the active site divalent metal ion. The SAMDI peptide screen enabled a broad survey of enzyme metalloform selectivity, and the enzyme assays in solution demonstrated a range of Fe^{2+}/Zn^{2+} ratios towards substrates of physiological relevance. There is no direct evidence that metal switching plays an important regulatory role in cells. However, our data alludes to the possibility that cellular conditions dictate the active site divalent metal ion and this seems to regulate deacetylation of specific protein targets.

Acknowledgements

We thank Dr. Eric D. Sullivan for collaborating with protein purification. This work was funded by the National Institutes of Health (Grants NIGMS GM040602 [C.A.F.], F31-GM-116619 [J.E.L.]), the University of Michigan Chemistry-Biology Interface training (CBI) program (T32-GM-008597 [C.A.P.]) and the Rackham Graduate School [C.A.P.] [J.E.L]

Bibliography

(1) Verdin, E., and Ott, M. (2014) 50 years of protein acetylation: from gene regulation to epigenetics, metabolism and beyond. *Nat. Rev. Mol. Cell Biol. 16*, 258–64.

(2) Norris, K. L., Lee, J.-Y., and Yao, T.-P. (2009) Acetylation Goes Global: The Emergence of Acetylation Biology. *Sci. Signal. 2*, pe76-pe76.

(3) Khoury, G. A., Baliban, R. C., and Floudas, C. A. (2011) Proteome-wide post-translational modification statistics: frequency analysis and curation of the swiss-prot database. *Sci. Rep. 1*.

(4) Smith, K. T., and Workman, J. L. (2009) Introducing the acetylome. *Nat. Biotechnol. 27*, 917–919.

(5) Haberland, M., Montgomery, R. L., and Olson, E. N. (2009) The many roles of histone deacetylases in development and physiology: implications for disease and therapy. *Nat. Rev. Genet. 10*, 32–42.

(6) Waltregny, D., de Leval, L., Glénisson, W., Ly Tran, S., North, B. J., Bellahcène, A., Weidle, U., Verdin, E., and Castronovo, V. (2004) Expression of Histone Deacetylase 8, a Class I Histone Deacetylase, Is Restricted to Cells Showing Smooth Muscle Differentiation in Normal Human Tissues. *Am. J. Pathol. 165*, 553–564.

(7) Hu, E., Chen, Z., Fredrickson, T., Zhu, Y., Kirkpatrick, R., Zhang, G. F., Johanson, K., Sung, C. M., Liu, R., and Winkler, J. (2000) Cloning and characterization of a novel human class I histone deacetylase that functions as a transcription repressor. *J. Biol. Chem. 275*, 15254–64.

(8) Deardorff, M. A., Bando, M., Nakato, R., Watrin, E., Itoh, T., Minamino, M., Saitoh, K., Komata, M., Katou, Y., Clark, D., Cole, K. E., De Baere, E., Decroos, C., Di Donato, N., Ernst, S., Francey, L. J., Gyftodimou, Y., Hirashima, K., Hullings, M., Ishikawa, Y., Jaulin, C., Kaur, M., Kiyono, T., Lombardi, P. M., Magnaghi-Jaulin, L., Mortier, G. R., Nozaki, N., Petersen, M. B., Seimiya, H., Siu, V. M., Suzuki, Y., Takagaki, K., Wilde, J. J., Willems, P. J., Prigent, C., Gillessen-Kaesbach, G., Christianson, D. W., Kaiser, F. J., Jackson, L. G., Hirota, T., Krantz, I. D., and Shirahige, K. (2012) HDAC8 mutations in Cornelia de Lange syndrome affect the cohesin acetylation cycle. *Nature 489*, 313–7.

(9) Buggy, J. J., Sideris, M. L., Mak, P., Lorimer, D. D., McIntosh, B., and Clark, J. M. (2000) Cloning and characterization of a novel human histone deacetylase, HDAC8. *Biochem. J. 350 Pt 1*, 199–205.

(10) Gao, J., Siddoway, B., Huang, Q., and Xia, H. (2009) Inactivation of CREB mediated gene transcription by HDAC8 bound protein phosphatase. *Biochem. Biophys. Res. Commun. 379*, 1–5.

(11) Olson, D. E., Udeshi, N. D., Wolfson, N. A., Pitcairn, C. A., Sullivan, E. D., Jaffe, J. D., Svinkina, T., Natoli, T., Lu, X., Paulk, J., McCarren, P., Wagner, F. F., Barker, D., Howe, E., Lazzaro, F., Gale, J. P., Zhang, Y.-L., Subramanian, A., Fierke, C. A., Carr, S. A., and Holson, E. B. (2014) An unbiased approach to identify endogenous substrates of

“histone” deacetylase 8. *ACS Chem. Biol. 9*, 2210–6.

(12) Wilson, B. J., Tremblay, A. M., Deblois, G., Sylvain-Drolet, G., and Giguère, V. (2010) An acetylation switch modulates the transcriptional activity of estrogen-related receptor alpha. *Mol. Endocrinol. 24*, 1349–1358.

(13) Wolfson, N. A., Ann Pitcairn, C., and Fierke, C. A. (2013) HDAC8 substrates: Histones and beyond. *Biopolymers 99*, 112–26.

(14) Vannini, A., Volpari, C., Filocamo, G., Casavola, E. C., Brunetti, M., Renzoni, D., Chakravarty, P., Paolini, C., De Francesco, R., Gallinari, P., Steinkühler, C., and Di Marco, S. (2004) Crystal structure of a eukaryotic zinc-dependent histone deacetylase, human HDAC8, complexed with a hydroxamic acid inhibitor. *Proc. Natl. Acad. Sci. U. S. A. 101*, 15064–9.

(15) Gantt, S. L., Gattis, S. G., and Fierke, C. A. (2006) Catalytic activity and inhibition of human histone deacetylase 8 is dependent on the identity of the active site metal ion. *Biochemistry 45*, 6170–8.

(16) Dowling, D. P., Gattis, S. G., Fierke, C. A., and Christianson, D. W. (2010) Structures of metal-substituted human histone deacetylase 8 provide mechanistic inferences on biological function . *Biochemistry 49*, 5048–56.

(17) Bozym, R. A., Thompson, R. B., Stoddard, A. K., and Fierke, C. A. (2006) Measuring Picomolar Intracellular Exchangeable Zinc in PC-12 Cells Using a Ratiometric Fluorescence Biosensor. *ACS Chem. Biol. 1*, 103–111.

(18) Vinkenborg, J. L., Nicolson, T. J., Bellomo, E. A., Koay, M. S., Rutter, G. A., and Merkx, M. (2009) Genetically encoded FRET sensors to monitor intracellular Zn2+ homeostasis. *Nat. Methods 6*, 737–740.

(19) Epsztejn, S., Kakhlon, O., Glickstein, H., Breuer, W., and Cabantchik, I. (1997) Fluorescence analysis of the labile iron pool of mammalian cells. *Anal. Biochem. 248*, 31–40.

(20) Kim, A. M., Vogt, S., O’Halloran, T. V, and Woodruff, T. K. (2010) Zinc availability regulates exit from meiosis in maturing mammalian oocytes. *Nat Chem Biol 6*, 674–681.

(21) Kim, B., Pithadia, A. S., and Fierke, C. A. (2015) Kinetics and thermodynamics of metal-binding to histone deacetylase 8. *Protein Sci. 24*, 354–365.

(22) Gattis, S. G. (2010) Mechanism and Metal Specificity of Zinc-dependent deacetylases. University of Michigan.

(23) Gurard-Levin, Z. A., Kilian, K. A., Kim, J., Bähr, K., and Mrksich, M. (2010) Peptide Arrays Identify Isoform-Selective Substrates for Profiling Endogenous Lysine Deacetylase Activity. *ACS Chem. Biol. 5*, 863–873.

(24) Gurard-Levin, Z. A., Kim, J., and Mrksich, M. (2009) Combining mass spectrometry and peptide arrays to profile the specificities of histone deacetylases. *ChemBioChem 10*, 2159–2161.

(25) Gurard-Levin, Z. A., and Mrksich, M. (2008) The activity of HDAC8 depends on local and distal sequences of its peptide substrates. *Biochemistry 47*, 6242–50.

(26) Mrksich, M. (2008) Mass Spectrometry of Self-Assembled Monolayers : A New Tool for Molecular. *ACS Nano 2*, 7–18.

(27) Kim, B. (2014) Probing the determinants of Molecular Recognition in metal-dependent deacetylases. University of Michigan.

(28) Wolfson, N. A., Pitcairn, C. A., Sullivan, E. D., Joseph, C. G., and Fierke, C. A. (2014) An enzyme-coupled assay measuring acetate production for profiling histone deacetylase specificity. *Anal. Biochem. 456*, 61–69.

(29) Alam, N., Zimmerman, L., Wolfson, N. A., Joseph, C. G., Fierke, C. A., and Schueler-Furman, O. (2016) Structure-Based Identification of HDAC8 Non-histone Substrates. *Structure 24*, 458–468.

(30) Alam, N., Zimmerman, L., Wolfson, N. A., Joseph, C. G., Fierke, C. A., and Schueler-Furman, O. (2016) Structure-Based Identification of HDAC8 Non-histone Substrates. *Structure 24*, 458–68.

(31) Gantt, S. M. L., Decroos, C., Lee, M. S., Gullett, L. E., Bowman, C. M., Christianson, D. W., and Fierke, C. A. (2016) General Base-General Acid Catalysis in Human Histone Deacetylase 8. *Biochemistry*.

(32) Dowling, D. P., Gantt, S. L., Gattis, S. G., Fierke, C. A., and Christianson, D. W. (2008) Structural studies of human histone deacetylase 8 and its site-specific variants complexed with substrate and inhibitors. *Biochemistry 47*, 13554–63.

(33) Vannini, A., Volpari, C., Gallinari, P., Jones, P., Mattu, M., Carfí, A., De Francesco, R., Steinkühler, C., and Di Marco, S. (2007) Substrate binding to histone deacetylases as shown by the crystal structure of the HDAC8–substrate complex. *EMBO Rep. 8*, 879–884.

(34) Decroos, C., Christianson, N. H., Gullett, L. E., Bowman, C. M., Christianson, K. E., Deardorff, M. A., and Christianson, D. W. (2015) Biochemical and Structural Characterization of HDAC8 Mutants Associated with Cornelia de Lange Syndrome Spectrum Disorders. *Biochemistry 54*, 6501–6513.

(35) Kim, B., Lopez, J. E., Pitcairn, C. A., and Fierke, C. A. (2017) Second Shell Residues Modulate the Reactivity and Metal Selectivity of Histone Deacetylase 8. *Prep.*

(36) Kim, A. M., Bernhardt, M. L., Kong, B. Y., Ahn, R. W., Vogt, S., Woodruff, T. K., and O'Halloran, T. V. (2011) Zinc sparks are triggered by fertilization and facilitate cell cycle resumption in mammalian eggs. *ACS Chem. Biol. 6*, 716–723.

(37) Maret, W., and Krezel, A. (2007) Cellular zinc and redox buffering capacity of metallothionein/thionein in health and disease. *Mol. Med. 13*, 1.

(38) Gattis, S. G., Hernick, M., and Fierke, C. A. (2010) Active site metal ion in UDP-3-O-((R)-3-hydroxymyristoyl)-N-acetylglucosamine deacetylase (LpxC) switches between Fe(II) and Zn(II) depending on cellular conditions. *J. Biol. Chem. 285*, 33788–96.

Chapter 5

Conclusions and Future Directions

Overview

Since the discovery of acetylation of histone tails[1], the acetylome has been expanded and many non-histone acetylated proteins have been predicted and discovered[2,3]. Acetylation has been recognized to affect proteins in many cellular processes, such as cell cycle regulation, metabolism and gene expression[2]. With the ongoing expansion of the acetylome, research has focused on understanding how this post-translational modification is regulated. The enzymes that catalyze acetylation and deacetylation are the lysine acetyltransferases and histone (or acetyllysine) deacetylases. To date, there are 18 deacetylases that catalyzing deacetylation, 11 of which are metal dependent enzymes.

One crucial piece of information that the acetylation field is currently attempting to unravel is the substrate specificity of each HDAC isozyme. These data would allow a better understanding of the role of each isozyme in the cell. In this thesis, I have presented work that improves upon the understanding of the function of HDAC8 by characterizing regulation by metal switching and the role that alterations in metal affinity could play in Cornelia de Lange spectrum disorders. Additionally, I have improved upon traditional

HDAC-substrate recognition methods using chemical covalent capture and discovered new HDAC8 substrates. Overall, these findings describe a new set of techniques that could be adapted for use in analyzing the function of other HDAC isozymes and, potentially, other enzymes that catalyze posttranslational modifications.

Chemical Covalent Capture of HDAC8 Substrates

One of the most important goals in the acetylation field is to profile HDAC-specific substrates. This specific profiling has proven difficult due to the continuous discovery of new acetylated proteins, the dynamic nature of HDAC-substrate interactions and the reactivity of multiple HDAC isozymes with particular substrates[4]. Efforts to map the acetylome include computational modeling of acetylation[3], SILAC studies along with both pan-HDAC and HDAC specific inhibitors[4], and HDAC-eGFP fusion proteins expressed in mammalian cells[5]. Although these methods have proven useful in providing insight into HDAC substrates, they remain limited in identifying transient HDAC-substrate interactions and highlighting HDAC-specific substrates. Here, we report an improved chemical covalent capture method to identify transient complexes using HDAC8 as a model isozyme. This approach takes advantage of site specific labeling with a cross linker followed by mass spectrometry and proteomics to identify HDAC8 binding proteins and potential substrates.

Previous work in the Fierke laboratory demonstrated crosslinking using Bpa-labeled Rpd3, HDAC8's yeast ortholog. I elaborated on this concept and developed an HDAC8 co-immunoprecipitation and crosslinking assay using HEK293 lysate. We coupled this assay with LC-MS/MS, proteomics and the Flex-Pep-Bind algorithm[6] to

predict reactive acetyl lysine residues in proteins that were covalently trapped with HDAC8. I then tested the highest scoring protein-based peptides using an enzyme-coupled assay[7] and demonstrated that many of the peptides tested have equal and/or faster deacetylation than an SMC3-based peptide, the best validated HDAC8 substrate.

This improved approach has allowed us to identify 139 HDAC8 potential substrates that had not been found by any other previous techniques. We identified proteins involved in a variety of cellular pathways, including metabolism, DNA repair, protein folding, among others. Many of these putative substrates were primarily new HDAC targets but some have been identified in previous studies[5,8]. We found PFKP and TUBA1A, both identified as potential HDAC8 substrates by proteome chips[8] and HDAC8-eGFP fusion protein immunoprecipitation studies[5], respectively. Further studies of intact protein substrates, beyond peptide deacetylation, will be needed to further validate the pool of HDAC8-specific substrates.

Some of the most interesting HDAC8 substrates identified through crosslinking are heat shock protein 90-beta (HSP90AB1), ATP-citrate lyase (ACLY), integrin beta-1 (ITGB1) and the regulator of nonsense transcripts (UFP1). I measured HDAC8-catalyzed deacetylation of the best scoring peptides for each of these proteins and found rate constants of over 100 $M^{-1}s^{-1}$.

The next step is to further validate this approach. One method would be to express and purify these proteins recombinantly using amber suppression methods to incorporate single, non-natural acetyl lysine residue at positions observed in cells and measure HDAC8-catalyzed deacetylation visualized using an anti-acetyl lysine antibody. To start this project, I have prepared constructs for expressing HSP90AB1 (WT and K429ac) with

site specific incorporation of a single acetyl lysine in *E. coli* and I plan to purify these enzymes and measure rates of deacetylation of the full-length protein substrate.

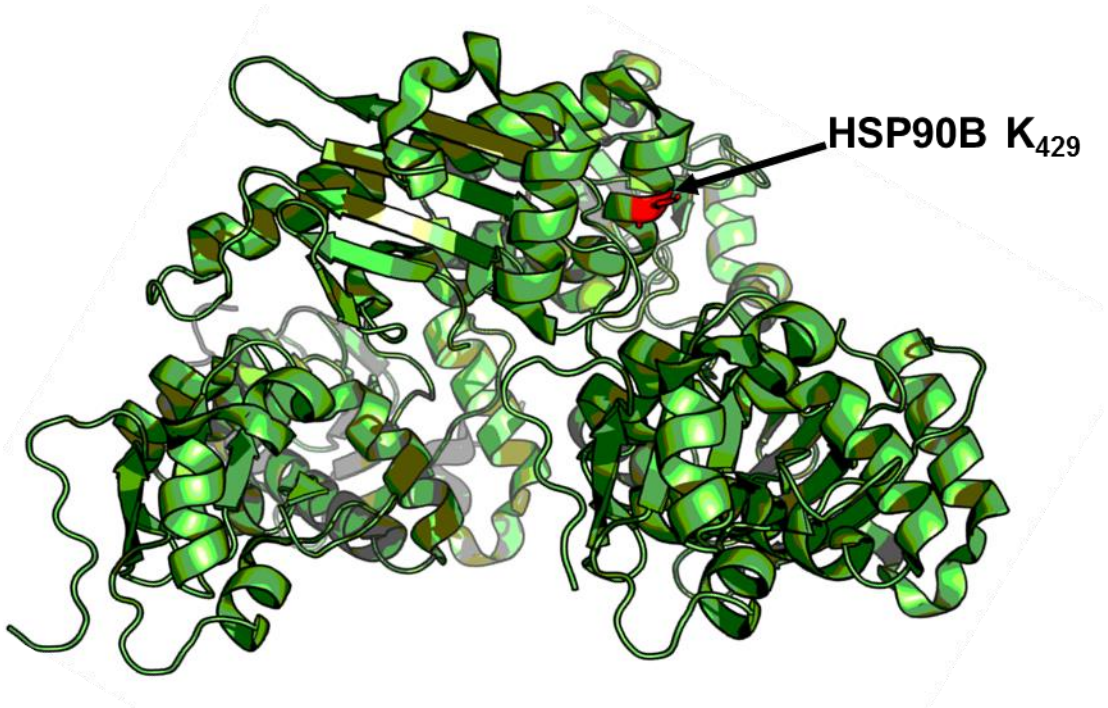

Figure 5.1: Proposed acetylation site of HSP90B

Full-length structure of HSP90B (PDB: 3PRY). My work has shown that a small acetylated peptide based on the sequence around K429 is readily deacetylated by HDAC8 (Table 2.2 and Figure 2.5A). Purification of HSP90B with acetylated K429 and testing HDAC8-catalyzed deacetylation will further validate this protein as an HDAC8 target in the cytoplasm.

Additionally, further validation would require *in vivo* evidence showing an increase in acetylation of these proteins upon HDAC8 specific inhibition. Acetylation of cellular proteins before and after treatment with the inhibitor could be visualized using an anti-acetyl lysine antibody and/or quantified using mass spectrometry. The effect of acetylation on the function of these proteins is currently unknown. However, a comparison of the properties of the native and singly acetylated protein will begin to answer this question as well as provide insight into HDAC8's role in cellular processes.

We expect that further work in the Fierke laboratory will incorporate non-natural amino acid cross linkers into other HDAC isozymes in order to gain further knowledge of the acetylome as well as the specific role of each HDAC.

However, this method still requires optimization to be carried out inside mammalian cells rather than in cell lysates. Protein-substrate localization is a problem when working with cellular lysates and some of the proteins that crosslinked to HDAC8 are proposed to be exclusively located in the mitochondria, a cell compartment where HDAC8 has not observed. Unfortunately, the main problem with incorporation of non-natural amino acids is the slow expression of tRNA and slow growth in mammalian cells, which decreases the fidelity and synthesis of the target protein. Currently, optimization of this system by increasing tRNA/tRNA synthetase levels in combination with engineered release factors (RFs) has shown promise in non-natural amino acid protein synthesis fidelity in both mammalian cells and *E.coli*[9,10]. We anticipate that the development of these systems will allow us to further optimize, incorporate and diversify our crosslinking system into mammalian cells in the near future.

Effects of HDAC8 CdLS mutants on Catalysis

HDAC8's best known biological role is the deacetylation of SMC3, a component of the cohesin complex[11]. The cohesin complex is responsible for the proper separation of sister chromatids during mitosis. Mutations in the genes that encode these complex components are responsible for the Cornelia de Lange spectrum (CdLS) disorders. It was recently discovered that missense mutations in the HDAC8 gene can also lead to CdLS

phenotypes[11]. These missense mutations result in partial to complete loss of deacetylase activity. Basic biochemical characterization of some of these mutants has been performed[12,13] but many questions remain about how these mutations affect deacetylase activity. Many of these mutations are not close to the active site and are not in residues that are known to be involved in catalysis. In our work, we studied three mutations (P91L, I243N and T311M) with different effects on catalysis using multiple biochemical approaches. We hypothesize that the effects of these mutations on catalytic activity could be attributed to small, minimal changes in the internal bonding network of HDAC8 while still retaining its overall secondary structure.

We demonstrated that although each mutant retains its overall secondary structure, the effects on catalysis are varied. The P91L mutant retained properties most similar to WT-HDAC8. The P91L mutation has been hypothesized to affect substrate binding by altering the positioning and flexibility of the L1 loop, decreasing peptide-substrate affinity and increasing product release[12,14,15]. Our data indicates that this mutation has little effect on the catalytic activity with peptides (Table 3.1 and Table 3.3) suggesting that it does not significantly alter peptide-substrate affinity, however, it is possible that peptide substrate affinity does not reflect the effects on full-length protein substrate affinity. The T311M mutation has a larger effect on the catalytic activity and this mutation has been proposed to alter the internal bonding network that helps coordinate product release and to possibly affect substrate affinity by leading to a reorganization of the L1 loop[14,15]. Our data demonstrate that both the T311M and I243 mutations significantly decrease Zn^{2+} binding affinity while retaining Fe^{2+} binding affinity. This loss of zinc binding affinity likely leads to loss of deacetylase activity in cells where the readily

exchangeable zinc concentration is in the pM range[16,17]. However, it is unclear what structural alterations occur in the T311M mutant that specifically affect Zn^{2+} affinity.

I243N HDAC8 is the most interesting mutant to perform follow up work. This mutant is located near one of the monovalent ion (K^+) binding sites that activates HDAC8 in a time-dependent manner[18], likely by stabilizing protein structure. We hypothesize that mutations near this site could either significantly decrease K^+ binding to this site and inhibit activation or allow K^+ binding that is uncoupled to enzyme activation. The unexpected effect of decreasing Zn^{2+} but not Fe^{2+} affinity leads to the suggestion that there could be multiple conformations that Fe^{2+} binds to with similar affinity while high affinity Zn^{2+} binding requires a specific enzyme conformation to be activated (Figure 5.2).

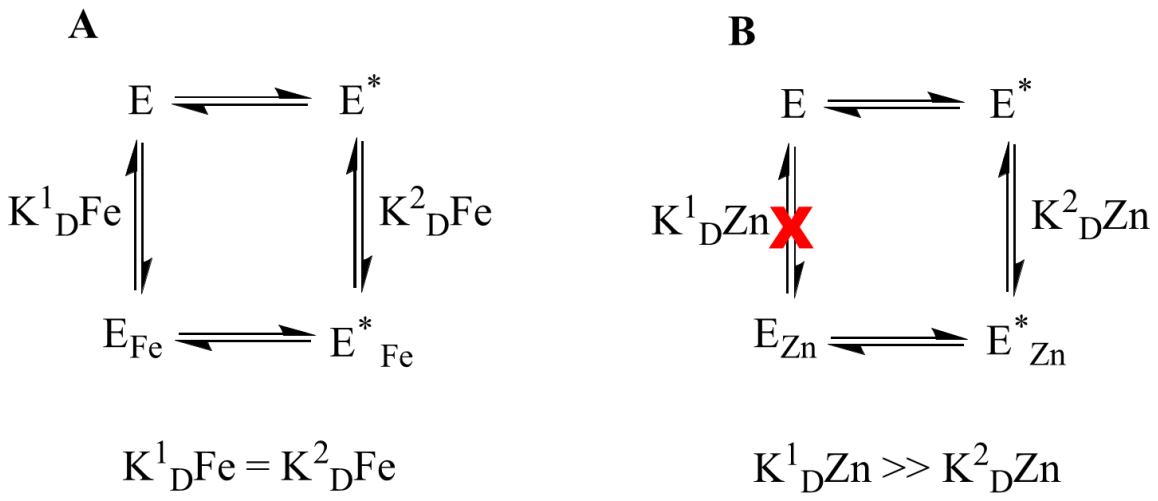

Figure 5.2: Potential mechanisms of divalent metal ion binding

Proposed mechanism of how the I243N mutation affects Fe^{2+} (A) and Zn^{2+} (B) binding and activation. We hypothesize that Fe^{2+} is capable of binding to two different enzyme forms with similar affinities, and that both forms possess some degree of catalytic efficiency while Zn^{2+} can only bind a form of the enzyme that is not activated. In order to probe this mechanism, we must identify the intrinsic differences between Fe^{2+} and Zn^{2+} bound HDAC8.

A future way to investigate this proposed mechanism would be to monitor deacetylase activity as a function of K^+ concentration as well as following changes in secondary structure as a function of K^+ concentration using circular dichroism for both WT and the mutants. Additionally, investigation of more CdLS mutations would provide insight into structural changes in HDAC8 that are important for catalysis.

Overall, these studies have provided insight into how HDAC8-catalyzed deacetylation is regulated by internal structural rearrangements.

HDAC8 Substrate Specificity Regulated Through Divalent Metal Switching

Previous studies have shown that HDAC8 is activated by by either Fe^{2+} or Zn^{2+}. and metal chelating inhibitors, such as suberanilohydroxamic acid (SAHA), exhibit efficacy towards both enzyme metalloforms[15]. This brings into question the identity of the catalytic metal ion *in vivo*. HDAC deacetylase activity in mammalian and *E. coli* lysates, as well as immunopurified HDAC8 from HeLa cells, have shown oxygen sensitivity[16]. We hypothesize that based on oxidative stress and/or other cellular conditions, HDAC8 is capable of exchanging between Zn^{2+} and Fe^{2+}, thus it could be possible for each metalloform to have different substrate specificities *in vivo*. Our data present evidence of metal-dependent substrate specificity through analyzing reactivity with both a high throughput peptide library as well as a library of peptides based on putative *in vivo* and methylcoumarin-bound substrates. We demonstrate that Fe^{2+}-HDAC8 catalyzes deacetylation faster than Zn^{2+}-HDAC8 of all but one of the substrates tested. The ratio of Fe/Zn deacetylation specificity rate constants varies between 0.3 and 15. Overall, we

have shown that Fe^{2+}-HDAC8 is significantly more active than Zn^{2+}-HDAC8 under the conditions tested and that the metal-dependent substrate selectivity is variable.

Additionally, our data suggest some determinants of HDAC8 substrate specificity including peptide length, stabilization by aromatic residues like Tyr and Phe at the +1 and +3 positions and potential inhibition of deacetylation by Met residues at the +1 residues. These data have provided insight on peptide-substrate selectivity for HDAC8 using biologically relevant metals.

However, the sample pool that we tested was not diverse enough to provide statistically significant validation of these determinants. Expanding the library of peptides tested using more peptides based on putative substrates and strategic varying of the peptide sequence would allow an enhanced understanding of the HDAC8 substrate selectivity. Additionally, HDAC8 reactivity could be altered by posttranslational modifications, particularly at the +1, -1 and +3 positions. This proposal could be tested by measuring reactivity of HDAC8 with peptides containing acetyl lysine, methyl lysine and/or phosphorylated residues at these sites. This would provide context into how other post-translational modifications affect acetylation in a direct manner.

Finally, a remaining question about HDAC8 substrate selectivity is the site(s) of additional interactions with full-length protein substrates that alter binding affinity relative to peptides. There are likely additional both positive and negative interactions, such as site flexibility, with proteins that alter selectivity relative to peptides. Despite this, our data clearly demonstrate that HDAC8 selectivity is altered depending on the identity of the active site metal ion. Investigating HDAC8 reactivity using full-length substrates will also examine how HDAC8 recognizes protein substrates based on the divalent metal bound.

Overall, our work demonstrates that peptide-substrate specificity of HDAC8 depends on the identity of the active site divalent metal ion. Our enzyme-coupled assays using physiologically relevant peptide substrates provide insight into the HDAC8's substrate recognition system. Understanding this specificity will provide avenues for substrate discovery and metal-specific inhibitor design.

Concluding remarks

The HDAC field is at an interesting crossroad where we are starting to understand what biological roles each isozyme plays in the cell. Particularly with HDAC8, great strides have been made to identify protein substrates and understand enzyme reactivity. The deacetylase field has acquired a lot of interest from the scientific community in recent years. More importantly, with the discovery of HDAC8's role in the Cornelia de Lange spectrum disorders, we have evidence of a disease in which HDAC8-catalyzed deacetylation plays an essential role in development. In the work presented here, we have made exciting breakthroughs, like the development of an improved HDAC8 co-immunoprecipitation approach along with the discovery of new HDAC8 substrates. The techniques described in this thesis will provide new tools to discover HDAC-specific substrates, understand how HDACs select their substrates *in vivo* and, in the nearby future, help to develop both isozyme-specific and metal-specific inhibitors.

Bibliography

(1) PHILLIPS, D. M. (1963) The presence of acetyl groups of histones. *Biochem. J. 87*, 258–63.

(2) Choudhary, C., Kumar, C., Gnad, F., Nielsen, M. L., Rehman, M., Walther, T. C., Olsen, J. V., and Mann, M. (2009) Lysine Acetylation Targets Protein Complexes and Co-Regulates Major Cellular Functions. *Science (80-.). 325*, 834–840.

(3) Khoury, G. A., Baliban, R. C., and Floudas, C. A. (2011) Proteome-wide post-translational modification statistics: frequency analysis and curation of the swiss-prot database. *Sci. Rep. 1*.

(4) Olson, D. E., Udeshi, N. D., Wolfson, N. A., Pitcairn, C. A., Sullivan, E. D., Jaffe, J. D., Svinkina, T., Natoli, T., Lu, X., Paulk, J., McCarren, P., Wagner, F. F., Barker, D., Howe, E., Lazzaro, F., Gale, J. P., Zhang, Y.-L., Subramanian, A., Fierke, C. A., Carr, S. A., and Holson, E. B. (2014) An unbiased approach to identify endogenous substrates of "histone" deacetylase 8. *ACS Chem. Biol. 9*, 2210–6.

(5) Joshi, P., Greco, T. M., Guise, A. J., Luo, Y., Yu, F., Nesvizhskii, A. I., and Cristea, I. M. (2013) The functional interactome landscape of the human histone deacetylase family. *Mol. Syst. Biol. 9*, 672.

(6) Alam, N., Zimmerman, L., Wolfson, N. A., Joseph, C. G., Fierke, C. A., and Schueler-Furman, O. (2016) Structure-Based Identification of HDAC8 Non-histone Substrates. *Structure 24*, 458–468.

(7) Wolfson, N. A., Pitcairn, C. A., Sullivan, E. D., Joseph, C. G., and Fierke, C. A. (2014) An enzyme-coupled assay measuring acetate production for profiling histone deacetylase specificity. *Anal. Biochem. 456*, 61–69.

(8) Sullivan, E. D. (2016) Unlocking an HDAC Toolbox: Methods towards understanding isozyme-specific activity. University of Michigan.

(9) Schmied, W. H., Elsässer, S. J., Uttamapinant, C., and Chin, J. W. (2014) Efficient Multisite Unnatural Amino Acid Incorporation in Mammalian Cells via Optimized Pyrrolysyl tRNA Synthetase/tRNA Expression and Engineered eRF1. *J. Am. Chem. Soc. 136*, 15577–15583.

(10) Kipper, K., Lundius, E. G., Ćurić, V., Nikić, I., Wiessler, M., Lemke, E. A., and Elf, J. (2017) Application of Noncanonical Amino Acids for Protein Labeling in a Genomically Recoded *Escherichia coli*. *ACS Synth. Biol. 6*, 233–255.

(11) Deardorff, M. A., Bando, M., Nakato, R., Watrin, E., Itoh, T., Minamino, M., Saitoh, K., Komata, M., Katou, Y., Clark, D., Cole, K. E., De Baere, E., Decroos, C., Di Donato, N., Ernst, S., Francey, L. J., Gyftodimou, Y., Hirashima, K., Hullings, M., Ishikawa, Y., Jaulin, C., Kaur, M., Kiyono, T., Lombardi, P. M., Magnaghi-Jaulin, L., Mortier, G. R., Nozaki, N., Petersen, M. B., Seimiya, H., Siu, V. M., Suzuki, Y., Takagaki, K., Wilde, J. J., Willems, P. J., Prigent, C., Gillessen-Kaesbach, G., Christianson, D. W., Kaiser, F. J., Jackson, L. G., Hirota, T., Krantz, I. D., and Shirahige, K. (2012) HDAC8 mutations in

Cornelia de Lange syndrome affect the cohesin acetylation cycle. *Nature 489*, 313–7.

(12) Decroos, C., Bowman, C. M., Moser, J. A. S., Christianson, K. E., Deardorff, M. A., and Christianson, D. W. (2014) Compromised structure and function of HDAC8 mutants identified in Cornelia de Lange Syndrome spectrum disorders. *ACS Chem. Biol. 9*, 2157–2164.

(13) Decroos, C., Christianson, N. H., Gullett, L. E., Bowman, C. M., Christianson, K. E., Deardorff, M. A., and Christianson, D. W. (2015) Biochemical and Structural Characterization of HDAC8 Mutants Associated with Cornelia de Lange Syndrome Spectrum Disorders. *Biochemistry 54*, 6501–6513.

(14) Vannini, A., Volpari, C., Filocamo, G., Casavola, E. C., Brunetti, M., Renzoni, D., Chakravarty, P., Paolini, C., De Francesco, R., Gallinari, P., Steinkühler, C., and Di Marco, S. (2004) Crystal structure of a eukaryotic zinc-dependent histone deacetylase, human HDAC8, complexed with a hydroxamic acid inhibitor. *Proc. Natl. Acad. Sci. U. S. A. 101*, 15064–9.

(15) Dowling, D. P., Gantt, S. L., Gattis, S. G., Fierke, C. A., and Christianson, D. W. (2008) Structural studies of human histone deacetylase 8 and its site-specific variants complexed with substrate and inhibitors. *Biochemistry 47*, 13554–63.

(16) Bozym, R. A., Thompson, R. B., Stoddard, A. K., and Fierke, C. A. (2006) Measuring Picomolar Intracellular Exchangeable Zinc in PC-12 Cells Using a Ratiometric Fluorescence Biosensor. *ACS Chem. Biol. 1*, 103–111.

(17) Vinkenborg, J. L., Nicolson, T. J., Bellomo, E. A., Koay, M. S., Rutter, G. A., and Merkx, M. (2009) Genetically encoded FRET sensors to monitor intracellular Zn2+ homeostasis. *Nat. Methods 6*, 737–740.

(18) Gantt, S. L., Joseph, C. G., and Fierke, C. A. (2009) Activation and Inhibition of Histone Deacetylase 8 by Monovalent Cations. *J. Biol. Chem. 285*, 6036–6043.

(19) Gantt, S. L., Gattis, S. G., and Fierke, C. A. (2006) Catalytic activity and inhibition of human histone deacetylase 8 is dependent on the identity of the active site metal ion. *Biochemistry 45*, 6170–8.

(20) Gattis, S. G. (2010) Mechanism and Metal Specificity of Zinc-dependent deacetylases. University of Michigan.

Appendix

Table A1.1 - Proteins identified through HDAC8 covalent capture - Y100				
Protein ID	**UV/No UV FC**	**p-value (UV/No UV)**	**# peptides ID**	**Notes**
SYAC	24.311	0.024	2	Putative HDAC8 substrate
MCMBP	22.468	0.143	1	
GSTO1	18.313	0.264	2	
RADI	12.529	0.280	16	
SNX5	12.175	0.252	2	
T2FA	11.600	0.066	2	
FHL1	10.286	0.022	1	
GEMI	7.487	0.235	1	
PGAM4	7.266	0.027	5	
VIGLN	7.088	0.052	4	
H90B3	6.968	0.092	35	
H2BFM	6.941	0.188	1	
1433G	6.420	0.425	4	
TBA1A	5.206	0.063	56	Observed as an HDAC8 substrate
IF4B	5.189	0.110	3	
SYEP	5.163	0.016	4	
H14	4.968	0.017	5	Putative HDAC8 substrate
K1C9	4.770	0.015	30	
HNRPM	4.731	0.048	1	
SC24C	4.723	0.070	5	Putative HDAC8 substrate
COPA	4.577	0.020	8	Putative HDAC8 substrate
SYQ	4.544	0.022	2	
LDH6B	4.536	0.124	2	
ACTBL	4.271	0.051	26	
LARP1	4.254	0.037	4	Putative HDAC8 substrate
PDLI1	4.206	0.031	3	Putative HDAC8 substrate
ACTN2	4.191	0.032	11	
XRN2	4.175	0.030	1	
DHX9	4.158	0.024	5	
RL7A	4.131	0.050	10	
ESYT1	4.095	0.036	6	
LPPRC	4.093	0.032	18	

HSP72	**4.065**	**0.027**	**53**	
PSA	**4.031**	**0.039**	**23**	**Putative HDAC8 substrate**
ITB1	**4.025**	**0.038**	**7**	**Putative HDAC8 substrate**
CAPR1	**4.002**	**0.033**	**5**	
LRC47	**3.976**	**0.047**	**2**	
IF4G1	**3.970**	**0.063**	**13**	
DCTN2	**3.961**	**0.117**	**7**	
MSH2	**3.960**	**0.036**	**3**	**Putative HDAC8 substrate**
PGTB1	**3.955**	**0.075**	**4**	
TIF1B	**3.939**	**0.036**	**21**	**Binds NuRD complex (HDACs) reference**
CDK1	**3.937**	**0.052**	**5**	
EIF3B	**3.929**	**0.027**	**7**	**Putative HDAC8 substrate (Eric Sullivan thesis)**
VPS35	**3.924**	**0.026**	**4**	
ACTN3	**3.909**	**0.140**	**9**	
UBA1	**3.879**	**0.036**	**46**	
PGAM1	**3.875**	**0.133**	**9**	
DPP3	**3.779**	**0.027**	**9**	
RENT1	**3.766**	**0.026**	**10**	**Putative HDAC8 substrate**
HS90B	**3.758**	**0.037**	**87**	**Putative HDAC8 substrate**
SFPQ	**3.757**	**0.035**	**13**	**Putative HDAC8 substrate**
ACTN1	**3.736**	**0.021**	**16**	**Putative HDAC8 substrate**
ENPL	**3.724**	**0.038**	**51**	
PFKAP	**3.720**	**0.053**	**3**	**Putative HDAC8 substrate**
E41L2	**3.718**	**0.032**	**1**	
KINH	**3.713**	**0.027**	**19**	**Putative HDAC8 substrate**
SF3B2	**3.704**	**0.125**	**1**	
C1TC	**3.704**	**0.033**	**36**	
HNRL1	**3.702**	**0.040**	**2**	
UGDH	**3.695**	**0.021**	**1**	
RBBP7	**3.662**	**0.045**	**4**	
MCM6	**3.649**	**0.042**	**10**	
PARP1	**3.639**	**0.031**	**32**	
UBP5	**3.623**	**0.052**	**5**	
EZRI	**3.622**	**0.030**	**26**	
HS105	**3.619**	**0.033**	**19**	
PSMD2	**3.616**	**0.034**	**8**	
TPIS	**3.609**	**0.026**	**21**	
MSH6	**3.600**	**0.202**	**1**	**Putative HDAC8 substrate (Noah Wolfson thesis)**
CLH1	**3.597**	**0.027**	**45**	
ACLY	**3.584**	**0.036**	**20**	**Putative HDAC8 substrate**

BASI	**3.573**	**0.131**	**2**	
GANAB	**3.562**	**0.031**	**27**	
P5CS	**3.556**	**0.037**	**11**	
EIF3C	**3.528**	**0.045**	**9**	
AT1A1	**3.508**	**0.034**	**19**	
CAND1	**3.507**	**0.026**	**24**	
DDB1	**3.484**	**0.028**	**5**	
CPSF6	**3.477**	**0.021**	**6**	
CSDE1	**3.473**	**0.033**	**5**	
HSPB1	**3.462**	**0.060**	**3**	
RNH2A	**3.461**	**0.046**	**1**	
1433B	**3.456**	**0.065**	**10**	
IPO7	**3.451**	**0.027**	**3**	
PSD12	**3.451**	**0.020**	**5**	
ACON	**3.440**	**0.048**	**3**	
ACTN4	**3.422**	**0.032**	**35**	
DBNL	**3.403**	**0.178**	**5**	
EF2	**3.402**	**0.040**	**93**	
HNRPU	**3.396**	**0.045**	**22**	
COPB2	**3.395**	**0.023**	**9**	
ADH1_YEAST	**3.382**	**0.048**	**59**	
TERA	**3.380**	**0.044**	**34**	
HXK1	**3.367**	**0.026**	**6**	
AINX	**3.361**	**0.044**	**3**	
XRCC5	**3.359**	**0.033**	**20**	
STRAP	**3.343**	**0.047**	**4**	
TNPO1	**3.340**	**0.043**	**8**	
PRS6B	**3.332**	**0.147**	**2**	
SAE2	**3.324**	**0.036**	**4**	
MCM7	**3.319**	**0.030**	**12**	
SND1	**3.314**	**0.042**	**17**	
VINC	**3.299**	**0.034**	**40**	
GLRX3	**3.267**	**0.028**	**11**	
HS90A	**3.266**	**0.037**	**92**	**Putative HDAC8 substrate**
GLU2B	**3.261**	**0.056**	**9**	
GBLP	**3.253**	**0.070**	**6**	
LAP2B	**3.252**	**0.042**	**8**	
MYH9	**3.248**	**0.028**	**63**	
CAN1	**3.242**	**0.070**	**2**	
MYH14	**3.234**	**0.044**	**16**	
DCTN1	**3.206**	**0.067**	**4**	

MCM5	**3.201**	**0.036**	**11**	
VDAC1	**3.194**	**0.029**	**10**	**Putative HDAC8 substrate**
ANM1	**3.192**	**0.089**	**3**	
PRS6A	**3.181**	**0.194**	**3**	
ACOT9	**3.169**	**0.026**	**7**	
SF01	**3.148**	**0.028**	**7**	
DHX15	**3.140**	**0.041**	**6**	
STX11	**3.137**	**0.029**	**4**	
MIC60	**3.129**	**0.038**	**8**	
CPNE3	**3.127**	**0.051**	**12**	**Observed as an HDAC8 substrate**
IPYR	**3.127**	**0.039**	**6**	
DHE3	**3.123**	**0.032**	**12**	
COPG1	**3.104**	**0.044**	**8**	
AXA2L	**3.099**	**0.052**	**21**	
2-Sep	**3.072**	**0.120**	**3**	
U5S1	**3.070**	**0.043**	**18**	
PDIP2	**3.052**	**0.029**	**2**	
EF1B	**3.050**	**0.045**	**2**	
NUCL	**3.044**	**0.043**	**43**	
IPO5	**3.020**	**0.079**	**5**	
HSP7C	**3.019**	**0.050**	**91**	
AIP	**3.017**	**0.040**	**3**	
DDX17	**3.009**	**0.040**	**29**	
FUBP3	**2.997**	**0.052**	**3**	
RIR1	**2.996**	**0.037**	**10**	
FUS	**2.954**	**0.047**	**5**	
PRDX1	**2.905**	**0.040**	**4**	
UBQL1	**2.880**	**0.046**	**2**	
IF2B3	**2.874**	**0.120**	**4**	
ALDOC	**2.869**	**0.068**	**2**	
NSUN2	**2.868**	**0.033**	**9**	
FUBP1	**2.854**	**0.035**	**13**	
RL5	**2.853**	**0.123**	**11**	
IMB1	**2.852**	**0.044**	**25**	
PHB2	**2.843**	**0.032**	**18**	
GTF2I	**2.817**	**0.048**	**1**	
G0S2	**2.806**	**0.074**	**2**	
ACTZ	**2.804**	**0.012**	**5**	
RUVB2	**2.784**	**0.079**	**12**	
ROA1	**2.776**	**0.046**	**7**	
GRP75	**2.763**	**0.062**	**40**	

EIF3A	**2.740**	**0.044**	**24**	
STAU1	**2.732**	**0.049**	**4**	
PYGL	**2.720**	**0.044**	**8**	
FEN1	**2.706**	**0.081**	**3**	
FETUA	**2.701**	**0.043**	**8**	
SEPT9	**2.688**	**0.037**	**5**	
G3PT	**2.679**	**0.000**	**2**	
PABP4	**2.675**	**0.060**	**13**	
HSP74	**2.672**	**0.044**	**22**	
NDUS1	**2.664**	**0.169**	**2**	
PCBP1	**2.662**	**0.035**	**11**	
NYNRI	**2.659**	**0.066**	**1**	
GFAP	**2.655**	**0.126**	**4**	
RL4	**2.633**	**0.154**	**31**	
GDIA	**2.633**	**0.043**	**11**	
CORO7	**2.630**	**0.070**	**3**	
DNM1L	**2.628**	**0.084**	**4**	
HNRH1	**2.616**	**0.063**	**9**	
SRSF7	**2.615**	**0.030**	**2**	
MCM3	**2.613**	**0.057**	**12**	
OST48	**2.608**	**0.231**	**5**	
ALBU	**2.604**	**0.052**	**33**	
RL8	**2.595**	**0.048**	**15**	
BACH	**2.595**	**0.035**	**4**	
HMGB2	**2.594**	**0.212**	**5**	
7-Sep	**2.593**	**0.051**	**7**	
METK2	**2.589**	**0.141**	**4**	
KAD2	**2.587**	**0.192**	**4**	
MCM4	**2.579**	**0.072**	**11**	
ANXA2	**2.570**	**0.040**	**25**	
STML2	**2.550**	**0.189**	**3**	
GRP78	**2.548**	**0.065**	**53**	
HS74L	**2.547**	**0.046**	**10**	
LDHC	**2.544**	**0.044**	**3**	
PSMD1	**2.542**	**0.058**	**7**	
PRS10	**2.539**	**0.027**	**3**	
SYMC	**2.539**	**0.062**	**9**	
STIP1	**2.530**	**0.056**	**35**	
SF3B3	**2.528**	**0.087**	**7**	
SNX2	**2.525**	**0.142**	**4**	
MOES	**2.524**	**0.077**	**23**	

ATPB	**2.522**	**0.206**	**27**	
KCRB	**2.504**	**0.035**	**15**	
TBB2A	**2.503**	**0.040**	**55**	
LKHA4	**2.493**	**0.048**	**3**	
COPB	**2.481**	**0.089**	**10**	
QCR1	**2.475**	**0.060**	**1**	
RBM39	**2.469**	**0.079**	**2**	
IQGA1	**2.468**	**0.062**	**12**	
BIEA	**2.457**	**0.139**	**3**	
CHM4B	**2.453**	**0.043**	**2**	
1433T	**2.450**	**0.444**	**8**	
MPCP	**2.447**	**0.047**	**8**	
PLST	**2.436**	**0.063**	**43**	
KPYM	**2.427**	**0.072**	**57**	
PUF60	**2.425**	**0.063**	**3**	
ANXA5	**2.418**	**0.057**	**17**	
LA	**2.409**	**0.181**	**3**	
SET	**2.403**	**0.034**	**12**	
ATP4A	**2.398**	**0.065**	**2**	
RL6	**2.392**	**0.043**	**18**	
XPO2	**2.390**	**0.049**	**28**	
TRFL	**2.383**	**0.099**	**1**	
RFA1	**2.382**	**0.090**	**4**	
PYRG1	**2.361**	**0.060**	**2**	
CNDP2	**2.356**	**0.251**	**2**	
ENOA	**2.340**	**0.197**	**70**	
K22O	**2.331**	**0.071**	**17**	
TKT	**2.321**	**0.069**	**28**	
UBP14	**2.319**	**0.112**	**3**	
PUR2	**2.317**	**0.050**	**9**	
PABP1	**2.311**	**0.069**	**28**	
PHB	**2.308**	**0.061**	**8**	
MYH10	**2.296**	**0.072**	**31**	
NP1L4	**2.285**	**0.078**	**7**	
XRCC6	**2.266**	**0.084**	**22**	
SMC2	**2.265**	**0.079**	**5**	**Sequence similarity with SMC3 (25%)**
SRSF6	**2.261**	**0.086**	**3**	
TPM3	**2.255**	**0.277**	**2**	**Observed as an HDAC8 substrate**
HNRPF	**2.255**	**0.209**	**10**	
YBOX3	**2.252**	**0.087**	**6**	
MATR3	**2.246**	**0.069**	**14**	

BLMH	**2.245**	**0.059**	**2**	
PDIA4	**2.242**	**0.077**	**16**	
YBOX1	**2.232**	**0.280**	**5**	
RS3	**2.226**	**0.078**	**11**	
DLDH	**2.218**	**0.191**	**2**	
RPN1	**2.217**	**0.077**	**15**	
TXND5	**2.197**	**0.082**	**5**	**Observed as an HDAC8 substrate**
IMA1	**2.195**	**0.103**	**7**	
PAIRB	**2.193**	**0.068**	**9**	
DDX3X	**2.179**	**0.071**	**13**	
TCPQ	**2.174**	**0.081**	**39**	
SYRC	**2.171**	**0.098**	**1**	
RS8	**2.158**	**0.357**	**5**	
KATL2	**2.154**	**0.078**	**4**	
IF2G	**2.153**	**0.136**	**9**	
VAT1	**2.144**	**0.097**	**3**	
FUBP2	**2.131**	**0.100**	**32**	
KTN1	**2.126**	**0.086**	**6**	
CH60	**2.124**	**0.095**	**51**	
PRDX4	**2.124**	**0.296**	**4**	**Putative HDAC8 substrate (Eric Sullivan thesis)**
TCPH	**2.119**	**0.095**	**22**	
SRC8	**2.115**	**0.074**	**10**	
DDX5	**2.112**	**0.131**	**16**	
2AAA	**2.104**	**0.083**	**20**	
TCPE	**2.102**	**0.098**	**23**	
TCPG	**2.100**	**0.097**	**21**	
LMNA	**2.096**	**0.089**	**3**	
TRAP1	**2.093**	**0.109**	**19**	
RS4X	**2.091**	**0.423**	**7**	
ADT3	**2.089**	**0.088**	**9**	
FKBP4	**2.086**	**0.077**	**29**	
NONO	**2.082**	**0.082**	**14**	
PRDX2	**2.079**	**0.079**	**3**	
IF2B1	**2.077**	**0.095**	**19**	
CALX	**2.070**	**0.162**	**15**	
RL13	**2.062**	**0.105**	**8**	
EF1D	**2.045**	**0.014**	**16**	
IF4A1	**2.043**	**0.256**	**33**	
ROA2	**2.040**	**0.119**	**7**	
SAM15	**2.033**	**0.091**	**5**	
ADT2	**2.029**	**0.141**	**10**	

RS6	**2.027**	**0.066**	**8**	
NPM	**2.023**	**0.075**	**7**	
SGT1	**2.015**	**0.198**	**4**	
EWS	**2.010**	**0.090**	**3**	
OLA1	**2.008**	**0.088**	**2**	
OAT	**1.992**	**0.100**	**7**	
LDHA	**1.983**	**0.029**	**27**	
TBB3	**1.978**	**0.361**	**33**	
PABP3	**1.973**	**0.072**	**13**	
IF2A	**1.971**	**0.167**	**3**	
EIF3I	**1.970**	**0.088**	**3**	
PYGM	**1.966**	**0.168**	**7**	
IF4H	**1.965**	**0.089**	**5**	
HNRPR	**1.957**	**0.265**	**2**	
F10A1	**1.957**	**0.116**	**7**	
G3P	**1.950**	**0.017**	**33**	
TCPD	**1.949**	**0.123**	**26**	
PDIA3	**1.939**	**0.119**	**32**	
APEX1	**1.934**	**0.156**	**4**	
HNRPQ	**1.928**	**0.150**	**10**	
HCN3	**1.926**	**0.128**	**2**	
RD23B	**1.925**	**0.102**	**7**	
RCN1	**1.911**	**0.283**	**4**	
PGK1	**1.908**	**0.110**	**24**	
AT1A2	**1.898**	**0.075**	**13**	
ILF2	**1.882**	**0.221**	**3**	
G3BP1	**1.879**	**0.168**	**8**	
NASP	**1.867**	**0.066**	**25**	
TCPZ	**1.865**	**0.122**	**22**	
IF2B2	**1.855**	**0.153**	**5**	
ANXA1	**1.851**	**0.082**	**20**	
GUAA	**1.841**	**0.181**	**2**	
RSSA	**1.835**	**0.064**	**12**	
SYTC	**1.830**	**0.126**	**15**	
LSR	**1.825**	**0.037**	**4**	
PIPNA	**1.816**	**0.127**	**2**	
RUVB1	**1.813**	**0.132**	**9**	
UCHL1	**1.806**	**0.554**	**6**	
ALDOA	**1.795**	**0.018**	**28**	
MYH11	**1.793**	**0.145**	**14**	
CN119	**1.792**	**0.328**	**1**	

RTCB	**1.789**	**0.137**	**5**	
RAB1C	**1.782**	**0.191**	**2**	
PRDX6	**1.780**	**0.143**	**7**	
LMAN1	**1.775**	**0.176**	**5**	
NMT1	**1.775**	**0.176**	**2**	
PDIA6	**1.767**	**0.335**	**14**	
EIF3D	**1.764**	**0.286**	**3**	
6PGD	**1.759**	**0.165**	**11**	
NO66	**1.759**	**0.328**	**4**	
ANXA6	**1.758**	**0.246**	**6**	
RLA0	**1.758**	**0.405**	**11**	
IF4A3	**1.751**	**0.116**	**11**	
EMD	**1.748**	**0.093**	**4**	
PAP1L	**1.747**	**0.184**	**7**	
TBB6	**1.741**	**0.411**	**27**	
CISY	**1.738**	**0.135**	**18**	
EIF2A	**1.735**	**0.319**	**1**	**Putative HDAC8 substrate (Eric Sullivan thesis)**
API5	**1.733**	**0.217**	**4**	
SERA	**1.732**	**0.197**	**13**	
CAP1	**1.722**	**0.155**	**10**	
IMDH2	**1.721**	**0.204**	**12**	
RAB1B	**1.700**	**0.356**	**2**	
ACTBM	**1.699**	**0.173**	**10**	
RINI	**1.697**	**0.196**	**3**	
PSD13	**1.675**	**0.347**	**4**	
GDIB	**1.672**	**0.239**	**11**	
ILF3	**1.671**	**0.260**	**6**	
PSMD4	**1.668**	**0.090**	**6**	
SMC1A	**1.666**	**0.227**	**3**	**Observed as an HDAC8 substrate**
RL3	**1.658**	**0.178**	**15**	
HNRH2	**1.652**	**0.394**	**6**	
TADBP	**1.648**	**0.073**	**4**	
DDX6	**1.642**	**0.282**	**3**	
SSRP1	**1.639**	**0.197**	**9**	
TAGL2	**1.620**	**0.302**	**3**	
SYHC	**1.620**	**0.590**	**4**	
PDIA1	**1.611**	**0.211**	**33**	**Putative HDAC8 substrate (Eric Sullivan thesis)**
TCPB	**1.606**	**0.220**	**33**	
NACAM	**1.603**	**0.203**	**19**	
PA2G4	**1.588**	**0.280**	**20**	

PAK2	**1.587**	**0.224**	**6**	
PRS4	**1.570**	**0.271**	**7**	
DDX1	**1.567**	**0.514**	**4**	
ENOG	**1.561**	**0.277**	**8**	
WDR1	**1.553**	**0.370**	**6**	
UBP7	**1.546**	**0.261**	**2**	
LDHB	**1.530**	**0.044**	**28**	
C1QBP	**1.521**	**0.542**	**4**	
THIL	**1.519**	**0.157**	**10**	
G6PI	**1.518**	**0.354**	**21**	
CL054	**1.517**	**0.454**	**1**	
CLIC1	**1.507**	**0.303**	**7**	
AT1A3	**1.495**	**0.422**	**9**	
HMCS1	**1.494**	**0.359**	**6**	
EIF3F	**1.492**	**0.303**	**2**	
LRC59	**1.488**	**0.398**	**4**	
NDE1	**1.479**	**0.305**	**3**	
TBB5	**1.478**	**0.524**	**62**	
VATB2	**1.477**	**0.374**	**8**	
KPYR	**1.473**	**0.300**	**8**	
EF1G	**1.465**	**0.257**	**28**	
NP1L1	**1.459**	**0.402**	**8**	
HS905	**1.456**	**0.634**	**17**	
PLSI	**1.450**	**0.205**	**14**	
PSMD3	**1.446**	**0.461**	**10**	
RPR1B	**1.446**	**0.506**	**2**	
GSHR	**1.438**	**0.501**	**5**	
VDAC2	**1.434**	**0.169**	**8**	
PTBP1	**1.434**	**0.434**	**9**	
LS14B	**1.420**	**0.669**	**1**	
IF4A2	**1.419**	**0.369**	**17**	
PUR9	**1.408**	**0.333**	**14**	
ERF1	**1.404**	**0.578**	**2**	
EIF3L	**1.403**	**0.532**	**1**	
1433Z	**1.398**	**0.440**	**10**	
BASP1	**1.388**	**0.458**	**8**	
ANX11	**1.386**	**0.446**	**7**	
CAZA1	**1.380**	**0.315**	**3**	
RAN	**1.378**	**0.614**	**2**	
TCPA	**1.376**	**0.445**	**22**	
CKAP4	**1.375**	**0.347**	**18**	

HNRPK	**1.365**	**0.468**	**24**	
4F2	**1.344**	**0.423**	**4**	
ETFA	**1.332**	**0.659**	**4**	
AATM	**1.331**	**0.251**	**7**	
SAHH	**1.308**	**0.384**	**17**	
TALDO	**1.303**	**0.289**	**17**	
TPM4	**1.290**	**0.451**	**3**	**Observed as an HDAC8 substrate**
M3K14	**1.286**	**0.336**	**6**	
PDCD4	**1.277**	**0.683**	**3**	
COPD	**1.258**	**0.613**	**1**	
GLYM	**1.253**	**0.630**	**12**	
SFXN1	**1.245**	**0.551**	**2**	
1433E	**1.239**	**0.611**	**17**	
PSA1	**1.239**	**0.567**	**6**	
HNRPC	**1.232**	**0.583**	**3**	
RPAP3	**1.231**	**0.444**	**3**	
PSPC1	**1.225**	**0.729**	**3**	
PUR1	**1.221**	**0.641**	**2**	
MCM2	**1.191**	**0.791**	**6**	
TBB4B	**1.184**	**0.758**	**64**	
AL7A1	**1.181**	**0.739**	**7**	
MDHM	**1.167**	**0.414**	**15**	
HMGB1	**1.163**	**0.694**	**9**	
1433F	**1.155**	**0.771**	**6**	
GSTP1	**1.138**	**0.819**	**6**	
RL7	**1.131**	**0.715**	**12**	
AMPL	**1.111**	**0.859**	**5**	
2ABA	**1.110**	**0.829**	**4**	**Observed as an HDAC8 substrate**
MARCS	**1.102**	**0.868**	**3**	
SERPH	**1.100**	**0.855**	**15**	
DPOD1	**1.083**	**0.860**	**1**	
FSCN1	**1.042**	**0.933**	**11**	
RANG	**1.035**	**0.860**	**2**	
OTUB1	**1.030**	**0.933**	**7**	
PCNA	**1.027**	**0.872**	**13**	
TBA1C	**1.018**	**0.985**	**55**	
PRP19	**1.002**	**0.997**	**7**	
HS71L	**0.996**	**0.991**	**61**	**Putative HDAC8 substrate (Eric Sullivan thesis)**
CTCFL	**0.983**	**0.963**	**7**	
HDAC8	**0.969**	**0.876**	**207**	**HDAC8 control**
DX39A	**0.952**	**0.946**	**9**	

ATPA	**0.949**	**0.913**	**27**	
ENOB	**0.920**	**0.839**	**13**	
RS3A	**0.920**	**0.765**	**21**	
ALDOB	**0.916**	**0.909**	**3**	
MDHC	**0.912**	**0.788**	**10**	
RPN2	**0.909**	**0.820**	**4**	
EFHD1	**0.906**	**0.849**	**1**	
HNRPD	**0.883**	**0.783**	**4**	
RL10A	**0.871**	**0.858**	**3**	
EIF3G	**0.869**	**0.706**	**2**	
MARE1	**0.866**	**0.838**	**4**	
SYDC	**0.862**	**0.797**	**4**	
NUDC	**0.847**	**0.707**	**8**	
U2AF2	**0.832**	**0.899**	**1**	
RL19	**0.774**	**0.567**	**3**	
RS2	**0.759**	**0.524**	**8**	
RL13A	**0.749**	**0.431**	**1**	
HPTR	**0.743**	**0.661**	**2**	
CALR	**0.727**	**0.503**	**12**	
GBB4	**0.685**	**0.208**	**2**	
SNX1	**0.683**	**0.694**	**2**	
SPEE	**0.675**	**0.226**	**3**	
INO1	**0.669**	**0.603**	**1**	
RCC2	**0.660**	**0.358**	**11**	
AT1B3	**0.653**	**0.516**	**1**	
RAB14	**0.628**	**0.350**	**4**	
PUR6	**0.626**	**0.344**	**11**	
STRA8	**0.621**	**0.343**	**1**	
SCMC1	**0.614**	**0.302**	**1**	
LDH6A	**0.610**	**0.035**	**5**	
UBXN1	**0.580**	**0.445**	**1**	
ENPLL	**0.532**	**0.389**	**8**	
ACTY	**0.531**	**0.089**	**3**	
POTEI	**0.518**	**0.418**	**30**	
NSF1C	**0.491**	**0.254**	**4**	
CPSF5	**0.474**	**0.416**	**1**	
TBB2B	**0.430**	**0.112**	**54**	
FKBP3	**0.422**	**0.112**	**3**	
EF1A2	**0.340**	**0.172**	**31**	**Sequence similarity with EF1A1 (96%)**
CBR1	**0.331**	**0.065**	**2**	
H90B2	**0.308**	**0.289**	**30**	

EFTU	**0.278**	**0.175**	**10**	
PCBP2	**0.268**	**0.082**	**9**	
AL9A1	**0.239**	**0.102**	**2**	
RL14	**0.196**	**0.053**	**3**	
MAOM	**0.196**	**0.220**	**1**	
RL15	**0.173**	**0.078**	**1**	
1433S	**0.010**	**0.059**	**4**	
PSA5	**0.009**	**0.139**	**2**	
PLSL	**0.001**	**0.084**	**10**	
RL18	**0.000**	**0.000**	**1**	**Undefined due to zero unique peptides and overflow abundance***
TBA4A	**0.000**	**0.000**	**36**	**Undefined due to zero unique peptides and overflow abundance***
TBA8	**0.000**	**0.000**	**21**	**Undefined due to zero unique peptides and overflow abundance***
KIF5C	**0.000**	**0.000**	**1**	**Undefined due to zero unique peptides and overflow abundance***
EIFCL	**0.000**	**0.000**	**6**	**Undefined due to zero unique peptides and overflow abundance***
IMDH1	**0.000**	**0.000**	**1**	**Undefined due to zero unique peptides and overflow abundance***
TBA3E	**0.000**	**0.000**	**35**	**Undefined due to zero unique peptides and overflow abundance***
K1C12	**0.000**	**0.000**	**2**	**Undefined due to zero unique peptides and overflow abundance***
TBA3C	**0.000**	**0.000**	**44**	**Undefined due to zero unique peptides and overflow abundance***
RS4Y2	**0.000**	**0.000**	**4**	**Undefined due to zero unique peptides and overflow abundance***
TBA1B	**0.000**	**0.000**	**57**	**Undefined due to zero unique peptides and overflow abundance***
LMNB1	**0.000**	**0.000**	**1**	**Undefined due to zero unique peptides and overflow abundance***
PSD11	**0.000**	**0.000**	**3**	**Undefined due to zero unique peptides and overflow abundance***
EF1A3	**0.000**	**0.000**	**50**	**Undefined due to zero unique peptides and overflow abundance***
ACTA	**0.000**	**0.000**	**58**	**Undefined due to zero unique peptides and overflow abundance***
ACTC	**0.000**	**0.000**	**59**	**Undefined due to zero unique peptides and overflow abundance***
EF1A1	**0.000**	**0.000**	**51**	**Putative HDAC8 substrate (Noah Wolfson thesis)**
TBB1	**0.000**	**0.000**	**9**	**Undefined due to zero unique peptides and overflow abundance***
TXNL1	**0.000**	**0.000**	**1**	**Undefined due to zero unique peptides and overflow abundance***
NACA	**0.000**	**0.000**	**5**	**Undefined due to zero unique peptides and overflow abundance***
CMC2	**0.000**	**0.000**	**1**	**Undefined due to zero unique peptides and overflow abundance***

HSP77	**0.000**	**0.000**	**25**	**Undefined due to zero unique peptides and overflow abundance***
KIF5A	**0.000**	**0.000**	**1**	**Undefined due to zero unique peptides and overflow abundance***
SYVC	**0.000**	**0.000**	**1**	**Undefined due to zero unique peptides and overflow abundance***
ACTH	**0.000**	**0.000**	**58**	**Undefined due to zero unique peptides and overflow abundance***
ACTS	**0.000**	**0.000**	**58**	**Undefined due to zero unique peptides and overflow abundance***
IF2P	**0.000**	**0.000**	**1**	**Undefined due to zero unique peptides and overflow abundance***
DHE4	**0.000**	**0.000**	**4**	**Undefined due to zero unique peptides and overflow abundance***
RAB10	**0.000**	**0.000**	**1**	**Undefined due to zero unique peptides and overflow abundance***
RS27A	**0.000**	**0.000**	**12**	**Undefined due to zero unique peptides and overflow abundance***
UBC	**0.000**	**0.000**	**12**	**Undefined due to zero unique peptides and overflow abundance***
K2C7	**0.000**	**0.000**	**3**	**Undefined due to zero unique peptides and overflow abundance***
K2C75	**0.000**	**0.000**	**3**	**Undefined due to zero unique peptides and overflow abundance***
CDK3	**0.000**	**0.000**	**1**	**Undefined due to zero unique peptides and overflow abundance***
CDK2	**0.000**	**0.000**	**1**	**Undefined due to zero unique peptides and overflow abundance***
POTEJ	**0.000**	**0.000**	**27**	**Undefined due to zero unique peptides and overflow abundance***
CSK21	**0.000**	**0.000**	**1**	**Observed as an HDAC8 substrate**
K1C27	**0.000**	**0.000**	**4**	**Undefined due to zero unique peptides and overflow abundance***
IDH3A	**0.000**	**0.000**	**1**	**Undefined due to zero unique peptides and overflow abundance***
CSK23	**0.000**	**0.000**	**1**	**Undefined due to zero unique peptides and overflow abundance***
PGAM2	**0.000**	**0.000**	**4**	**Undefined due to zero unique peptides and overflow abundance***
HSP76	**0.000**	**0.000**	**48**	**Undefined due to zero unique peptides and overflow abundance***
RBBP4	**0.000**	**0.000**	**2**	**Undefined due to zero unique peptides and overflow abundance***
FKBP8	**0.000**	**0.000**	**1**	**Undefined due to zero unique peptides and overflow abundance***
HS71A	**0.000**	**0.000**	**123**	**Undefined due to zero unique peptides and overflow abundance***
HS71B	**0.000**	**0.000**	**123**	**Undefined due to zero unique peptides and overflow abundance***
SYNC	**0.000**	**0.000**	**2**	**Undefined due to zero unique peptides and overflow abundance***
UBB	**0.000**	**0.000**	**12**	**Undefined due to zero unique peptides and overflow abundance***

KRT85	**0.000**	**0.000**	**1**	**Undefined due to zero unique peptides and overflow abundance***
PAP1M	**0.000**	**0.000**	**1**	**Undefined due to zero unique peptides and overflow abundance***
RL40	**0.000**	**0.000**	**12**	**Undefined due to zero unique peptides and overflow abundance***
ACTB	**0.000**	**0.000**	**79**	**Undefined due to zero unique peptides and overflow abundance***
ACTG	**0.000**	**0.000**	**79**	**Undefined due to zero unique peptides and overflow abundance***
AT2A2	**0.000**	**0.000**	**2**	**Undefined due to zero unique peptides and overflow abundance***
H90B4	**0.000**	**0.000**	**16**	**Undefined due to zero unique peptides and overflow abundance***
GSHB	**0.000**	**0.000**	**2**	**Undefined due to zero unique peptides and overflow abundance***
K2C3	**0.000**	**0.000**	**4**	**Undefined due to zero unique peptides and overflow abundance***
K1C24	**0.000**	**0.000**	**3**	**Undefined due to zero unique peptides and overflow abundance***
SETLP	**0.000**	**0.000**	**10**	**Undefined due to zero unique peptides and overflow abundance***
DX39B	**0.000**	**0.000**	**8**	**Undefined due to zero unique peptides and overflow abundance***
CTCF	**0.000**	**0.000**	**2**	**Undefined due to zero unique peptides and overflow abundance***
HS904	**0.000**	**0.000**	**4**	**Undefined due to zero unique peptides and overflow abundance***
ESTD	**0.000**	**0.000**	**2**	**Undefined due to zero unique peptides and overflow abundance***
PP2AB	**0.000**	**0.000**	**1**	**Undefined due to zero unique peptides and overflow abundance***
TBAL3	**0.000**	**0.000**	**4**	**Undefined due to zero unique peptides and overflow abundance***
HV317	**0.000**	**0.000**	**1**	**Undefined due to zero unique peptides and overflow abundance***
KRT36	**0.000**	**0.000**	**2**	**Undefined due to zero unique peptides and overflow abundance***
PGK2	**0.000**	**0.000**	**2**	**Undefined due to zero unique peptides and overflow abundance***
K1H1	**0.000**	**0.000**	**2**	**Undefined due to zero unique peptides and overflow abundance***
DDX3Y	**0.000**	**0.000**	**7**	**Undefined due to zero unique peptides and overflow abundance***
UBQL4	**0.000**	**0.000**	**1**	**Undefined due to zero unique peptides and overflow abundance***
PSAL	**0.000**	**0.000**	**11**	**Undefined due to zero unique peptides and overflow abundance***
DPYL2	**0.000**	**0.000**	**3**	**Undefined due to zero unique peptides and overflow abundance***
KT33B	**0.000**	**0.000**	**2**	**Undefined due to zero unique peptides and overflow abundance***
KRT38	**0.000**	**0.000**	**2**	**Undefined due to zero unique peptides and overflow abundance***

H12	**0.000**	**0.000**	**5**	**Undefined due to zero unique peptides and overflow abundance***
KRT37	**0.000**	**0.000**	**2**	**Undefined due to zero unique peptides and overflow abundance***
H13	**0.000**	**0.000**	**4**	**Undefined due to zero unique peptides and overflow abundance***
RA1L2	**0.000**	**0.000**	**3**	**Undefined due to zero unique peptides and overflow abundance***
HAT1	**0.000**	**0.000**	**1**	**Undefined due to zero unique peptides and overflow abundance***
HS902	**0.000**	**0.000**	**11**	**Undefined due to zero unique peptides and overflow abundance***
POTEF	**0.000**	**0.000**	**31**	**Undefined due to zero unique peptides and overflow abundance***
POTEE	**0.000**	**0.000**	**36**	**Undefined due to zero unique peptides and overflow abundance***
TBB4A	**0.000**	**0.000**	**49**	**Undefined due to zero unique peptides and overflow abundance***
TCPW	**0.000**	**0.000**	**7**	**Undefined due to zero unique peptides and overflow abundance***
PCBP3	**0.000**	**0.000**	**4**	**Undefined due to zero unique peptides and overflow abundance***
LAP2A	**0.000**	**0.000**	**8**	**Undefined due to zero unique peptides and overflow abundance***
PABP5	**0.000**	**0.000**	**1**	**Undefined due to zero unique peptides and overflow abundance***
RS4Y1	**0.000**	**0.000**	**5**	**Undefined due to zero unique peptides and overflow abundance***
IF2GL	**0.000**	**0.000**	**5**	**Undefined due to zero unique peptides and overflow abundance***
TBB8L	**0.000**	**0.000**	**23**	**Undefined due to zero unique peptides and overflow abundance***
TBB8	**0.000**	**0.000**	**25**	**Undefined due to zero unique peptides and overflow abundance***
ZYX	**0.000**	**0.000**	**2**	**Undefined due to zero unique peptides and overflow abundance***
F10A5	**0.000**	**0.000**	**2**	**Undefined due to zero unique peptides and overflow abundance***
ADT1	**0.000**	**0.000**	**6**	**Undefined due to zero unique peptides and overflow abundance***
GBB1	**0.000**	**0.000**	**1**	**Undefined due to zero unique peptides and overflow abundance***
GBB2	**0.000**	**0.000**	**1**	**Undefined due to zero unique peptides and overflow abundance***
RAGP1	**0.000**	**0.000**	**1**	**Undefined due to zero unique peptides and overflow abundance***
ANR66	**0.000**	**0.000**	**1**	**Undefined due to zero unique peptides and overflow abundance***
TBA4B	**0.000**	**0.000**	**3**	**Undefined due to zero unique peptides and overflow abundance***
K2C6A	**0.000**	**0.000**	**19**	**Undefined due to zero unique peptides and overflow abundance***
K2C6C	**0.000**	**0.000**	**20**	**Undefined due to zero unique peptides and overflow abundance***

ST134	**0.000**	**0.000**	**5**	**Undefined due to zero unique peptides and overflow abundance***
K2C8	**0.000**	**0.000**	**5**	**Undefined due to zero unique peptides and overflow abundance***
AATC	**0.000**	**0.000**	**2**	**Putative HDAC11 substrate (Eric Sullivan thesis)**
ADT4	**0.000**	**0.000**	**4**	**Undefined due to zero unique peptides and overflow abundance***
PYGB	**0.000**	**0.000**	**7**	**Undefined due to zero unique peptides and overflow abundance***
GDIR1	**0.000**	**0.000**	**1**	
K1C26	**0.000**	**0.012**	**3**	**Undefined due to zero unique peptides and overflow abundance***
RS7	**0.000**	**0.126**	**1**	
RLA0L	**0.000**	**0.347**	**9**	**Undefined due to zero unique peptides and overflow abundance***

Table A1.2 - Proteins identified through HDAC8 covalent capture - I94

Protein ID	UV/No UV FC	p-value (UV/No UV)	# peptides ID	Notes
TDRP	**45.413**	**0.000**	**1**	
HUS1B	**39.205**	**0.001**	**2**	
ADT1	**10.596**	**0.002**	**7**	**Putative HDAC8 substrate**
S10A9	**5.431**	**0.001**	**5**	**Tested peptide**
TXLNA	**5.421**	**0.002**	**4**	
VDAC1;VDAC3	**5.178**	**0.001**	**6**	**Putative HDAC8 substrate**
HS71L	**3.914**	**0.007**	**5**	**Tested peptide**
COX41	**3.654**	**0.032**	**2**	**Tested peptide**
RL3	**3.486**	**0.003**	**18**	**Tested peptide**
PHB	**2.678**	**0.040**	**10**	**Tested peptide**
PLMN	**2.664**	**0.005**	**5**	
HBA	**2.542**	**0.017**	**1**	
RRAS	**2.350**	**0.006**	**1**	
HS90B;HS902	**2.345**	**0.006**	**16**	**Putative HDAC8 substrate**
AGO1;AGO4	**2.306**	**0.002**	**20**	
LR10B	**2.244**	**0.010**	**7**	
TIF1B	**2.186**	**0.010**	**15**	
CD3E	**2.165**	**0.091**	**1**	
BRCC3	**2.061**	**0.025**	**1**	
CALM	**2.049**	**0.045**	**3**	
ANXA7	**2.034**	**0.115**	**2**	
MATR3	**2.023**	**0.012**	**16**	
MRGBP	**2.014**	**0.020**	**1**	
PZP	**1.972**	**0.060**	**1**	
RS3A	**1.949**	**0.005**	**18**	

ROA3	**1.944**	**0.035**	**13**	
HSP76	**1.924**	**0.010**	**8**	
HSP72	**1.921**	**0.012**	**8**	
RL29	**1.887**	**0.116**	**7**	
KHDR1	**1.882**	**0.047**	**5**	
LAP2A	**1.854**	**0.072**	**10**	
RL26L	**1.841**	**0.081**	**9**	
HS90A	**1.830**	**0.028**	**9**	
TADBP	**1.818**	**0.062**	**6**	
LMNA	**1.812**	**0.019**	**29**	
HNRL1	**1.806**	**0.007**	**5**	
AIMP2	**1.795**	**0.057**	**4**	
RL4	**1.794**	**0.063**	**28**	
KRT85	**1.790**	**0.138**	**4**	
HV309;HV312	**1.786**	**0.023**	**3**	
SRSF9	**1.782**	**0.019**	**5**	
RL13A;R13AX	**1.768**	**0.104**	**5**	
ANX11	**1.756**	**0.085**	**8**	
THOC4	**1.730**	**0.028**	**1**	
POTEI;POTEJ	**1.725**	**0.027**	**20**	
WFD12	**1.723**	**0.049**	**1**	
MUCB;IGHM	**1.721**	**0.048**	**2**	
RL21	**1.707**	**0.034**	**3**	
K2C7	**1.703**	**0.076**	**26**	
HNRPR	**1.699**	**0.041**	**20**	
CDK1	**1.679**	**0.101**	**10**	
DAZP1	**1.678**	**0.079**	**1**	
H2BFS;H2B1A	**1.676**	**0.059**	**14**	
H2B2E;H2B1B	**1.676**	**0.059**	**13**	
PERI	**1.671**	**0.027**	**16**	
ACTBM	**1.660**	**0.051**	**9**	
RL15	**1.657**	**0.079**	**11**	
ADT2;ADT3	**1.651**	**0.063**	**14**	
ML12A;ML12B	**1.650**	**0.049**	**1**	
Z280A	**1.647**	**0.097**	**1**	
RAB3B	**1.640**	**0.125**	**1**	
HNRL2	**1.632**	**0.199**	**12**	
K1H1	**1.632**	**0.117**	**11**	
RS9	**1.626**	**0.059**	**16**	
RL30	**1.618**	**0.007**	**3**	
AIMP1	**1.616**	**0.034**	**6**	

TIA1	**1.604**	**0.005**	**5**	
RL19	**1.603**	**0.027**	**3**	
EF1A1;EF1A2	**1.602**	**0.126**	**9**	
RMXL2	**1.602**	**0.070**	**7**	
RL7	**1.599**	**0.056**	**11**	
RS13	**1.592**	**0.062**	**10**	
K2C73	**1.582**	**0.095**	**17**	
TRAP1	**1.580**	**0.048**	**5**	
IMMT	**1.578**	**0.030**	**17**	
RL14	**1.574**	**0.077**	**7**	
LMNB2	**1.573**	**0.108**	**48**	
RUVB2	**1.565**	**0.115**	**9**	
LMNB1	**1.554**	**0.087**	**79**	
HNRPC	**1.550**	**0.057**	**10**	
RL32	**1.537**	**0.019**	**7**	
HNRH1	**1.533**	**0.091**	**22**	
HNRH2	**1.533**	**0.091**	**18**	
RAB25	**1.531**	**0.110**	**2**	
ROAA	**1.531**	**0.136**	**7**	
RL22	**1.525**	**0.078**	**3**	
RL28	**1.515**	**0.075**	**14**	
DDX3X	**1.515**	**0.002**	**9**	
RS25	**1.514**	**0.072**	**5**	
FUBP2	**1.512**	**0.152**	**13**	
RL8	**1.509**	**0.083**	**19**	
RL9	**1.505**	**0.092**	**2**	
HNRPU	**1.496**	**0.143**	**38**	
POTEE;POTEF	**1.493**	**0.159**	**25**	
NOSIP	**1.492**	**0.235**	**1**	
RS15A	**1.489**	**0.008**	**6**	
PIPNA	**1.489**	**0.111**	**1**	
RS8	**1.489**	**0.107**	**17**	
RL18	**1.487**	**0.143**	**9**	
RB39A	**1.485**	**0.133**	**2**	
K1C9	**1.482**	**0.109**	**42**	
HSP71;HSP77	**1.481**	**0.176**	**9**	
KRT35	**1.476**	**0.041**	**13**	
ADH1_YEAST	**1.476**	**0.169**	**69**	
RS17L;RS17	**1.475**	**0.046**	**2**	
RBM39	**1.475**	**0.001**	**4**	
EFTU	**1.472**	**0.148**	**2**	

K2C3	**1.469**	**0.135**	**28**	
HNRCL	**1.468**	**0.076**	**8**	
H4	**1.467**	**0.060**	**13**	
RS26	**1.464**	**0.130**	**2**	
ACTA;ACTC	**1.463**	**0.093**	**30**	
RALY;RALYL	**1.462**	**0.119**	**12**	
RL11	**1.460**	**0.094**	**6**	
RL18A	**1.460**	**0.154**	**11**	
DHX9	**1.459**	**0.068**	**32**	
RS6	**1.457**	**0.016**	**8**	
NFM	**1.456**	**0.062**	**16**	
RL36	**1.444**	**0.023**	**4**	
DESM	**1.442**	**0.067**	**29**	
ROA2	**1.440**	**0.148**	**32**	
HDA11	**1.437**	**0.157**	**20**	
RLA2	**1.435**	**0.093**	**4**	
ODP2	**1.425**	**0.041**	**3**	
RL34	**1.422**	**0.039**	**4**	
SRSF6;SRSF4	**1.418**	**0.114**	**8**	
ILF3	**1.415**	**0.203**	**11**	
CCD73	**1.414**	**0.217**	**27**	
H1X	**1.413**	**0.005**	**10**	
HNRH3	**1.413**	**0.154**	**17**	
ACTB;ACTG	**1.412**	**0.118**	**40**	
VDAC2	**1.411**	**0.326**	**8**	
AINX	**1.410**	**0.143**	**15**	
K2C4	**1.405**	**0.206**	**24**	
HNRPK	**1.404**	**0.078**	**16**	
IF2B3	**1.399**	**0.117**	**6**	
K1C17	**1.399**	**0.105**	**34**	
HNRPD	**1.397**	**0.187**	**12**	
KRT84;KRT86	**1.394**	**0.090**	**26**	
K2C1	**1.393**	**0.197**	**75**	
AGO3	**1.390**	**0.215**	**13**	
PHB2	**1.390**	**0.247**	**5**	
LRC36	**1.388**	**0.232**	**3**	
RS11	**1.387**	**0.057**	**11**	
CO1A1	**1.381**	**0.213**	**22**	
K1C19;KT222	**1.381**	**0.091**	**54**	
RL10	**1.379**	**0.042**	**13**	
UBP2L	**1.376**	**0.141**	**13**	

RA1L2	**1.372**	**0.013**	**17**	
S10A8	**1.368**	**0.171**	**3**	
SKIL	**1.368**	**0.032**	**5**	
SYRC	**1.366**	**0.116**	**4**	
NEDD1	**1.365**	**0.201**	**3**	
HNRPF	**1.365**	**0.050**	**21**	
HSPB1	**1.363**	**0.127**	**5**	
RBMX;RMXL1	**1.363**	**0.062**	**22**	
RL5	**1.356**	**0.237**	**6**	
K1C10	**1.356**	**0.152**	**58**	
K1C14	**1.354**	**0.091**	**43**	
EMB	**1.354**	**0.141**	**1**	
RS4X;RS4Y1	**1.354**	**0.050**	**19**	
RS2	**1.353**	**0.115**	**13**	
RL1D1	**1.353**	**0.103**	**2**	
SRSF7	**1.351**	**0.026**	**9**	
MYL6	**1.349**	**0.139**	**3**	
ZN638	**1.349**	**0.035**	**2**	
K1C28;K1C27	**1.345**	**0.034**	**16**	
TBA1A;TBA1B	**1.344**	**0.196**	**24**	
NOP56	**1.337**	**0.120**	**4**	
ADT4	**1.335**	**0.069**	**6**	
PWP2B	**1.334**	**0.013**	**6**	
RS3	**1.334**	**0.243**	**18**	
K1C18	**1.333**	**0.181**	**51**	
RL35A	**1.329**	**0.099**	**4**	
RAN	**1.322**	**0.105**	**13**	
ILF2	**1.318**	**0.281**	**4**	
RL6	**1.315**	**0.174**	**17**	
RL36A	**1.315**	**0.365**	**1**	
TBB4B;TBB8	**1.314**	**0.175**	**22**	
RL13	**1.314**	**0.175**	**15**	
RL10A	**1.310**	**0.211**	**16**	
K2C80	**1.305**	**0.526**	**2**	
SRSF1	**1.304**	**0.234**	**14**	
ATPA	**1.303**	**0.029**	**13**	
RL40;RS27A	**1.298**	**0.620**	**2**	
RL35	**1.296**	**0.141**	**6**	
DDX5	**1.292**	**0.188**	**26**	
K2C5	**1.289**	**0.179**	**42**	
RL24	**1.286**	**0.165**	**6**	

CP013	**1.280**	**0.114**	**2**	
TRA2B	**1.280**	**0.180**	**8**	
FBRL	**1.277**	**0.118**	**11**	
RL12	**1.273**	**0.250**	**12**	
RAB10;RAB13	**1.271**	**0.240**	**2**	
K2C78	**1.268**	**0.288**	**12**	
RS23	**1.265**	**0.095**	**1**	
K1C26	**1.257**	**0.421**	**4**	
HSP7C	**1.255**	**0.044**	**10**	
SRSF5	**1.254**	**0.048**	**3**	
NFL	**1.241**	**0.049**	**11**	
CL076	**1.236**	**0.214**	**2**	
EMD	**1.234**	**0.219**	**1**	
H12;H13	**1.222**	**0.304**	**7**	
SFPQ	**1.217**	**0.210**	**14**	
RS20	**1.216**	**0.271**	**4**	
H31T;H31	**1.215**	**0.291**	**4**	
RBM14	**1.212**	**0.240**	**11**	
RAB5C	**1.206**	**0.443**	**2**	
RAB37;RAB12	**1.205**	**0.041**	**3**	
K2C71	**1.205**	**0.337**	**18**	
PCBP2;PCBP3	**1.203**	**0.210**	**5**	
K1C12	**1.202**	**0.327**	**17**	
TBB5	**1.196**	**0.226**	**21**	
RL23	**1.192**	**0.000**	**7**	
GFAP	**1.185**	**0.335**	**17**	
NFH	**1.182**	**0.259**	**17**	
RL17	**1.177**	**0.284**	**7**	
RL31	**1.176**	**0.078**	**7**	
ROA0	**1.173**	**0.144**	**12**	
SRSF3	**1.163**	**0.187**	**5**	
LRC59	**1.159**	**0.344**	**3**	
RLA0	**1.157**	**0.194**	**16**	
UTP23	**1.154**	**0.291**	**3**	
KT33B	**1.154**	**0.260**	**7**	
1433Z	**1.149**	**0.610**	**2**	
KV403;KV401	**1.132**	**0.482**	**13**	
RS5	**1.131**	**0.327**	**10**	
SYDC	**1.126**	**0.337**	**12**	
AGO2	**1.117**	**0.687**	**25**	
G3P	**1.116**	**0.522**	**6**	

K2C1B	**1.116**	**0.460**	**22**	
RL27A	**1.102**	**0.188**	**6**	
K22E	**1.100**	**0.625**	**65**	
RL23A	**1.097**	**0.547**	**7**	
RL27	**1.093**	**0.649**	**9**	
KV306	**1.085**	**0.663**	**7**	
HNRDL	**1.081**	**0.736**	**18**	
MCUR1	**1.077**	**0.611**	**1**	
H2A3;H2A1	**1.076**	**0.623**	**9**	
KV113	**1.067**	**0.732**	**10**	
RS10	**1.060**	**0.847**	**2**	
NTHL1	**1.057**	**0.704**	**1**	
K1H2	**1.057**	**0.862**	**8**	
PCBP1	**1.055**	**0.787**	**6**	
RS27L	**1.054**	**0.788**	**1**	
YTHD3	**1.044**	**0.838**	**7**	
K1C16	**1.042**	**0.861**	**31**	
DDX17	**1.039**	**0.774**	**33**	
NTPCR	**1.033**	**0.814**	**2**	
K2C75	**1.028**	**0.903**	**38**	
RS16	**1.016**	**0.898**	**17**	
ROA1	**1.012**	**0.927**	**20**	
TBB2A;TBB2B	**1.001**	**0.997**	**18**	
HDAC8	**1.000**	**0.998**	**134**	
TIAR	**0.979**	**0.815**	**7**	
RS14	**0.966**	**0.811**	**5**	
GBLP	**0.957**	**0.764**	**8**	
HNRPM	**0.956**	**0.795**	**45**	
CDK3	**0.955**	**0.683**	**2**	
RMXL3	**0.939**	**0.744**	**4**	
LAP2B	**0.939**	**0.704**	**12**	
HNRPQ	**0.919**	**0.587**	**13**	
RS12	**0.906**	**0.252**	**6**	
RS18	**0.903**	**0.484**	**28**	
TANC2	**0.894**	**0.784**	**6**	
VIME	**0.893**	**0.356**	**94**	
K1C13	**0.857**	**0.367**	**21**	
K2C6B	**0.833**	**0.354**	**45**	
K2C8;KRT81	**0.833**	**0.210**	**105**	
RLA1	**0.820**	**0.357**	**1**	
NDUAD	**0.778**	**0.608**	**1**	

DDX3Y	**0.759**	**0.107**	**8**	
SLMAP	**0.749**	**0.285**	**5**	
RL7A	**0.747**	**0.198**	**22**	
TBB6	**0.671**	**0.004**	**4**	
RS19	**0.648**	**0.024**	**9**	
N2DL4	**0.617**	**0.007**	**1**	
SPR1A	**0.552**	**0.171**	**1**	
SYEP	**0.502**	**0.161**	**17**	
K2C6A	**0.460**	**0.021**	**43**	
SYIC	**0.372**	**0.007**	**10**	
LEG7	**0.337**	**0.054**	**6**	
ALBU	**0.230**	**0.000**	**37**	
NDUB4	**0.211**	**0.017**	**1**	
RAB3A	**0.044**	**0.000**	**1**	
RL26	**0.000**	**0.000**	**8**	**Undefined due to zero unique peptides and overflow abundance***
TBB4A	**0.000**	**0.000**	**15**	**Undefined due to zero unique peptides and overflow abundance***
K1C15	**0.000**	**0.000**	**18**	**Undefined due to zero unique peptides and overflow abundance***
ACTBL	**0.000**	**0.000**	**15**	**Undefined due to zero unique peptides and overflow abundance***
KRT83	**0.000**	**0.000**	**4**	**Undefined due to zero unique peptides and overflow abundance***
TBB3	**0.000**	**0.000**	**14**	**Undefined due to zero unique peptides and overflow abundance***
DUX5	**0.000**	**0.000**	**1**	**Undefined due to zero unique peptides and overflow abundance***
RLA0L	**0.000**	**0.000**	**12**	**Undefined due to zero unique peptides and overflow abundance***
H90B3	**0.000**	**0.000**	**3**	**Undefined due to zero unique peptides and overflow abundance***
K2C6C	**0.000**	**0.000**	**42**	**Undefined due to zero unique peptides and overflow abundance***
RAB43;RB43L	**0.000**	**0.000**	**1**	**Undefined due to zero unique peptides and overflow abundance***
CHCH3	**0.000**	**0.000**	**1**	**Undefined due to zero unique peptides and overflow abundance***

KV201;KV206	0.000	0.000	1	Undefined due to zero unique peptides and overflow abundance*
TMCC3	0.000	0.000	1	Undefined due to zero unique peptides and overflow abundance*
NOP58	0.000	0.000	1	Undefined due to zero unique peptides and overflow abundance*
TBA3E	0.000	0.000	18	Undefined due to zero unique peptides and overflow abundance*
RAB3D	0.000	0.000	2	Undefined due to zero unique peptides and overflow abundance*
H90B2	0.000	0.000	2	Undefined due to zero unique peptides and overflow abundance*

Table A1.3 - Proteins identified through HDAC8 covalent capture - F191

Protein ID	UV/No UV FC	p-value (UV/No UV)	# peptide ID	Notes
RS9	6.087	0.013	1	
ROA1;RA1L2	3.911	0.001	3	
IL6	3.745	0.005	3	
SRSF3	3.661	0.000	1	
TIAR	2.507	0.000	3	
ATPB	2.105	0.003	4	
HNRPF	2.073	0.101	2	
FBRL	2.066	0.013	2	
RAB1C;RAB1A;RAB1B	1.981	0.005	1	
ROAA	1.976	0.008	7	
ILF2	1.862	0.018	1	
CKAP4	1.838	0.021	1	
OAT	1.776	0.026	6	
THIL	1.727	0.289	1	
RL4	1.654	0.016	6	
SERPH	1.561	0.000	7	
TBB2A;TBB2B;TBB6	1.550	0.019	10	
RS7	1.547	0.005	7	
HNRDL	1.529	0.048	5	
TBB4B;TBB4A;TBB8	1.527	0.009	16	
RLA1	1.499	0.054	2	
TBA1B;TBA1A;TBA1C	1.486	0.006	17	
ASSY	1.477	0.061	2	

RLA0	**1.457**	**0.119**	**2**	
ACTBM	**1.457**	**0.078**	**9**	
RL30	**1.452**	**0.095**	**3**	
RL35	**1.452**	**0.193**	**5**	
ROA0	**1.422**	**0.258**	**1**	
POTEE;POTEF;POTEI;POTEJ	**1.394**	**0.014**	**14**	
RL6	**1.372**	**0.007**	**12**	
RS29	**1.367**	**0.035**	**3**	
ADT2	**1.359**	**0.077**	**3**	
AN18A	**1.353**	**0.001**	**1**	
H3C;H31;H31T;H32;H33	**1.351**	**0.023**	**7**	
RT23	**1.346**	**0.387**	**1**	
RL8	**1.335**	**0.109**	**8**	
HSPB1	**1.324**	**0.040**	**5**	
K1C18	**1.312**	**0.089**	**5**	
SFPQ	**1.281**	**0.511**	**2**	
TBB5	**1.275**	**0.142**	**15**	
RL17	**1.268**	**0.370**	**2**	
HDAC8	**1.262**	**0.082**	**25**	
RLA2	**1.259**	**0.075**	**9**	
RL7	**1.259**	**0.253**	**3**	
RL27	**1.257**	**0.009**	**2**	
GRP78	**1.233**	**0.186**	**5**	
ELAV1	**1.211**	**0.557**	**3**	
RS20	**1.208**	**0.599**	**1**	
RL19	**1.207**	**0.337**	**5**	
RL32	**1.207**	**0.361**	**7**	
RS3A	**1.194**	**0.030**	**7**	
RS16	**1.185**	**0.808**	**1**	
H2B1K;H2B1A;H2B1B	**1.182**	**0.367**	**12**	
ETFA	**1.174**	**0.037**	**6**	
RL14	**1.167**	**0.491**	**2**	
RL38	**1.154**	**0.389**	**4**	
VIME;KRT81;KRT83;KRT86	**1.145**	**0.358**	**23**	
TAGAP	**1.143**	**0.224**	**2**	
RL23A	**1.140**	**0.206**	**5**	
HSP7C;HSP72	**1.125**	**0.341**	**7**	
E1B55_ADE05;E1B55_ADE02	**1.124**	**0.566**	**9**	
RS5	**1.100**	**0.565**	**3**	
ETFB	**1.087**	**0.315**	**12**	

PHB	**1.084**	**0.492**	**4**	
FUBP2	**1.079**	**0.524**	**27**	
ROA3	**1.079**	**0.792**	**2**	
P4K2A	**1.072**	**0.711**	**3**	
H2A1J;H2A1;H2A1B	**1.070**	**0.473**	**11**	
H4	**1.060**	**0.650**	**17**	
RL18	**1.057**	**0.751**	**5**	
RS3	**1.056**	**0.488**	**4**	
ACTB;ACTA;ACTBL	**1.051**	**0.672**	**16**	
STAU1	**1.050**	**0.817**	**5**	
DAZP1	**1.050**	**0.787**	**8**	
TIF1B	**1.033**	**0.663**	**4**	
ROA2	**1.030**	**0.876**	**6**	
ATP5H	**1.027**	**0.886**	**3**	
RS2	**1.021**	**0.922**	**9**	
RBM14	**1.020**	**0.907**	**6**	
CH60	**1.006**	**0.939**	**56**	
HNRPC;HNRC1;HNRC2;	**1.006**	**0.977**	**10**	
DHX9	**1.003**	**0.991**	**2**	
RL23	**1.000**	**0.998**	**6**	
RL3	**0.999**	**0.997**	**9**	
SREK1	**0.999**	**0.995**	**5**	
UBQL1;UBQL4	**0.998**	**0.987**	**2**	
ATPA	**0.988**	**0.939**	**22**	
K2C5	**0.982**	**0.905**	**5**	
AINX	**0.975**	**0.783**	**2**	
MKX	**0.971**	**0.576**	**4**	
FUBP3	**0.963**	**0.785**	**24**	
RS28	**0.963**	**0.755**	**5**	
RL31	**0.955**	**0.825**	**2**	
PABP1	**0.954**	**0.804**	**6**	
HNRH3	**0.952**	**0.851**	**5**	
RS4X;RS4Y1;RS4Y2	**0.951**	**0.523**	**9**	
ADH1_YEAST	**0.943**	**0.702**	**9**	
RS19	**0.937**	**0.610**	**13**	
STML2	**0.925**	**0.666**	**2**	
H14;H11;H12;H13	**0.921**	**0.499**	**24**	
TRAP1	**0.919**	**0.507**	**1**	
GFAP	**0.914**	**0.619**	**3**	
TNIP2	**0.909**	**0.491**	**1**	
SGT1	**0.901**	**0.073**	**2**	

HNRPM	**0.894**	**0.398**	**41**	
RS18	**0.893**	**0.458**	**9**	
RL15	**0.891**	**0.634**	**2**	
RS11	**0.891**	**0.670**	**6**	
GRP75	**0.888**	**0.391**	**14**	
HNRH1;HNRH2	**0.888**	**0.225**	**10**	
IF2B1	**0.888**	**0.462**	**5**	
CDK1	**0.885**	**0.317**	**5**	
RL34	**0.884**	**0.647**	**3**	
DDX5	**0.879**	**0.382**	**5**	
RL11	**0.869**	**0.403**	**5**	
MATR3	**0.869**	**0.338**	**15**	
RL27A	**0.860**	**0.438**	**10**	
RL10A	**0.858**	**0.105**	**7**	
RLA0L	**0.854**	**0.533**	**2**	
RALYL	**0.848**	**0.706**	**1**	
RL13	**0.846**	**0.112**	**14**	
CERKL	**0.841**	**0.011**	**2**	
COX41	**0.841**	**0.432**	**1**	
RL7A	**0.835**	**0.210**	**16**	
HNRPD	**0.832**	**0.135**	**6**	
RL28	**0.832**	**0.351**	**2**	
RL3L	**0.830**	**0.048**	**5**	
RS8	**0.825**	**0.098**	**8**	
RBM4	**0.824**	**0.222**	**4**	
HNRPU	**0.824**	**0.297**	**18**	
NPM	**0.819**	**0.042**	**16**	
PSB2	**0.817**	**0.296**	**3**	
RS14	**0.810**	**0.215**	**7**	
EIF3F	**0.809**	**0.138**	**1**	
RS25	**0.803**	**0.064**	**7**	
RS12	**0.799**	**0.134**	**4**	
RS30	**0.787**	**0.355**	**2**	
ATPO	**0.786**	**0.215**	**2**	
NSUN2	**0.783**	**0.066**	**9**	
H2AY	**0.782**	**0.253**	**1**	
COX5B	**0.779**	**0.292**	**4**	
G3P	**0.779**	**0.319**	**1**	
RL9_MACFA;RL9	**0.766**	**0.157**	**3**	
EF1A2	**0.763**	**0.020**	**10**	
EF1A3;EF1A1	**0.763**	**0.020**	**10**	

PCBP1	**0.760**	**0.476**	**2**	
MYL6	**0.754**	**0.037**	**2**	
RL24	**0.749**	**0.227**	**4**	
PB2_I56A3	**0.748**	**0.004**	**3**	
CX6B1	**0.744**	**0.316**	**1**	
LMNB1	**0.743**	**0.000**	**16**	
EFTU	**0.739**	**0.012**	**17**	
K2C8;K22O;K2C3	**0.728**	**0.168**	**15**	
KV404;KV401;KV402;KV403	**0.725**	**0.168**	**4**	
ODPB	**0.715**	**0.022**	**6**	
RL12	**0.697**	**0.186**	**3**	
RS6	**0.694**	**0.021**	**9**	
HS71A;HS71B;HSP76	**0.693**	**0.069**	**14**	
PRDX4	**0.664**	**0.322**	**1**	
VP35_EBOSU	**0.655**	**0.025**	**1**	
KV310;KV113;KV306	**0.645**	**0.033**	**6**	
RM12	**0.628**	**0.131**	**5**	
RL36	**0.628**	**0.028**	**2**	
PGS1	**0.618**	**0.001**	**1**	
RMXL1;RBMX	**0.592**	**0.005**	**3**	
RAB7A	**0.587**	**0.037**	**4**	
RL22	**0.576**	**0.114**	**2**	
FUBP1	**0.470**	**0.103**	**5**	
SLIRP	**0.452**	**0.020**	**2**	
TIA1	**0.445**	**0.210**	**2**	
ITB1	**0.439**	**0.202**	**3**	
IKBP1	**0.387**	**0.015**	**1**	
RL13A	**0.385**	**0.067**	**2**	
CB044	**0.222**	**0.067**	**2**	
LMNA	**0.132**	**0.360**	**1**	
GLYM	**0.099**	**0.278**	**1**	
K2C78	**0.017**	**0.075**	**2**	
LR10B	**0.002**	**0.161**	**4**	
XPO2	**0.000**	**0.000**	**2**	**Undefined due to zero unique peptides and overflow abundance***
TBA4A	**0.000**	**0.000**	**12**	**Undefined due to zero unique peptides and overflow abundance***
K2C79	**0.000**	**0.000**	**4**	**Undefined due to zero unique peptides and overflow abundance***

K2C6B;K2C75	**0.000**	**0.000**	**4**	**Undefined due to zero unique peptides and overflow abundance***
HS71L	**0.000**	**0.000**	**5**	**Undefined due to zero unique peptides and overflow abundance***
CK040	**0.000**	**0.000**	**1**	**Undefined due to zero unique peptides and overflow abundance***
YAED1	**0.000**	**0.000**	**1**	**Undefined due to zero unique peptides and overflow abundance***
TBB3	**0.000**	**0.000**	**8**	**Undefined due to zero unique peptides and overflow abundance***
RL36A	**0.000**	**0.000**	**1**	**Undefined due to zero unique peptides and overflow abundance***